5-2014

Geomorphic Change Detection Using Multi-Beam Sonar

James Hensleigh
Utah State University

GEOMORPHIC CHANGE DETECTION USING MULTI-BEAM SONAR

by

James Hensleigh

A thesis submitted in partial fulfillment
of the requirements for the degree

of

MASTER OF SCIENCE

in

Watershed Sciences

Approved:

Dr. Joseph M. Wheaton Major Professor	Dr. Patrick Belmont Committee Member
Dr. Mac McKee Committee Member	Dr. Mark R. McLellan Dean of Graduate Studies

UTAH STATE UNIVERSITY
Logan, Utah

2014

ABSTRACT

Geomorphic Change Detection Using Multi-beam SONAR

by

James Hensleigh, Master of Science

Utah State University, 2014

Major Professor: Dr. Joseph M. Wheaton
Department: Watershed Sciences

The emergence of multi-beam echo sounders (MBES) as an applicable surveying technology in shallow water environments has expanded the extent of geomorphic change detection studies to include river environments that historically have not been possible to survey or only small portions have been surveyed. The high point densities and accuracy of MBES has the potential to create highly accurate digital elevation models (DEM). However, to properly use MBES data for DEM creation and subsequent analysis, it is essential to quantify and propagate uncertainty in surveyed points and surfaces derived from them through each phase of data collection and processing. Much attention has been given to the topic of spatially variable uncertainty propagation in the context of the construction of DEM and their use in geomorphic change detection studies. However little work has been done specifically with applying spatially varying uncertainty models for MBES data in shallow water environments. To address this need, this report presents a review of literature and methodology of uncertainty quantification in a geomorphic change detection study. These methods are then applied and analyzed in a geomorphic change detection study using MBES as the data collection technique.

(122 pages)

ACKNOWLEDGMENTS

This paper could not have been written without the help of a number of patient and knowledgeable individuals in my corner. I would like to personally thank Chris Welcker, Kelvin Anderson, and Mike Butler of Idaho Power Company for their readiness to provide feedback and encouragement throughout the process. I would also like to thank my committee members Patrick Belmont and Mac McKee for their advice and insightful feedback. I cannot thank my advisor Joe Wheaton enough for taking a chance on me and providing instrumental guidance and feedback without which none of this would have been possible. Additionally I would like to recognize all of the lab members of ET-AL for their help as well as Chris Garrard for sharing her vast knowledge of Python with me. Last and certainly not least much love and thanks to my family for providing me unconditional support in this endeavor and in life.

James Hensleigh

CONTENTS

Page

LIST OF TABLES

Table Page

LIST OF FIGURES

ACRONYMS

ANOVA	Analysis of Variance
DEA	David Evans & Associates
DEM	Digital Elevation Model(s)
DoD	DEM of Difference
FIS	Fuzzy Inference System
GCD	Geomorphic Change Detection
GIS	Geographic Information System(s)
HRP	Heave-Roll-Pitch Sensor
IDW	Inverse Distance Weighting
IPC	Idaho Power Company
MB	Megabytes
MBES	Multi-beam echo sounder
MBB	Multi-beam Bathymetry
MBBS	Multi-beam Bathymetric Survey
ME	Mean Error
MRBF	Multiquadratic radial basis function
OK	Ordinary Kriging
RBF	Radial Basis Functions
RMSE	Root Mean Square Error
RST	Regularized Spline with Tension
SONAR	Sound Navigation & Ranging
SVP	Sound Velocity Profiler
TIN	Triangulated Irregular Network
TLS	Terrestrial Laser Scanner(s)
TPU	Total Propagated Uncertainties
UK	Universal Kriging
USGS	United States Geological Survey
VRU	Vertical Reference Unit

Section 1

Introduction

The emergence of multi-beam echo sounders (MBES) as an applicable surveying technology in shallow water environments has expanded the extent of geomorphic change detection studies to include river environments that historically have not been possible to survey or only small portions have been surveyed (Hazel et al., 2010). The high point densities and accuracy of MBES has the potential to create highly accurate digital elevation models (DEM). Through repeat surveying of the same area, DEM can be created from the surveyed points, and by differencing the DEM be used to track the change in sediment storage through reaches of interest. However, to properly use MBES data for DEM creation and subsequent analysis, it is essential to quantify and propagate uncertainty in surveyed points and surfaces derived from them through each phase of data collection and processing.

Much attention has been given to the topic of uncertainty propagation in the context of the construction of DEM and their use in geomorphic change detection studies (Milan et al., 2011; Wheaton, 2008; Wheaton et al., 2010). To obtain an accurate model of geomorphic change it is necessary to account for survey uncertainty, surface uncertainty, and data processing error when creating DEM that will be differenced to determine geomorphic change. Surveying uncertainty is not spatially random but varies across a surveyed area due to quantifiable spatial parameters. For this reason methods have been developed to better quantify the relationship between survey and surface uncertainty and spatial attributes. To accomplish this it is essential to quantify uncertainties and distribute them across the surveyed area based on parameters influencing survey and processing uncertainties. However little work has been done specifically with applying spatially varying uncertainty models for MBES data in shallow water environments.

To address this need, this report presents a review of literature and methodology of the

pertinent steps to limit and quantify uncertainty in a geomorphic change detection study. The topics of estimating sample resolution, determining cell resolution of analysis, proper interpolation techniques, quantification of surface uncertainties, integration of a fuzzy inference system to model uncertainty, probabilistic thresholding, and Bayesian probability updating will all be discussed in the context of limiting and quantifying uncertainty.

Idaho Power Company (IPC) has provided data collected from MBES surveys from their ongoing development of a long-term monitoring program of sediment fluxes below Hells Canyon Dam Complex. This data is used as a case study to illuminate and expand upon examples from the literature as well as to act as a template to demonstrate best practice methodologies for MBES data in this river environment. High quality data can easily be degraded (e.g. working in an improper cell resolution, applying unacceptable interpolation methods, not practicing orthogonality and concurrency in map algebra operations) within a geographic information system (GIS) through the application of incorrect methodology. By exploring and implementing best practice methodologies discussed in the literature this paper aims to maintain the quality of data throughout the study.

There are three main objectives addressed in this report. The first objective is to outline the key themes of past work on the topic of uncertainty propagation in geomorphic change detection studies. The second is to apply these themes with consideration to MBES data. The third objective is the analysis of common GIS data preparation methodologies and the identification of best practice methodology for MBES data. These objectives are not sequential and are woven into each section of the paper. By addressing these three objectives the goal is to provide a context for applying a spatially varying uncertainty model in a geomorphic change detection study from repeat surveys using MBES.

Section 2

Case Study Site and Concept

2.1 Concept and Structure of Paper

The data used in this study was collected in separate surveys in 2008 and 2009 with a RESON SeaBat 8101 MBES as part of IPC's development of a repeat surveying methodology for the area below Hells Canyon Dam Complex. The data has been collected with the specific goal of developing a long term monitoring program of the movement of sediment through the reach. In this paper the data will be used as a template to explore different data processing and uncertainty incorporation methodologies. By comparing different techniques, a methodology is developed for both limiting and accounting for uncertainty within a multi-beam bathymetric survey (MBBS) project. The emphasis of this paper is not on the results of the geomorphic change study but on optimizing a workflow for MBES through exploring different ideas and methodologies discussed in literature.

Section 2 begins as a brief overview of the study site, the data produced from the surveys and the MBES used in this study. Section 3 is a discussion of multi-beam SONAR basics and its place among other highly accurate surveying techniques. Issues unique to multi-beam SONAR are addressed to provide a background for their contribution to uncertainty. This section provides methods for determining the sampling resolution during a MBBS. Section 4 discusses the construction of a DEM from a MBBS and builds upon concepts presented in Section 3. An information sensitivity loss analysis is performed in Section 4.1.1 to aid in the choosing of a cell resolution of analysis. Additionally a study exploring the influence of interpolation on DEM uncertainty is presented and a method for quantifying this uncertainty is presented.

Section 5 discusses landscape features contributing to uncertainty in the surfaces produced from data from a MBBS. To explore the relationship between landscape morphology and survey uncertainty an initial method for estimating survey uncertainty is provided. The relationship between this estimate of survey uncertainty and landscape morphology, surface roughness and slope, are statistically explored which provides the background for emerging concepts in geomorphic change studies discussed in Section 6. A case study which outlines the use of these new techniques is presented, specifically a spatially distributed uncertainty model, application of a fuzzy inference system to handle uncertainty, probabilistic thresholding, and the use of Bayesian probability to assess and update the resulting probabilities. In addition to presenting emerging techniques in geomorphic change detection, Section 6 briefly discusses historical methods and their potential shortcomings. Section 7 interprets the effects of implementing these new methods on the output of a geomorphic change detection study. Section 8 summarizes the workflow and gives recommendations for those working with MBES technology. Section 9 is a discussion section that brings up shortcomings and identifies potential areas of improvement and future research, while Section 10 presents conclusions drawn from this study.

The result of the paper is a basic workflow for a geomorphic change detection study using data from an MBES that is comprised of six basic steps:

1. Determine sampling resolution
2. Determine grid resolution
3. Create an interpolation error grid
4. Create survey uncertainty grids
5. Create a fuzzy inference system
6. Difference DEMs to 95% confidence using probabilistic thresholding and a fuzzy inference system, Bayesian updating and an interpolation error term.

2.2 Study Site and Data Collection Specifications

The Hells Canyon Reach of the Snake River flows north 95 kilometers from Hells Canyon Dam to the confluence with the Salmon River. The reach has an average bed slope of approximately 0.002%, contains numerous rapids, has an average bankfull width of 245 to 330 ft., and is extremely confined with a bankfull width to floodplain width ratio of 1 (Anderson et al., 2011). The surrounding canyon walls and deep fast-moving water of the reach exclude traditional surveying methods and require a sonar system to be surveyed. Due to the extensive area covered in the surveying project a sub reach, known as Wild Sheep Reach, has been chosen to use in this study.

This study site was chosen because it contains a healthy variety of geomorphic features (e.g. breaks in slope, boulders, shelves, sand bars, etc.) and the surveys have produced point clouds of adequate memory requirements, greater than 125 megabytes (MB), to pose a challenge to GIS operations. The point clouds cover an area of approximately 0.06 mi^2. Within this reach the Snake River runs from southwest to northeast and has a length of approximately 1.8 miles. The study site, which can be seen in Figure 2.1, runs through a deep rugged canyon where from bottom of canyon to ridge is over 1000 ft. The river channel ranges in width from about 70 ft. at its narrowest to about 375 ft. at is widest points. Considering all of the facies and features in the channel, the reach has an average slope of 12° and steep banks of greater than 60° characterize distinct areas of the reach. Overall the channel of Wild Sheep Reach is characterized by a relatively smooth surface with a mean surface roughness estimate of about 6 inches but has many areas with high surface roughness greater than 2 ft. with some areas containing boulders greater than 10 ft. in height.

Data was collected on two different surveying trips in 2008 and 2009 with the RESON SeaBat 8101 MBES. This MBES utilizes 101 uniform beams of 1.5° x 1.5° at 240 kHz to produce a swath with the potential to cover 150°. Depending on water depth the MBES

was used at a ping rate of 21 to 10 Hz (Butler, 2002).

The point clouds produced from these surveys contain over 10.8 million (10,824,618) points and 4.5 million (4,559,106) points and are roughly 382 MB and 135 MB for the 2008 and 2009 datasets respectively. The difference is due to a different surveying strategy and increased passes of specific areas in 2008 which resulted in an increase in points surveyed and average point density. Files of this size have the potential to significantly slow down calculations and visualization within popular GIS like ArcGIS and are best handled with an efficient workflow.

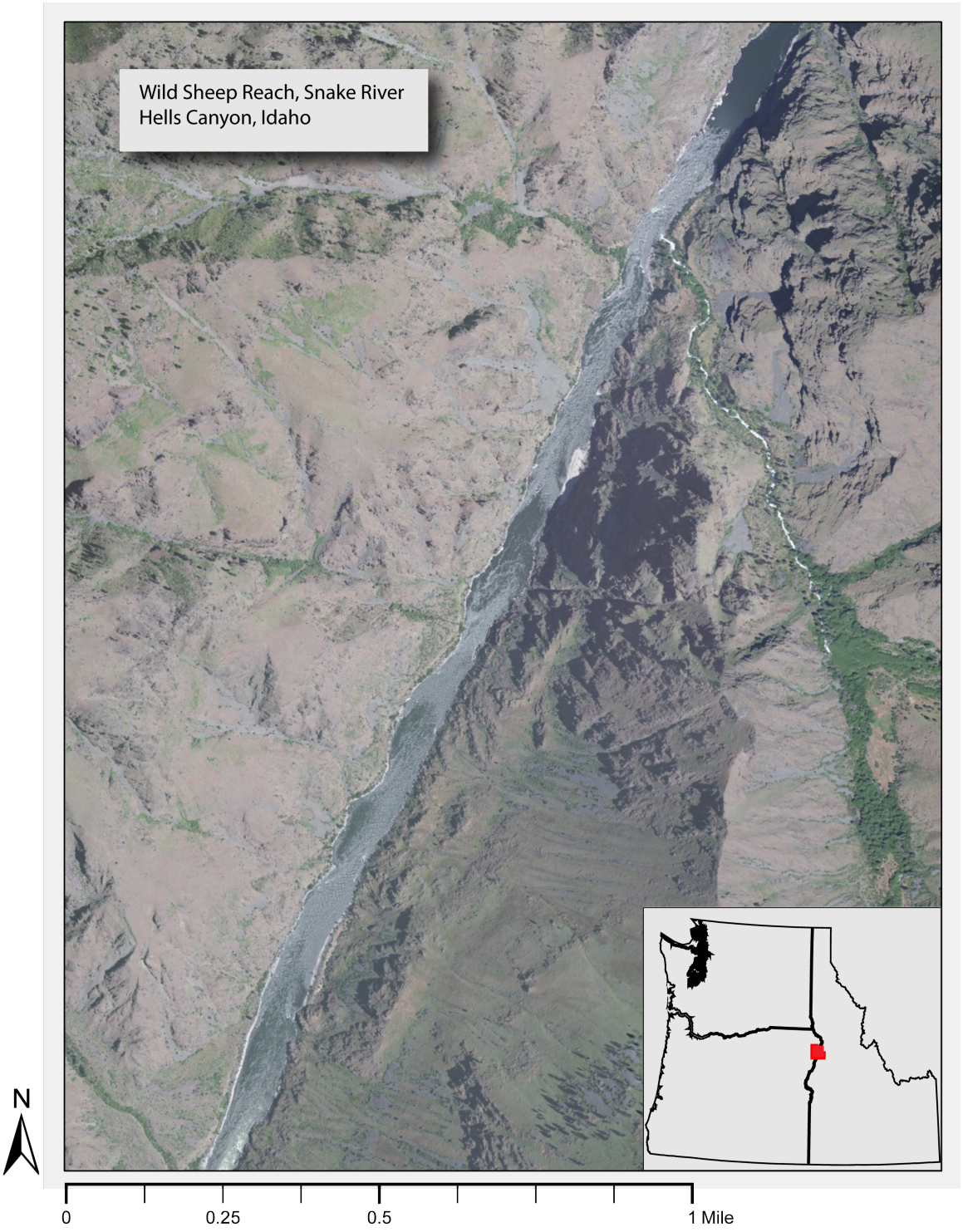

Figure 2.1. Study Site Wild Sheep Reach, Snake River, Hells Canyon, Idaho.

Section 3

Multi-beam Bathymetric SONAR Surveys

3.1 Multi-beam SONAR and Beam Footprints

MBES are mounted to a vessel and use sound navigation and ranging (SONAR) to measure elevations of a water-body floor. Elevation measurements are collected by creating sound waves and measuring the time it takes them to return to the MBES. By the time the sound wave reaches the water-body floor it has expanded resulting in the beam reporting an elevation for a region of the water-body floor, not a single point. The area providing an elevation measurement for an individual sonar beam is known as the beam footprint. In MBES this process is done with multiple beams which create a swath shaped region providing near complete coverage of the water-body floor. A basic depiction of this process for one beam is shown in Figure 3.1. For a more complete description of how a SONAR beam provides elevation measurements refer to the Appendix A.1.

Swath data collection creates non-uniform beam footprints resulting in a non-uniform sampling resolution. The across-track and along-track sampling resolutions are a function of distance from the boat or depth, angle of incidence, and beam width (Diaz, 2000; International-Hydrographic-Bureau, 2005). It is given by Equation 3.1:

$$beam footprint = \frac{2z}{cos^2(\beta)} \times tan(\frac{\phi r}{2}) \tag{3.1}$$

where z is the mean depth, β is the beam angle, ϕr is the width of the reception beam in the athwartship (across-track) direction (1.5° in RESON SeaBat 8101). The same equation is used to calculate beam footprint in the along-track direction with the exception that the cosine term in the denominator is not squared. When surveying a sloping surface the

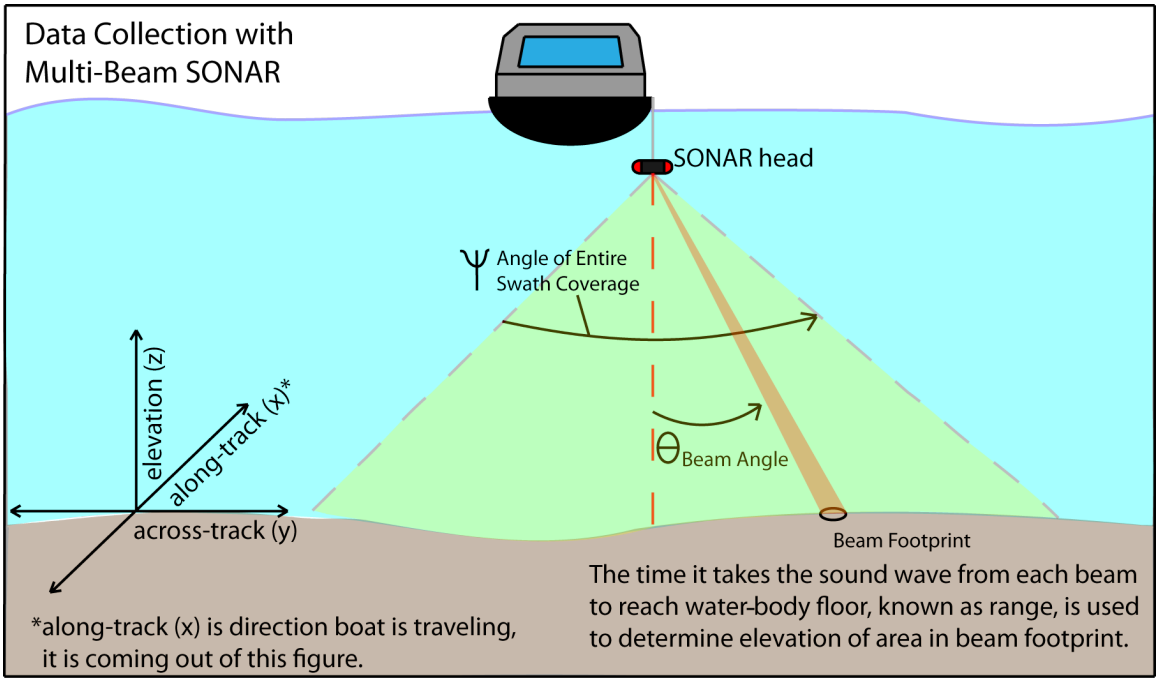

Figure 3.1. Basic data collection of a multi-beam echo sounder (MBES). The MBES produces a sound wave which upon striking the river bottom a portion of the sound wave reflects back to the MBES producing a depth measurement.

equation adds a term ζ to represent the slope of the surface (International-Hydrographic-Bureau, 2005). Equation 3.2 is used:

$$beam footprint = \frac{2z}{cos(\beta) - cos(\beta - \zeta)} \times tan(\frac{\phi r}{2}) \tag{3.2}$$

The concept of a beam footprint that varies in size is essential to understanding how a MBES works as the beam footprint is the determining factor for the size of object that can be determined by the MBES (de Jong et al., 2002; Diaz, 2000; International-Hydrographic-Bureau, 2005). Using Equation 3.1 and a constant depth, as beam angle increases the size of the footprint increases resulting in a decreased sampling resolution. The effect of beam angle at different depths for the RESON SeaBat 8101 is shown in Figures 3.2, 3.3, and 3.4. These figures reveal that a larger range of footprints exists in the across-track direction than along-track.

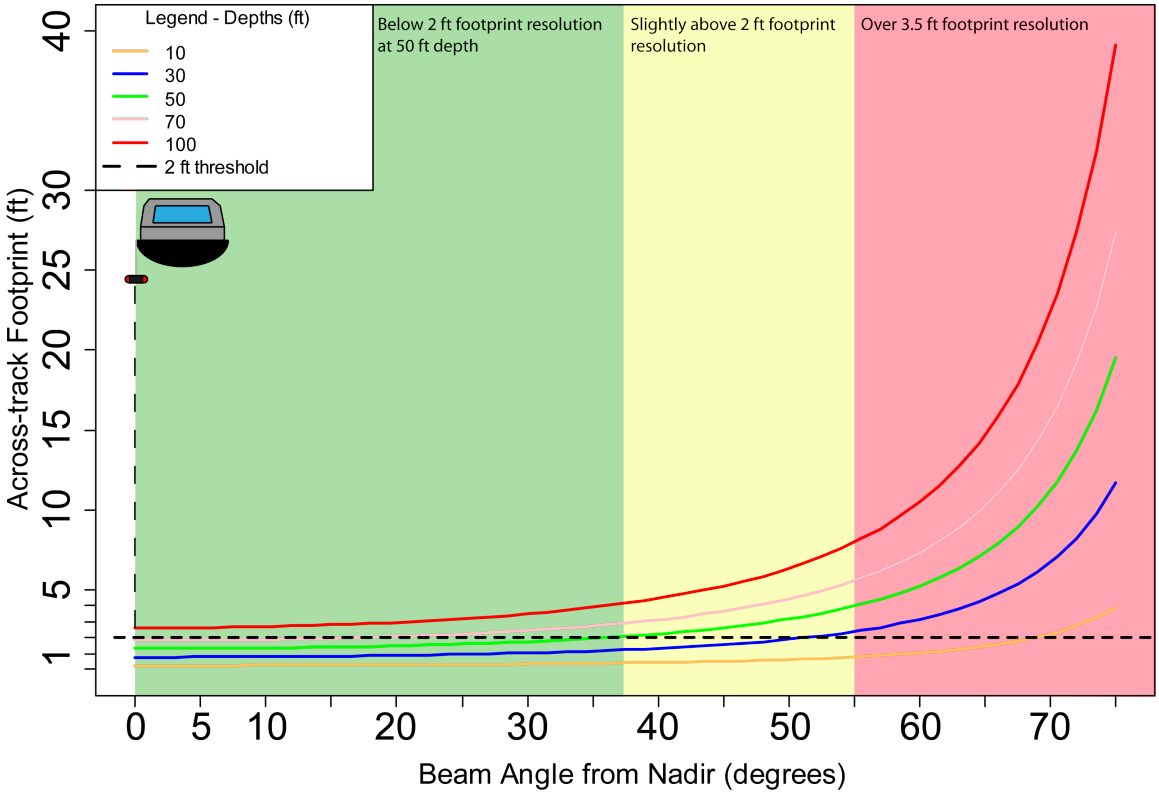

Figure 3.2. Change in footprint size by beam at different depths in the athwarthship (across-track) dimension. The colored regions designate beam angles when surveying at 50 ft. depth or greater producing a footprint less than 2 ft. (green), slightly greater above 2 ft. (yellow), or over 3.5 ft. (red).

A typical range of depths in the Wild Sheep Reach is 10 to 50 ft. and the calculated along-track, across-track, and total beam footprints for depths of 10, 30 and 50 ft. are shown in Table 3.1. This table shows there is a distinct change in resolution from nadir to the outer beams. For example at 30 ft. depth there is a range of 0.79 to 11.73 ft. in the across-track direction, 0.79 to 3.03 ft. in the along-track direction, and 0.62 to 35.58 ft^2 in total beam footprint.

The total coverage of a swath in the across-track direction can be calculated by Equation 3.3:

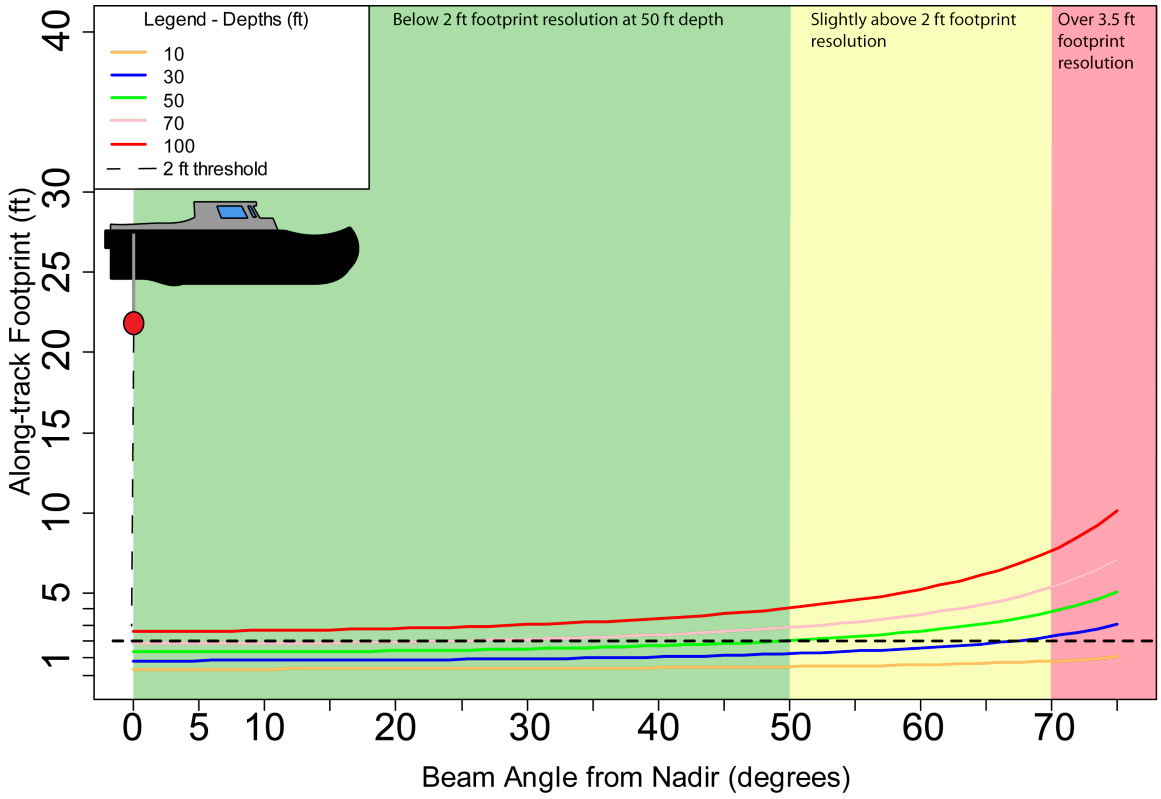

Figure 3.3. Change in footprint size by beam at different depths in the fore-aft (along-track) direction. The colored regions designate beam angles when surveying at 50 ft. depth or greater producing a footprint less than 2 ft. (green), slightly greater above 2 ft. (yellow), or over 3.5 ft. (red).

Table 3.1. Change in beam footprints for across-track , along-track and total footprints at different beam angles. At each depth the first column is across-track dimension in ft., second column is along-track dimension in ft., and the third column is total footprint in ft^2.

	Depth (ft.)								
	Ten			**Thirty**			**Fifty**		
Beam Angle (°)									
0	0.26	0.26	0.07	0.79	0.79	0.62	1.31	1.31	1.71
15	0.28	0.27	0.08	0.84	0.81	0.68	1.40	1.36	1.90
30	0.35	0.30	0.11	1.05	0.91	0.95	1.75	1.51	2.64
45	0.52	0.37	0.19	1.57	1.11	1.74	2.62	1.85	4.85
60	1.05	0.52	0.55	3.14	1.57	4.94	5.24	2.62	13.71
75	3.91	1.01	3.95	11.73	3.03	35.58	19.54	5.06	98.84
Swath-Width (ft.)	75			234			373		

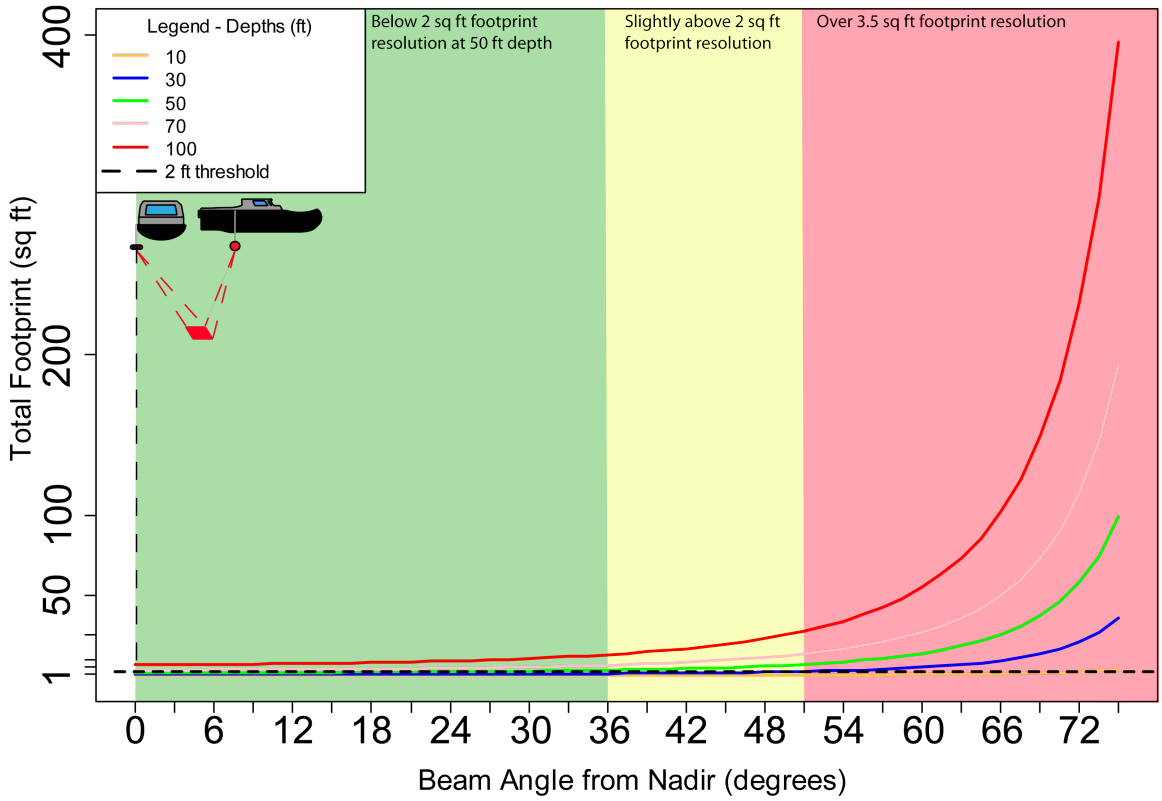

Figure 3.4. Change in total footprint size by beam at different depths. The colored regions designate beam angles when surveying at 50 ft. depth or greater producing a footprint less than 2 ft^2 (green), slightly greater above 2 ft^2 (yellow), or over 3.5 ft^2 (red).

$$swathwidth = 2z \times tan(\frac{\Delta\theta}{2}) \tag{3.3}$$

where z is depth and $\Delta\theta$ is the total angular coverage for the MBES (de Jong et al., 2002). As can be seen in Table 3.1; the total swath coverage for the RESON SeaBat 8101 in the across-track dimension ranges from 75 ft. to 373 ft. at 10 and 50 ft. depths respectively.

The variable footprint size of MBES is in contrast to the expansion observed in surveys with terrestrial laser scanners (TLS). Although TLS also has expansion of its laser this is in the magnitude of millimeters to centimeters when compared to the expansion of sound waves in MBES which is in the magnitude of centimeters to meters (Mechelke et al., 2007). A variable footprint has implications for the uncertainty involved in elevation measurements as the size of object that can be resolved varies depending on water depth and beam angle. This topic is expanded upon in Section 5.1.

It is important to note that the results in Figures 3.2, 3.3, and 3.4 as well as Table 3.1 from the equations presented in this section are estimates that assume a constant depth and a flat floor. A more applicable example of varying beam footprints with differing depths and slopes is calculated for an across-track profile taken from the 2009 Wild Sheep Reach survey in the next section, Section 3.2.

3.2 Case Study Application - Determining Sampling Resolution

Support is the concept that the size, shape, orientation, and distribution of data determine how it can be used (Huevelink, 1998). In general when surveying for elevation, data sampled at smaller intervals over a uniform spacing and distribution will provide a more accurate representation of the surface and provide a greater amount of support. For example data sampled over intervals of 1 ft. can be used to identify objects 1 ft. or greater but not any smaller, implying that the raster resolution of analysis should be no less than

1 ft. By determining the sampling resolution, the distribution and spacing of a survey are identified providing a metric for the amount of support that is provided by the survey. By knowing the amount of support provided by the survey a more informed determination of the raster resolution to be used in later analysis can be made.

In this section two methods are discussed to estimate the sampling resolution of an MBBS. The first method is a straightforward method made possible by the Average Nearest Neighbor tool standard in ArcGIS. This tool takes a point shapefile as input and iteratively calculates the average distance between nearest neighbor points. Running this tool on the study site point clouds reveals an average distance of 0.27 and 0.394 ft. for the 2008 and 2009 datasets respectively. This easy method provides a quick estimate of sampling resolution. However it falls short as it does not account for the difference in sampling resolution between the interior angles of the swath (0° to 35°) and the exterior angles of the swath (>35°).

The next method is to use the geometry and equations presented in the previous section to estimate sampling resolution for an across-track profile taken from the survey. This improves upon the previous method as it accounts for the change in beam footprint from nadir to the outer regions of the swath. Idaho Power Company (IPC) generally uses a 90° swath width, 45° to both sides of nadir, when not customizing the swath to specifically capture the banks of a river. Equation 3.2 is used to calculate the beam footprint in a more realistic example of varying depths typical of Wild Sheep Reach and sloping riverbanks. Specifically the nadir beam is measuring the deepest point and the depths decrease with increasing beam angle while the riverbank slope increases with increasing beam angle. The results of this more realistic analysis are presented in Table 3.2.

In Table 3.2 it can be seen that the decreased depth, z = 25, at the 45° beam reduces the beam footprint, which when compared at a uniform depth to lesser beam angles would

Table 3.2. Varying beam footprints calculated with changing slope and depths based on realistic conditions of varying slope in Wild Sheep Reach.

			Footprint (ft.)		
			Across-track	Along-track	Total (ft^2)
Depth	z	35	0.92	0.92	0.84
Beam Angle	β	0			
Slope	ζ	1.5			
Beam Width	ϕ	1.5			
Depth	z	33	0.89	0.89	0.80
Beam Angle	β	15			
Slope	ζ	3			
Beam Width	ϕ	1.5			
Depth	z	30	0.91	0.91	0.82
Beam Angle	β	30			
Slope	ζ	10			
Beam Width	ϕ	1.5			
Depth	z	25	0.93	0.93	0.86
Beam Angle	β	45			
Slope	ζ	45			
Beam Width	ϕ	1.5			

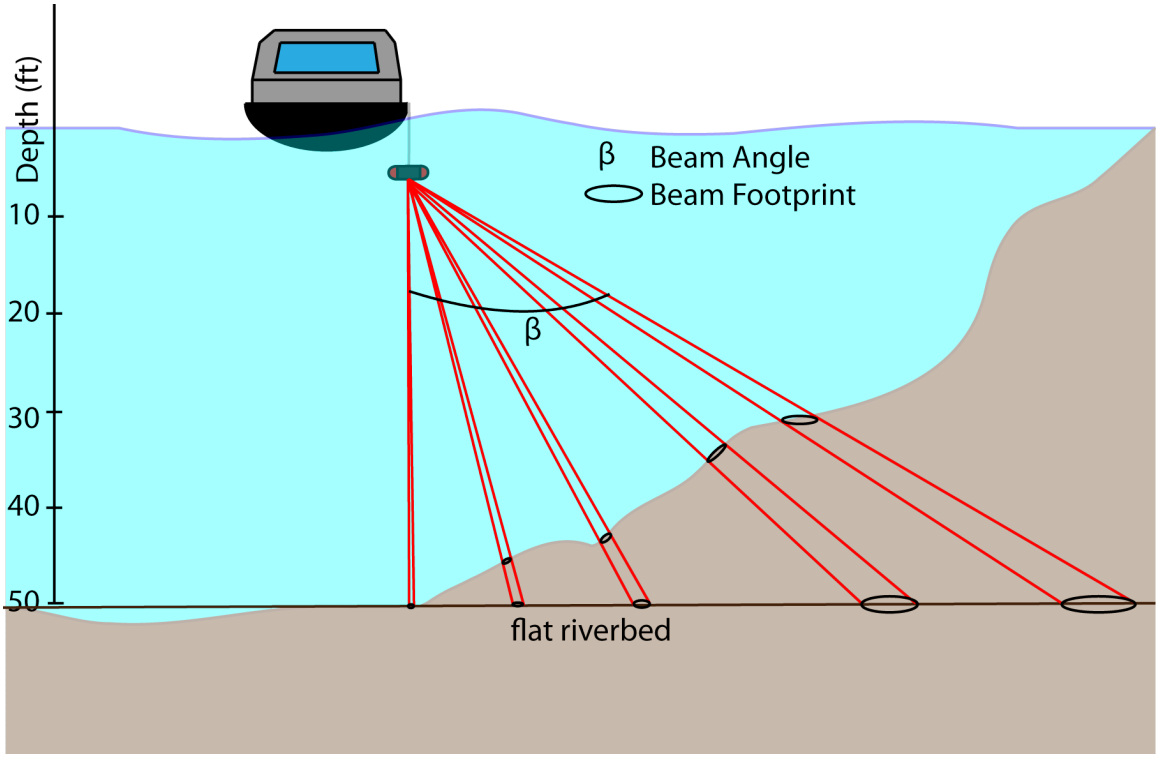

Figure 3.5. Hypothetical example of the expansion of beam footprints in a flat riverbed versus a variable riverbed.

be expected to have a significantly larger beam footprint. With a uniform depth it would be expected that the nadir beam has the smallest footprint; however, because this beam now travels the furthest distance it is subject to more expansion and has a larger footprint than all but the 45° beam angle footprint. Additionally, based on analysis of Equation 3.2 it can be understood that when the beam angle is close to the slope of the riverbed this will reduce the size of the beam footprint. The effect of beam expansion and a flat river bed versus a variable riverbed is presented graphically in Figure 3.5.

The example shown in Table 3.2 details the sampling resolution of one swath pass; however, the survey strategy used in this study made multiple passes of the riverbed to provide overlap. Therefore the true sampling resolution of the survey is higher than what is reported for the one swath pass example. Although it does not account for the difference in beam footprints the first method, using ArcGIS Nearest Neighbor Tool, gives a better

estimation of the true point density for the survey as a whole. For this reason 0.394 ft. (4.7 inches) will be referred to as the point density of the survey throughout this paper and used as the estimation of support when determining the raster resolution of analysis in Section 4.1.1.

Section 4
DEM Construction from MBES Data

4.1 Determining Cell Resolution

The cell resolution of a raster controls the amount of information included in the analysis and defines computation times of calculations. Due to the homogenous nature of raster cell values, features below the resolution cannot be properly represented (Bolstad, 2008). The surveying method is the main factor that regulates raster quality and in turn cell resolution through its control over point quality, point density and point distribution (Heritage and Milan, 2009a).

The sampling resolution and the greater concept of support are important when determining a cell resolution. In this study when accounting for overlapping swaths the 2008 survey had an average sampling resolution of 0.27 ft. and 2009 of 0.394 ft. These measurements represent the absolute minimum cell resolution that is possible without introducing unnecessary interpolation. However, in geomorphic change detection studies the surveyed data is often used to create other raster products, particularly surface roughness rasters, which require more than one point to calculate the surface roughness value for a raster cell. To use the data to its maximum level of support, 0.27 and 0.394 ft., does not allow for statistical calculations involving the z values within a cell. For this reason it is more realistic to expand the cell resolution beyond the maximum level of support to include more points. This concept is expanded upon in Section 5.2.

After analyzing point quality, density and distribution, considerations should be made for the level of accuracy required in the surface model and the size of the study area. It is important to recognize the level of accuracy that is required in a surface model and ultimately the use of the surface model. As cell resolution increases, the total number of cells increases

Table 4.1. Increasing number of cells with increased cell resolution

Cell Resolution(m)	Width(m)	Height(m)	Number of Cells
10	100	100	10000
5	200	200	40000
2.5	400	400	160000
1	1000	1000	1000000
0.5	2000	2000	4000000
0.1	10000	10000	800000000

exponentially. The number of cells in a raster will greatly impact computation times. For example the number of cells in a raster covering an area of 1 km^2 with width and height of 1 km each is presented in Table 4.1. The comparison of computation times and memory demands between cell resolutions is an exponential relationship, similar to the increase in number of cells observed in Table 4.1, which both drastically increase as resolutions become finer. For this reason size of the study area should be considered when determining the cell resolution as this will impact total number of cells which controls memory demands and computation times.

Although it may be attractive to choose the finest resolution this is not always correct. The potential information gained through finer resolutions may be overshadowed by an inability to realistically perform computations and view the data within a GIS. Information loss sensitivity analysis is recognized as a method for aiding in the determination of cell resolution for a study (personal communication Joe Wheaton). Determining a proper cell resolution is an important step in a geomorphic change study as improper cell resolutions have the potential to misrepresent the data and introduce uncertainty into the study (Hare et al., 2011).

4.1.1 Case Study Application - Determining Grid Resolution

In this section two different methods of information sensitivity loss are explored. The

first method uses the mean and standard deviation of a DEM derivative to explore the effect of different cell resolutions. While the second method uses an analysis of variance (ANOVA) to statistically prove differences in the amount of information a DEM derivative is able to present when moving from one resolution to another.

In the first method the mean and standard deviation of a profile curvature raster are plotted against different cell resolutions. Standard deviation is a measure of how much variation there is from the mean and mean is a measure of centrality. Analysis of the how the mean and standard deviation change with grid resolution gives an understanding of information lost or gained at each resolution.

In Figure 4.1 the result of the first method is shown. The changing of slope in the lines represents meaningful information gained or lost as resolution changes. An increase in slope from one grid resolution to the next indicates an increase in information while a leveling out indicates that a threshold has been crossed and little to no information is gained or lost from one resolution to the next. With the high level of support provided by surveys with MBES it is tempting to go with the finest spatial resolution; however, unless custom scripts or software will be used in the analysis of the data (or visualization is not important) the limitations of the software used to process the data need to be kept in mind. For example calculating slope for a 2-ft. resolution of the Wild Sheep Reach took approximately 1 second, while the same calculation for a 6-inch resolution raster took 12 seconds. An 11 second difference for such a basic raster calculation of slope will get exponentially larger with more complex calculations used later in a geomorphic change study.

In Figure 4.1 it is clear that there is little difference in the amount of information gained or lost when moving between grid resolutions from 10 ft. to 4 ft. The first gain is seen at 3 ft. where the slope begins to increase, this increasing slope trend increases until a threshold for the mean value is crossed at the 3 inch cell resolution. As determined in

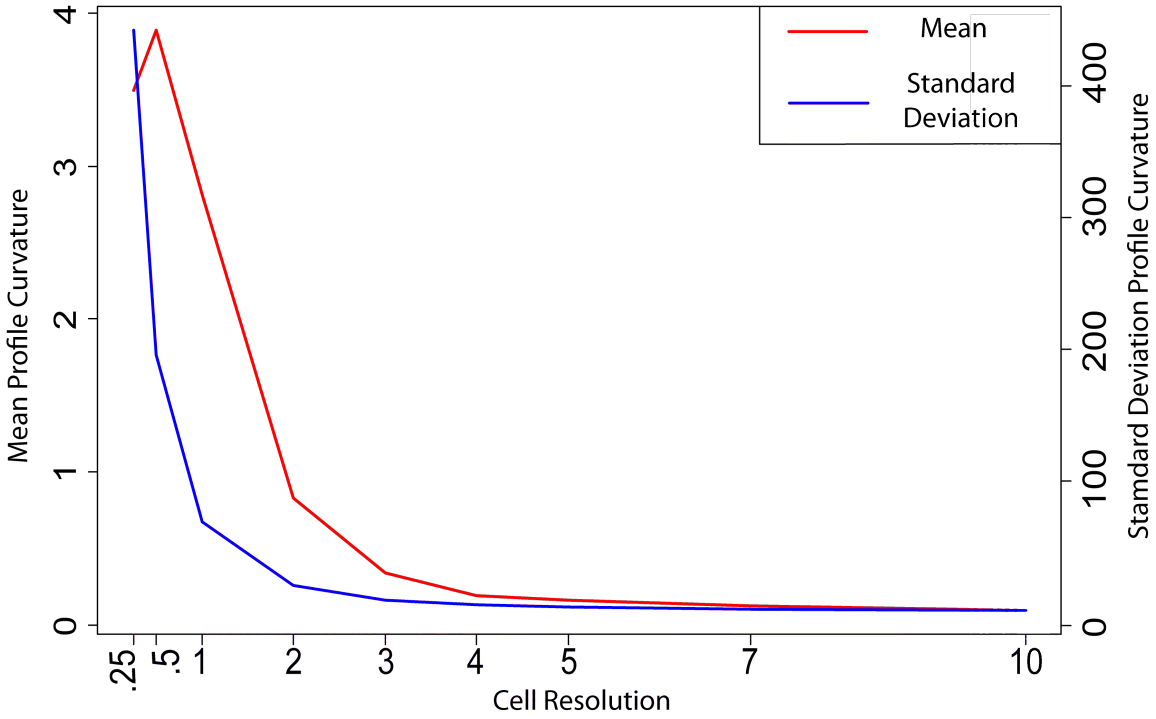

Figure 4.1. Information loss analysis.

the previous section, a cell resolution below 4.7 inches should not be selected as this was the highest level of support observed in both of the surveys. A resolution below this level should not be chosen as it will require more interpolation and does not allow for surface roughness rasters to be calculated.

The second method of determining cell resolution utilizes ANOVA to judge the amount of information gained when moving to finer grid resolutions. This method is more of a quantitative analysis than the method in the previous example. By comparing the mean and variance of curvature raster values between resolution sizes an F-statistic can be computed and a probability to determine if the difference between the two resolutions is statistically significant.

Results of this analysis are presented in Figure 4.2. Analysis of these plots reveal that moving from 3 ft. to 2 ft., 2 ft. to 1 ft., and 1 ft. to 6 inch resolution are all statistically

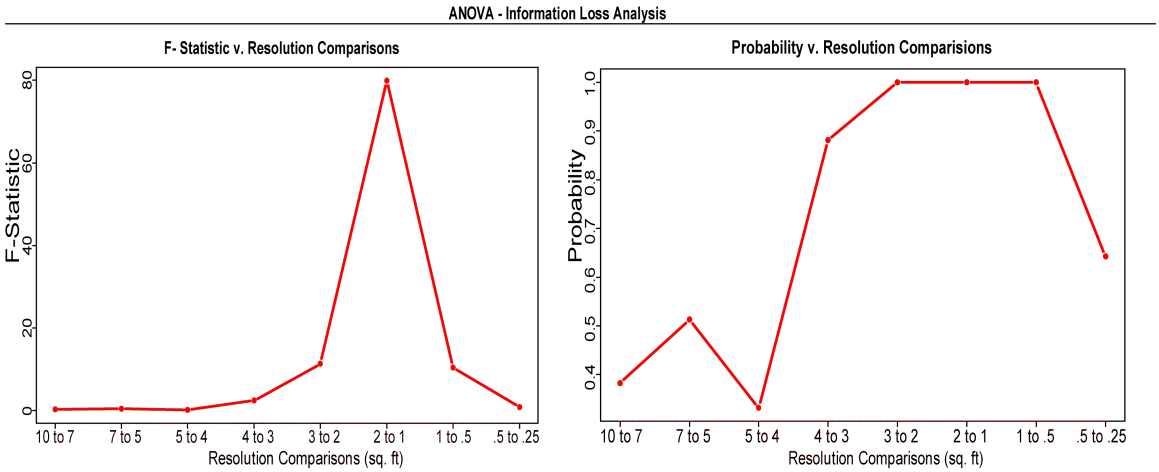

Figure 4.2. Left figure is F-statistic plotted against cell resolution change and right figure is probability plotted against cell resolution change.

significant. The most statistically significant increase between cell resolutions is when moving from 2 ft. to 1 ft. resolution. This analysis also reveals that little information is gained when moving from 6 inch to 3 inch resolution.

Based on these information sensitivity loss analyses the best resolutions are 2 ft., 1 ft., and 6 inches. Considering the large area this study covers and the many computations that will be performed in latter steps of analysis, 2 ft. resolution will be used moving forward in this paper. Although some information is lost by choosing a coarser resolution, much is gained in the ability to quickly perform computations and visualize the data.

4.2 Interpolation Techniques

4.2.1 Overview of Interpolation Techniques

The point collection nature of MBES requires the use of interpolation to create a continuous surface. GIS provides a plethora of interpolation options but unfortunately there is no best interpolation method for all applications. Instead, the best interpolation method depends on characteristics of the variable to be estimated, accuracy requirements of the

user, scale of the study, landscape morphology, quality of samples and sampling densities (Bolstad, 2008).

Data produced from MBES generally have high sampling densities in the depths observed in rivers (>100 ft.), points spaced an average of 0.394 ft. (2009 survey), and relatively high quality, a reported accuracy in the magnitude of inches Dix et al. (2012); Ernstsen et al. (2006); Hazel et al. (2010). Studies have shown that there is little difference observed between interpolation techniques when sampling density is high (Chaplot et al., 2006; Heritage and Milan, 2009a). However certain land morphology, specifically the presence of high surface roughness and large relief, has the potential to affect the accuracy of interpolation techniques (Heritage and Milan, 2009b). Analyzing the difference between the mathematics used, the assumptions, and the characteristics of different interpolation techniques helps to understand how each technique creates a final surface and aids in determining which technique or techniques are ultimately the best for a particular dataset. For an overview of interpolation techniques which have been identified as fit for geomorphic studies refer to Appendix B.

4.2.2 Known Sources of Uncertainty for Interpolation Techniques

Local form roughness has an association with increased error in survey and interpolation techniques (Heritage and Milan, 2009a; McKean et al., 2008). The local surface roughness has an influence on the accuracy of interpolation techniques, with areas of increasing complexity decreasing the effectiveness of interpolation techniques.

Breaks in slope pose a particular problem for interpolators. If the top and base of the break in slope are not each surveyed then the survey has the tendency to misrepresent the break in slope. This is particularly an issue with MBES because of an operatorś inability to choose specific points to survey. If a ping does not coincide with the top and base of the break in slope there is potential to badly misrepresent the surface. This concept is further explored and visually examined in Section 4.2.3.

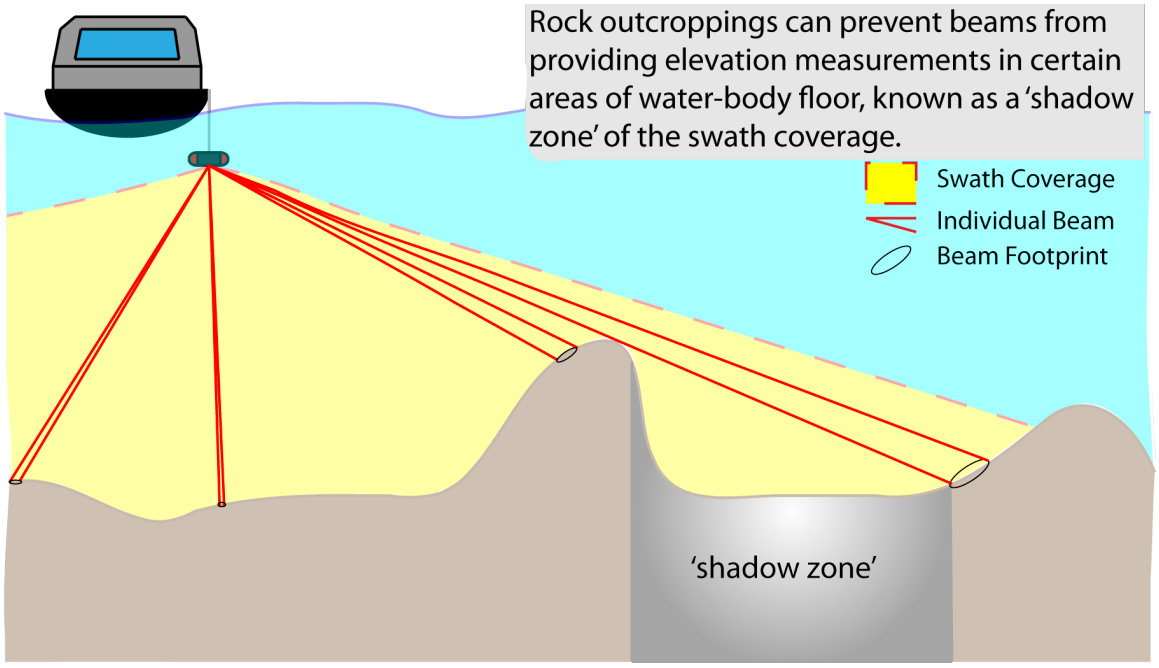

Figure 4.3. Example of the potential for a shadow zone where no data is collected due to the obstruction of a large boulder or rock outcrop and the swath style collection of MBES.

Large boulders and rock outcrops combined with the swath style data collection of MBES present a particular challenge for interpolation techniques. The swath data collection style does not accurately report the elevation of the backside of the boulder, creating a shadow zone where no depth measurement is reported on the side of the boulder further from the MBES. This shadow zone will increase in size with increasing depths, boulder size, and beam angles. This is shown conceptually in Figure 4.3 and an example from the Wild Sheep Reach point clouds is shown in Figure 4.4. This shadow zone has the potential to increase the size of boulders in the final surface created from interpolating from these values.

These examples of surface roughness and its influence on interpolation method are known as errors of generalization or inclusion. The homogenous nature of raster cell data and the determination of cell resolution dictate the level of detail that can be deciphered by a raster dataset (Bolstad, 2008). When a potential raster cell area has a large range in values the interpolation technique will tend to smooth these surfaces or not include the

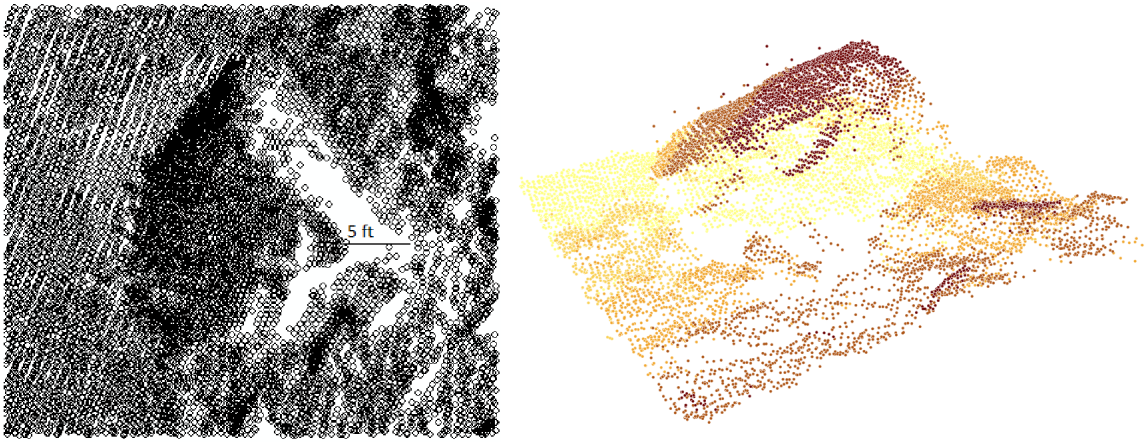

Figure 4.4. 2D and 3D visualization in GIS of the same point cloud collected in an area where a large rock is present. The 5 ft. gap is an example of a rock shadow and is on the side facing away from the MBES.

influence of large variations occurring over small scales. Specific examples of boulders and breaks in slope from the Wild Sheep Reach data are presented and explored in the next section.

4.2.3 Case Study Application - Interpolation Techniques

To further the exploration of interpolation techniques a study was performed to compare and contrast the different techniques: inverse distance weighting (IDW), multiquadratic radial basis function (MRBF), regularized spline with tension (RST), ordinary kriging (OK) and universal kriging (UK). Due to the large size of the study site a subset of data was taken from the Wild Sheep Reach. The northern most section of the river was selected as it is fairly representative of the entire reach with median roughness and slope values comparable to the entire reach and isolated areas of topographic complexity showing roughness of greater than 7 ft. and slope values greater than 70° (refer to Table E.1 in Appendix E). It is an area of about 0.01 mi^2 and is represented by a point cloud of 1,342,794 points. The point cloud was divided in half with one half being used as the training set to interpolate a surface from while the other half, the test set, was used to compare the interpolated values. The difference between the interpolated values at the test set locations is a measure of interpolation error.

Table 4.2. Comparison of the results of interpolation study for inverse distance weighting (IDW), multiquadratic radial basis function (MRBF), ordinary kriging (OK), regularized spline with tension (RST), and universal kriging (UK).

	Interpolation Techniques				
	IDW	**MRBF**	**OK**	**RST**	**UK**
RMSE	0.854	0.888	0.794	0.8083	0.8174
ME	0.0080	0.0002	-0.0001	0.0039	0.0075
Max	18.2585	18.1333	18.1565	18.3166	18.4449
Min	-14.3180	-16.0035	-13.4400	-13.4400	-13.4400
Percent Large Error	0.0489	0.0486	0.0495	0.0492	0.0498
Percent Positive Error	0.5086	0.4984	0.5028	0.5115	0.5158
Percent Positive when High Error	0.5134	0.5071	0.507	0.5106	0.5123

To assess precision root mean square error (RMSE) and mean error (ME) were calculated for each interpolation method. The results of this analysis are presented in Table 4.2.

All techniques performed quite well with all methods reporting a mean error below one inch. This is exceptional as on average the interpolation methods are not introducing error into the study. However, there are particular areas where interpolation overestimated by as much as 18 ft. and underestimated by as much as 16 ft.; this generally occurred where abrupt breaks in slope occur (an example of a feature causing these large errors is shown in row 2 of Figure 4.5). This is concerning because accuracy is paramount in a geomorphic change detection study. Although errors this high are isolated they have the potential to influence the overall volumetric sediment change reported by a study. An error of 18 ft. in a 2 x 2 cell represents a volume of 72 ft^3 of sediment.

Moran's I statistic was computed for the error of each interpolation technique to determine if spatial autocorrelation exists between interpolation error. Moranś I statistic was virtually the same value of 0.40 for all interpolation methods. This indicates that statistically significant clustering exists in errors of all interpolation methods. The clustering of

interpolation errors makes them easier to identify and account for than if they were completely random. Three examples of features where clusters of interpolation error occurred are presented in Figure 4.5.

Considering the normal distribution of the interpolation errors observed with all interpolation methods, the mean and standard deviation were used to establish large change that is outside of the normal distribution. To do this two times the standard deviations of error were added and subtracted from the mean error, $\mu \pm 2\ \sigma$. The location of the points outside of this range were analyzed and subsequently used to identify landforms causing the clusters of high interpolation error.

This exercise revealed that across all interpolation techniques about 5% of all errors are greater than 2 standard deviations from the mean. Analysis of row 7 in Table 4.2 reveals that of the errors existing in this upper 5% essentially 50% were underestimation and 50% were overestimation of the surveyed elevations; this suggests a normal distribution of interpolation error. Areas containing clusters of high interpolation errors as designated from the above exercise were examined in more detail to reveal the landforms creating these errors. These areas tended to contain landforms displaying abrupt change in elevation; either a rock outcropping, boulder, break in slope, shelf or shear wall. Examples of these features in relation to elevation, slope and surface roughness are examined in Figure 4.5, along with the profile and histogram of elevation values of the landforms.

Due to the high point density of MBES all interpolation techniques performed very well. The high point density led to virtually the same errors even in areas of extreme surface roughness. The choice of interpolation technique is more a choice of how many inputs the user is comfortable having control over. If simplicity and ease of use is valued then IDW is a good option but if more control over inputs is desired as well as statistical output with the surface then one of the kriging methods would be preferred.

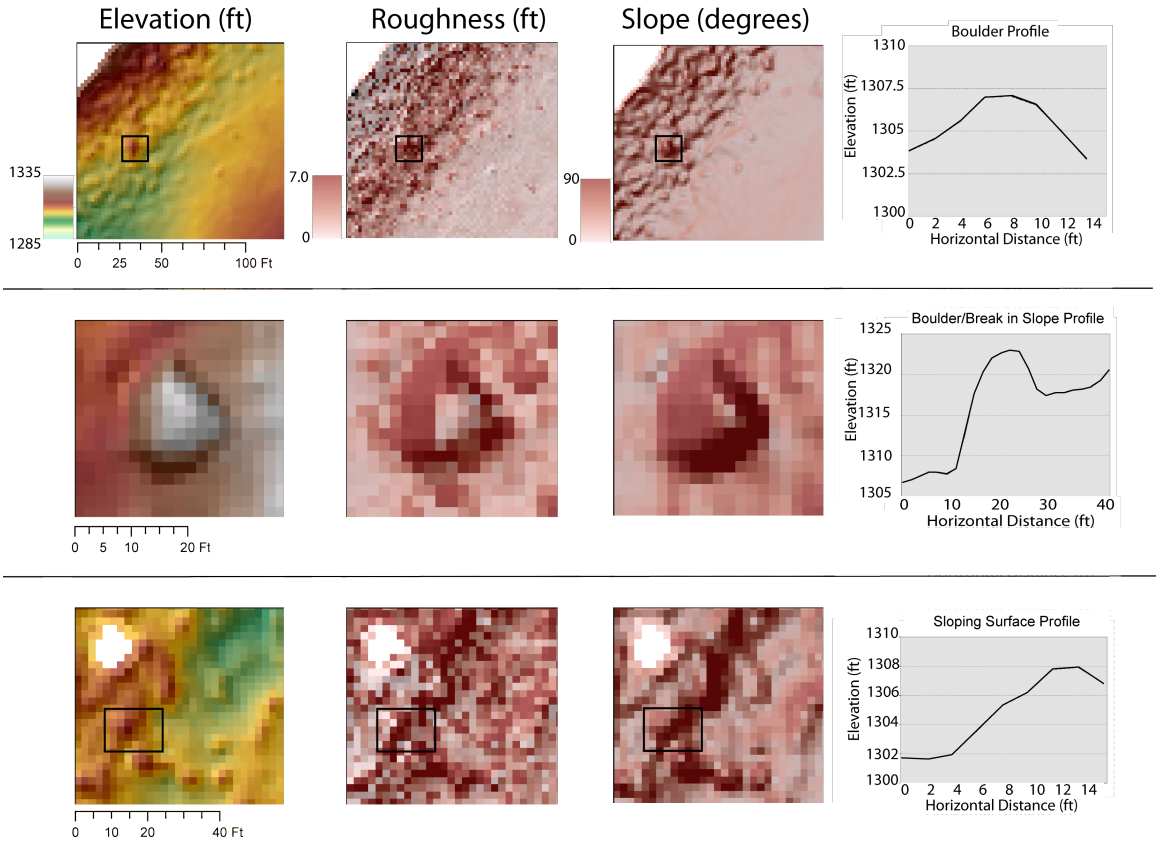

Figure 4.5. Example of areas that contained large amounts of interpolation error.

Errors due to interpolation are an unavoidable relic that occur because of the need to convert data to raster format in order to perform calculations. It is important to recognize and quantify interpolation error, particularly large interpolation error. A method for quantifying this error and adding it as a term to the total calculated propagated uncertainty for each raster cell is presented in Section 5.2 - Quantifying Surface Uncertainty from MBES.

Section 5

Uncertainty Estimation for DEM from MBES Data

5.1 Contributions to Surface Uncertainty Using MBES

The performance of MBES has been tested to provide horizontal and vertical accuracies of 0.02 and 0.03 m respectively (Dix et al., 2012). This is on par with the accuracies reported for TLS. Applied studies covering a wider area and more diverse landscape have reported horizontal and vertical accuracies of 0.10 m (Ernstsen et al., 2006; Hazel et al., 2010). Uncertainty and accuracy in surveying is not entirely random and has a spatial component. This is because in practice swath type collection style, surface roughness, slope, the inability to test for absolute accuracy and movement of the vessel can limit the performance test reported accuracy (Hare et al., 1995; International-Hydrographic-Bureau, 2005; Milan et al., 2011; Wheaton et al., 2010).

The non-uniform beam footprints of MBES have the potential to introduce uncertainty into the accuracy of a depth measurement when a beam has a large footprint. This is due to a single value being reported for each beam. When a beam has a large footprint over an area with high surface roughness or high slope the return depth measurement for this area will fail to represent the diversity of depth measurements existing within the footprint area. Generally the shortest path echo, highest elevation value will be reported for the depth of a beam footprint.

Further out in the swath angle or at increased depths the size of the beam footprint increases and consequently the point density of MBES surveys decreases (Diaz, 2000; International-Hydrographic-Bureau, 2005). The reduction in point densities can be quite drastic, for example in Section 3.1 it was shown that at a depth of 30 ft. the differences

between beam footprints in the across-track direction between the nadir beam and the outermost beam can be as much as ten feet. Additionally, if the across-track beam footprint of the maximum beam angle of the RESON Seabat (75°) is compared between 10 and 50 ft. of depth the difference can be as much as 15 ft. This potential lack of point density puts more reliance on a single point to report the value for a potentially large area.

The amount of surface roughness has a direct influence on the ability of the MBES to collect the minimum depth in the beam footprint region (de Jong et al., 2002; Hare et al., 1995). Figure 5.1 depicts this phenomenon in the across-track dimension. The depth measurement returned to the MBES is the shortest path, the point z_1 from both examples in Figure 5.1. The potential uncertainty in the final derived surfaces will increase with increasing surface roughness and increasing beam footprint.

The slope of a surface influences the MBES ability to accurately collect depth measurements (de Jong et al., 2002; International-Hydrographic-Bureau, 2005). This is a function of the beam footprint and slope of the surface. This phenomenon is shown in Figure 5.1. Similar to uncertainty due to surface roughness, surface uncertainty in the final derived surfaces due to slope will increase with an increasing beam footprint.

The nature of surveying sub-aqueous environments makes testing for absolute accuracy difficult. Overlap in surveying lines resulting in the same point being surveyed twice and surveying unchanging surfaces can be used as methods to test measurement accuracy (Hazel et al., 2010). However these methods may fall short of traditional stationary land based methods of ground truthing control points. The result is that often times measured points are not verified against an absolute control system (Dix et al., 2012).

Movement of the vessel has the potential to introduce uncertainty into measurements

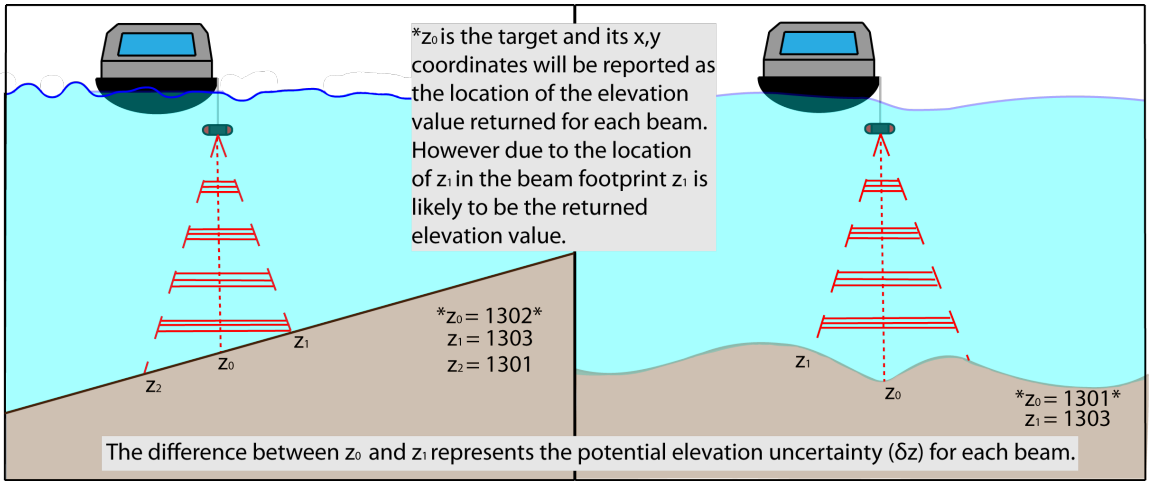

Figure 5.1. Depiction of how surface roughness and slope contribute to uncertainty in depth measurements. Surveying in the presence of slope is on the left and in the presence of surface roughness is on the right.

despite the presence of technology and mathematical formulas to account for them in real-time (de Jong et al., 2002; International-Hydrographic-Bureau, 2005). Although the depth measurements from MBES are accurate in the magnitude of inches, this accuracy is dependent upon the performance of the additional sensors which track vessel motion such as the heave-roll-pitch (HRP) sensor or vertical reference unit (VRU), the gyrocompass and the sound velocity profiler (SVP) (Hare et al., 1995). Roll, pitch, yaw, heave, sway and surge are all types of motion associated with a moving vessel. Heading is also essential and is a measurement of the exact orientation of the vessel. All of these variables must be accurately measured during an MBBS to produce reliable results.

Roll, pitch, and yaw are ways to describe the rotation of a boat around the lateral, longitudinal, and vertical axis respectively. Roll is the side to side rotation of a vessel, pitch is the rotation from front to back, and yaw is the rotation of the boat around its vertical axis. While heave, surge, and sway are linear motions along the same axes. Heave is the up and down motion of the boat, sway is the side to side movement, and surge is front to back movement (Hare et al., 2011).

These measurements of rotation and linear motion are collected by a motion sensor unit, HRP or VRU, at set time intervals. It is essential that all measurements are collected at a consistent timing and calibration of the motion sensor is performed before a survey.

Vessel motion detectors allow for near complete positional uncertainty budgets to be created (Hare et al., 1995). In a report by David Evans & Associates (DEA) an uncertainty budget of vessel motion for the 2008 and 2009 surveys was undertaken to compute the total propagated uncertainties (TPU) from positional influences. Utilizing the methodology from Hare et al 1995, the uncertainty budget mathematically takes into account the effect of vessel motion sensors along with their uncertainties and reports a positional and depth accuracy uncertainty estimate for each sounding (Hocker, 2012). The DEA report analyzed the contributing uncertainties of navigation, pitch, roll, yaw, heave, and sound velocity sensors. The results indicate that on average the horizontal and vertical accuracies for surveyed points are between 0.10 and 0.20 m for both the 2008 and 2009 surveys. In some areas uncertainty was higher than this amount and loss of satellite signals due to blocking of satellite signals near the shoreline of steep canyon walls was determined to generally be the cause.

The mathematical calculations used to compute the TPU are beyond the scope of this paper; however, analyzing the horizontal and vertical uncertainty and their relationship to beam angle is helpful in illuminating how the swath data collection nature of MBES influences survey uncertainty. Analysis of the findings from the TPU report from DEA revealed a strong relationship between beam angle and horizontal accuracy. Beam angles greater than 30° from nadir had statistically significant higher horizontal inaccuracies than beam angles lower than 30° from nadir. This phenomenon is reported in Figure 5.2. Although beam angles greater than 30° from nadir had an effect on vertical accuracy it had much less of an effect which may suggest that other factors such as surface roughness have a stronger effect on vertical accuracy.

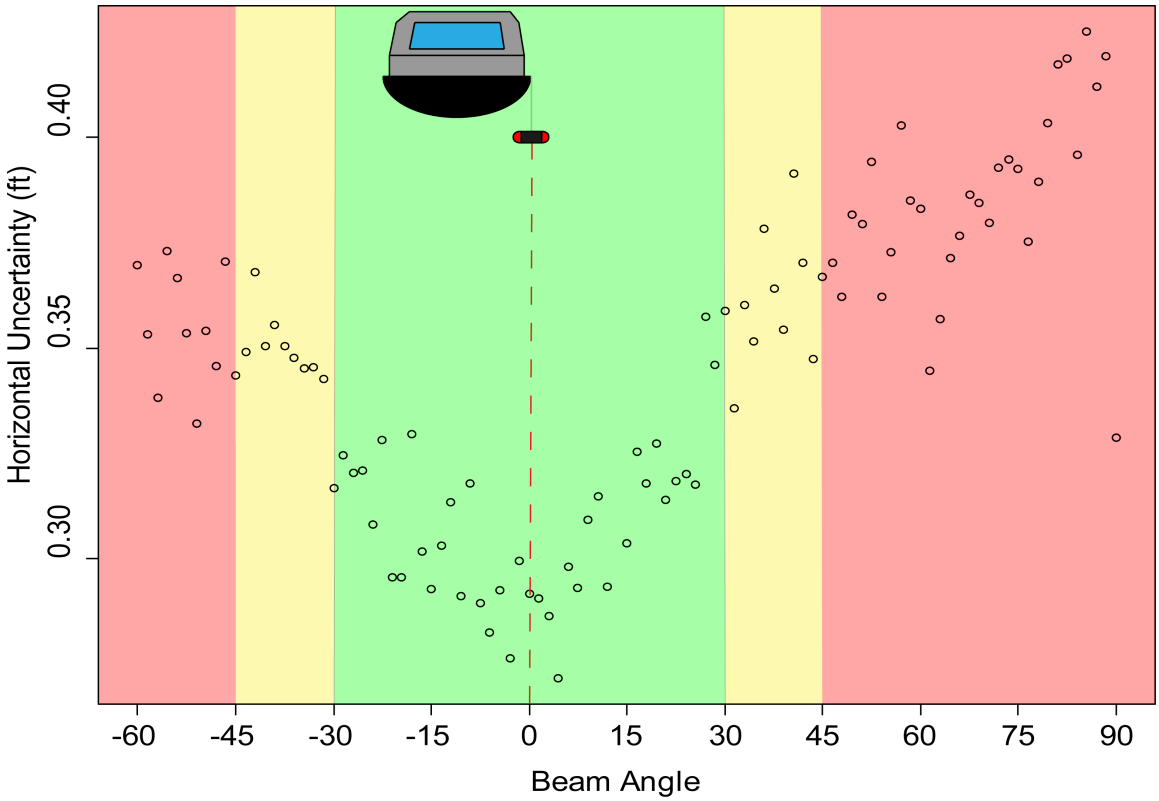

Figure 5.2. Beam angle (x-axis) is plotted against horizontal uncertainty (y-axis) reported in the Total Propagated Uncertainties (TPU) report from David Evans & Associates (DEA). There is a clear pattern of decreasing horizontal accuracy the further from nadir a beam angle is. The colored regions distinguish different groupings of accuracy.

To account for these surface uncertainties, rasters quantifying surface roughness, slope, and positional accuracies due to vessel motion can be developed and used as input to an uncertainty model to better quantify the surface uncertainty produced from MBES.

5.2 Quantifying Surface Uncertainty from MBES

In Section 6.2.2 the use of an uncertainty model to quantify the surface uncertainty in elevation values of surfaces derived from a MBES survey is introduced. To implement this uncertainty model it is necessary to have representations of the main contributors to surface uncertainties when using an MBES. This section covers how to compute the representations of surface roughness, slope, and interpolation error.

The standard deviation and the locally detrended standard deviation of a surface are metrics of surface roughness (Heritage and Milan, 2009b; Rychkov et al., 2012). Surface roughness can be computed in a number of different ways. A common method is the use of neighborhood and block statistic operations to compute cell by cell standard deviation of a surface. An emerging method is the classification of acoustic backscatter into sediment classes. These operations can be carried out with standard tools provided by many popular GIS.

Using neighborhood or block statistics to calculate the standard deviation on a cell by cell basis is a straightforward method that requires few user inputs. They are generally applied on a 3 x 3 or 5 x 5 cell window of the DEM and produce relatively reliable results. However these methods fall short on a sloping surface as standard deviation may be overestimated due to differences in elevation values because of the slope and not surface roughness. To avoid this inaccuracy it is necessary to locally detrend the surface of the influence of slope.

Locally detrending a surface before taking the standard deviation ensures that only

local variations in height are being modeled. On a cell by cell basis this operation is computationally expensive and is not a standard tool in popular GIS. Work done by Rychkov et al led to the creation of a software package called PcTools that efficiently applies a thinning algorithm on a cell by cell basis. Point cloud thinning or binning is common practice when using MBES and TLS data to reduce the computation times and memory requirements of their large point clouds (Kearns and Breman, 2010). Point thinning is the process of setting a defined grid size and using the point values that are contained within those grids to calculate a representative value for each grid cell. PcTools uses the point values contained within the defined grid size to calculate the minimum, maximum, mean, detrended mean, range, standard deviation, detrended standard deviation, skew, detrended skew, kurtosis, detrended kurtosis, and point density. A minimum number of points is necessary, generally four, to calculate the detrended standard deviation. The necessity to have more than one point within the cell resolution of analysis is in support of many of the concepts presented in Section 4.1. Having these statistics in a regularly spaced grid is invaluable for developing a detrended standard deviation raster to represent surface roughness.

Similar to the classifying of remote sensing imagery, patterns observed in acoustic backscatter can be associated with specific sediment types. By using training cells that represent specific values for different sediment types an automated classification can be performed in popular GIS software. The resulting surface can be used as a proxy for surface roughness. Monitoring acoustic backscatter was not implemented by IPC for the surveys used in this study; however, it is an emerging use of MBES and brief overview of acoustic backscatter is contained in Appendix A.2.

In Section 5.1 slope was also identified as having a relationship with surface uncertainty. The calculation of slope is a straight forward process in popular GIS software. The slope is calculated for each cell using a moving window. The slope value for each cell is calculated when it is the center of the moving window. This measurement gives an estimate

of slope; however, it is important to note that these calculations represent the steepest slope for the cell and do not give a measurement of the direction of slope. This is important to consider because depending on if the slope is facing the SONAR head or facing in an opposite direction, this will have an effect on how much the slope influences the size of the beam footprint. Slope should be calculated in degrees as opposed to percent rise. When calculated in degrees slopes can be compared between different study sites as opposed to percent rise which is relative to the data it is being calculated for.

As was presented in Section 4.2.3 interpolation can misrepresent areas of abrupt elevation change such as boulders and breaks in slope. To quantify this error a workflow, shown in Figure 5.3, in which half of the points in the original point cloud are withheld and the remaining points are used to interpolate a DEM. The points withheld are then compared to the interpolated value at their location. This step is then repeated by using the initially withheld points to interpolate a new DEM. As before, the withheld points are then compared to the values of this DEM and at their respective locations. The difference in values is a measure of interpolation error and these values are then used to create a raster surface. The resulting raster surface provides actual uncertainty values as it calculates the difference between actual surveyed values and interpolated points. This raster surface also serves as a proxy for point density as areas with few points will be represented by areas of high error in the interpolation surface because of the lack of points to compute a reliable DEM surface.

5.3 Case Study Application - Calculating Surface Uncertainty in MBES

Survey overlap from separate SONAR passes during the same survey creates situations where soundings have struck the exact same spot, as is depicted in Figure 5.4. Sites where this occurs create the opportunity to compare the elevation measurements between the points to get an estimation of the vertical accuracy of measurements. To acquire this information an algorithm was designed to cycle through the original point clouds and extract only the points that have multiple measurements. Points were considered to be matching

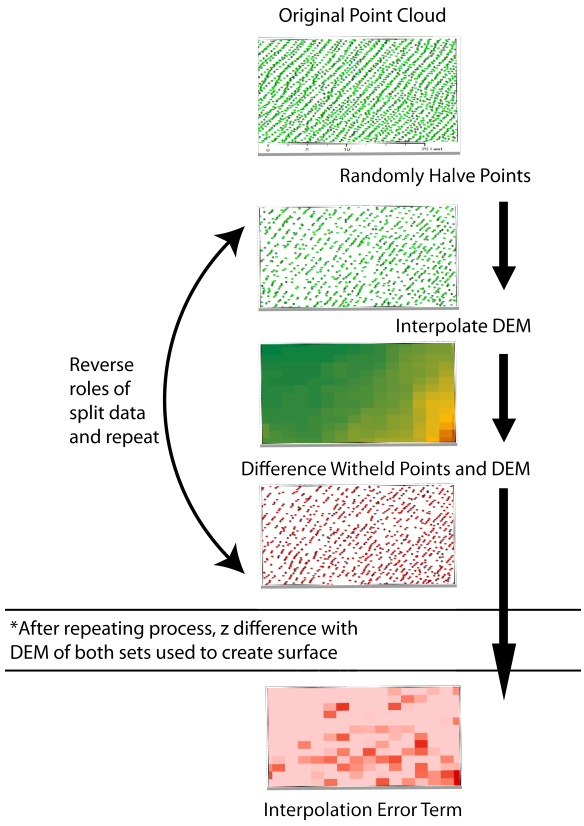

Figure 5.3. Creation of interpolation error term. In figure, DEM is a digital elevation model.

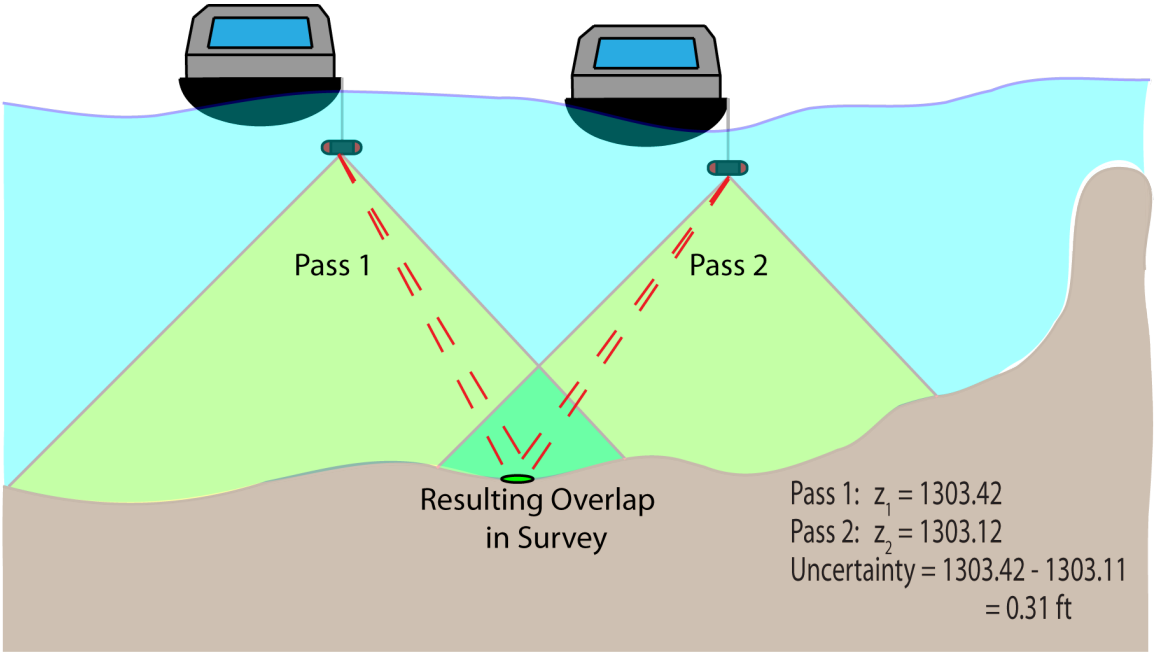

Figure 5.4. The survey collection strategy of many multi-beam echo sounder (MBES) surveys involves making multiple passes which provide overlap in the survey. When the swaths of these passes overlap they create situations when different beams provide elevation measurements for the exact same point. Differencing these elevations provides a method for estimating uncertainty.

only if they had the exact same x and y coordinates as measured by the Reson SEABAT 8101 which returns coordinates to hundredths of a foot. Through this process a sample of 19,049 points was collected at coinciding points.

The basic summary statistics and distribution of this sample are presented in Figure 5.5. The mean is approximately 7 inches with a standard deviation of 18 inches; however, this sample is highly skewed towards small measurement uncertainties and the median of approximately 2.4 inches is a better measure of centrality.

To gain a greater understanding of how the contributions to surface uncertainty presented in Section 5.1 relate to this estimation, scatter plots of measurement uncertainty explained by surface roughness and slope were created. These are presented in Figures 5.6 and 5.7.

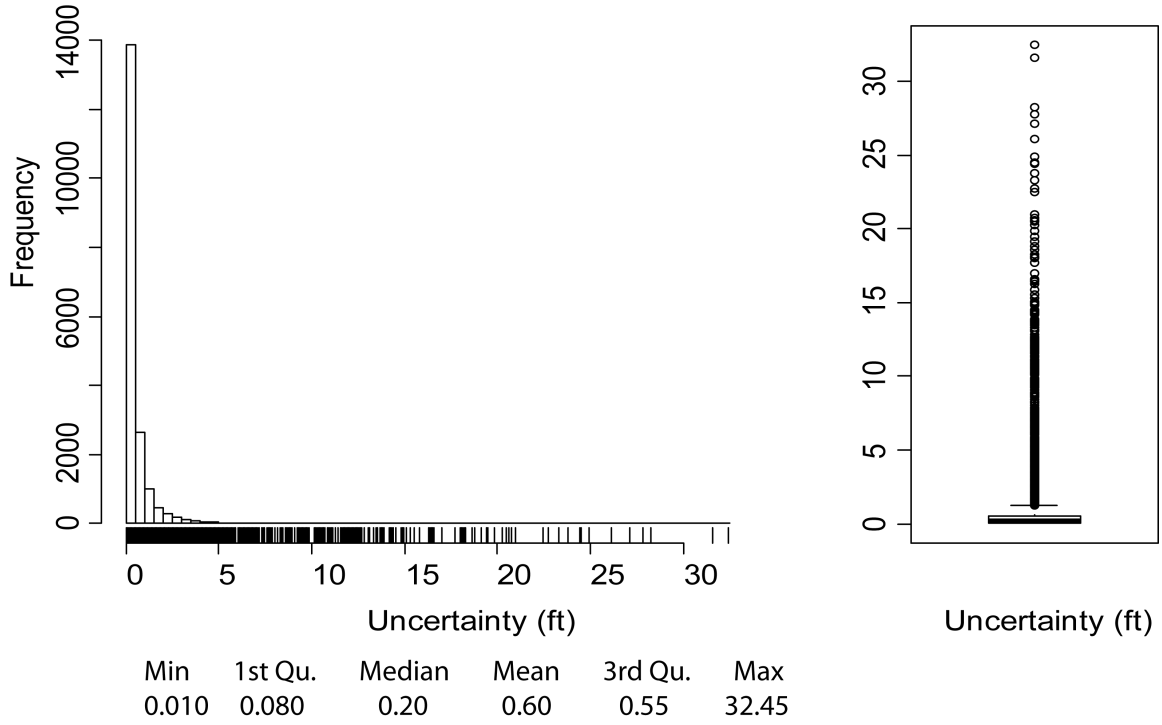

Figure 5.5. Exploration of the distribution of measurement uncertainty across Wild Sheep Reach.

Analysis of the Figures 5.6 and 5.7 reveal that both surface roughness and slope have a high statistical probability that an increase in either of these values will increase measurement uncertainty. However the 'megaphone' pattern seen in these figures shows that high measurement uncertainty is not always the case when high surface roughness and slope occur. While these situations increase the possibility for higher measurement uncertainty, accurate measurements are possible when high surface roughness and slope occur.

To identify a potential for spatial bias and analyze regions with differing spatial characteristics, Wild Sheep Reach was divided into nine sub-reaches each of approximately 1,000 ft. in length and the same analysis described above was performed on each sub-reach. A summary of the difference in surface roughness and slope for each of the sub-reaches can be seen in Table E.1 in Appendix E. Analysis of the sub-reaches revealed that the effect of slope and surface roughness on measurement uncertainty was statistically significant across all

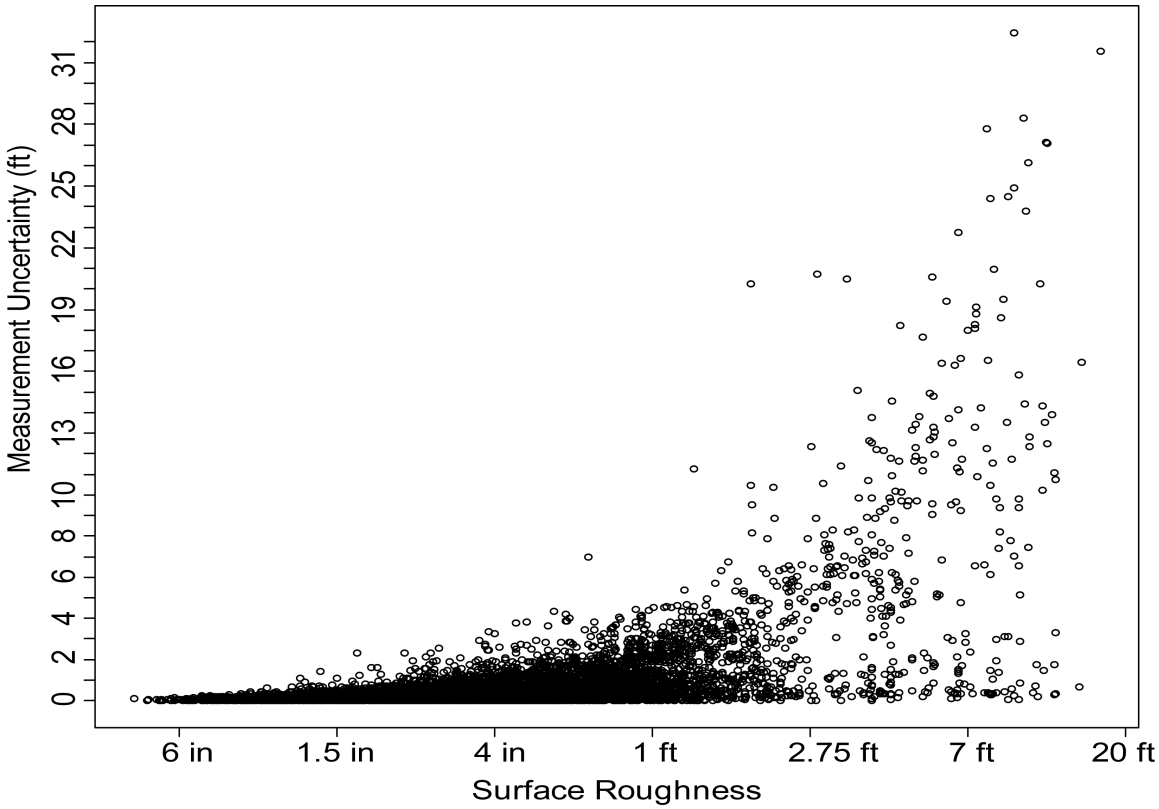

Figure 5.6. Measurement uncertainty described by surface roughness. Surface Rrughness is plotted on a natural log scale; however the labels are converted to relevant values. The relationship is statistically significant with a F-Statistic of 9899.97 at 10717 degrees of freedom.

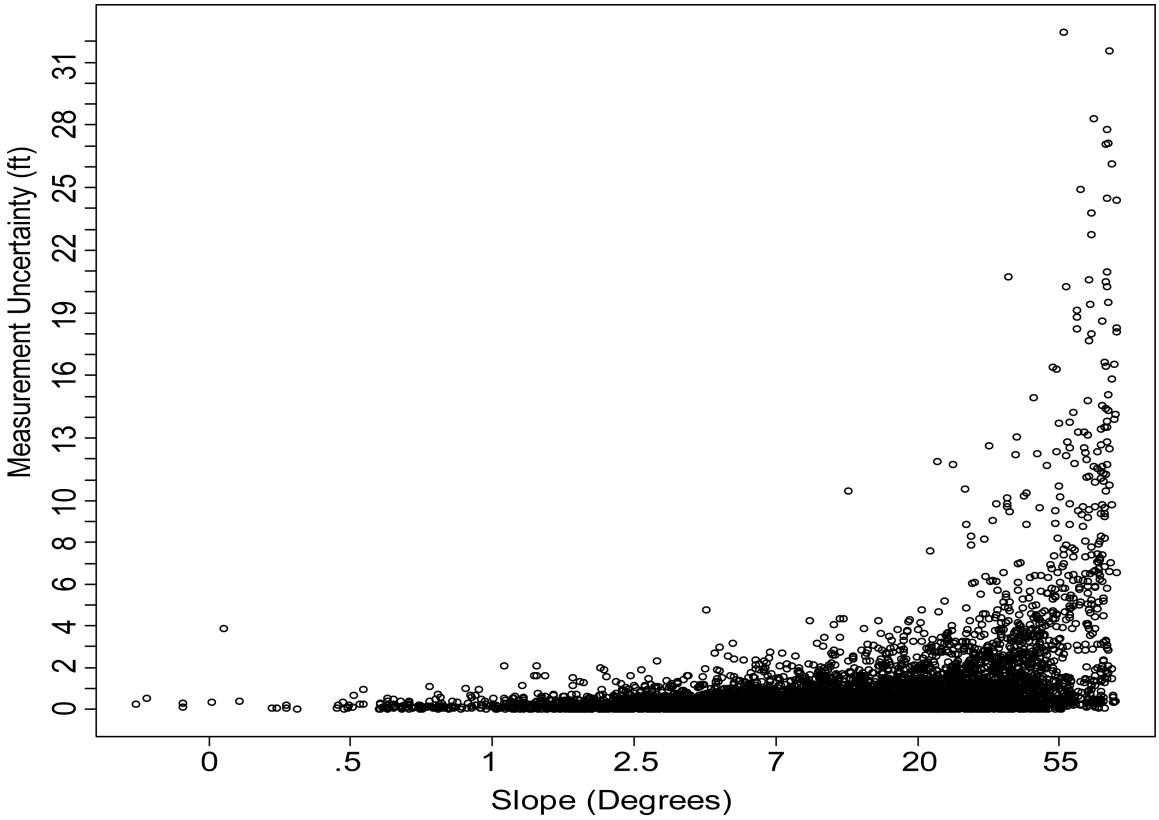

Figure 5.7. Measurement uncertainty described by slope. Slope is plotted on a natural log scale; however, the labels are converted to relevant values. The relationship is statistically significant with a F-Statistic of 4143.9 at 10757 degrees of freedom.

sub-reaches during both 2008 and 2009. In addition the scatter plots displayed essentially the same pattern of increased measurement uncertainty with increased values of slope or surface roughness. These results are presented in Table E.2 in Appendix E.

Statistical studies such as those presented in this section that have large degrees of freedom due to large samples (over 18,000 points) have a much greater likelihood of being statistically significant (Laan et al., 2010). To remove this tendency as well as the potential for a spatial influence, 100 points were randomly selected from the entire data set and the same statistical analysis was performed. This was performed iteratively 100 times to establish the true statistical significance of the influence of each parameter on measurement error. This analysis revealed that surface roughness was statistically significant above a 95% significance across all 100 tests, while slope was statistically significant above 95% significance in 97 out of 100 tests.

To further quantify the effect of surface roughness and slope on measurement error, surface roughness and slope were classified into three groups of low, medium and high values derived from the boxplot of each parameter, a non-parametric metric of distribution. To do this the boxplot was used to divide the data at understandable breaks that can be applied to other data sets and potentially other data types. The low class was designated as values less than or equal to the media; medium was greater than the median but less than or equal to the upper whisker of the boxplot; and high was classified as greater than the upper whisker of the boxplot. An ANOVA analysis assuming unequal variances was run on these groupings to determine if there was a difference in effect on the variance and mean of the measurement uncertainty values between groups. This analysis reveals there is a statistically significant difference in the mean and variance in the measurement uncertainty values based on slope and surface roughness groups. The statistical significance and graphical representation of this analysis is presented in Figure 5.8.

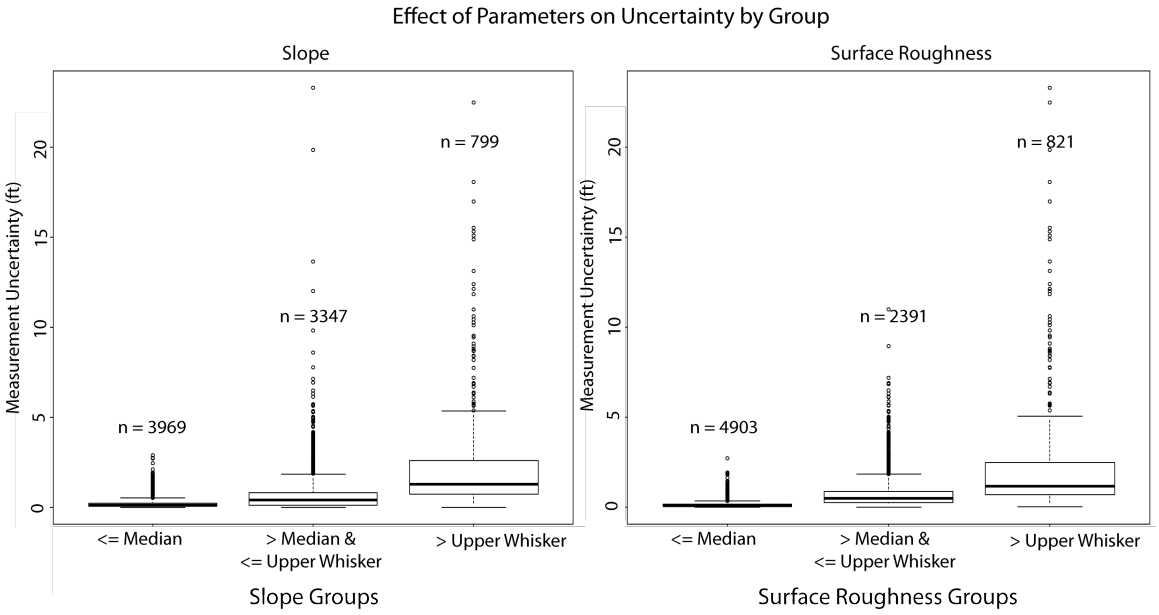

Figure 5.8. Measurement error by grouping of low, medium and high of both slope and surface roughness. ANOVA analysis of surface roughness groups resulted in a F-statistic of 1009 on 789 degrees of freedom while the same analysis of the slope groups resulted in a F-statistic of 435 on 930 degrees of freedom.

The findings of these analyses will be used in subsequent sections when quantifying the influence of surface roughness and slope on actual amounts of vertical uncertainty. This analysis reveals that the magnitude of effect that surface roughness has on uncertainty is slightly greater than slope. This is demonstrated in Tables 5.1 and 5.2 by the larger median uncertainty in the medium (0.53 ft.) and high (1.27 ft.) classes of the roughness when compared to the median of the medium (0.31 ft.) and high (1.08 ft.) classes of slope. This can also be seen in Figures 5.6 and 5.7 where in relation to the distribution of values an increased effect on uncertainty is seen sooner in surface roughness than slope. In addition the statistical significance of the influence of surface roughness on uncertainty, F-Statistic of 9899.97, is greater than that of slope, F-Statistic of 4143.9, indicating an effect of greater magnitude from surface roughness. In addition slope had a statistically significant effect in 97 of 100 random sample tests in comparison to surface roughness being significant across all 100 random sample tests.

Table 5.1. Summary of the surface roughness groups of low, medium, and high, and their effect on uncertainty. The areas labeled uncertainty are the specific values of uncertainty from each boxplot from Figure 5.8.

Influence of Roughness Class on Uncertainty							
			Uncertainty (ft.)				
Parameter Class	Observations	Outliers	Min	1^{st} Quartile	Median	3^{rd} Quartile	Max
Low	4903	413	0.01	0.05	0.11	0.21	0.44
Medium	2391	98	0.01	0.29	0.53	0.85	1.69
High	821	65	0.01	0.74	1.27	2.44	4.96

Table 5.2. Summary of the slope groups low, medium, and high, and their effect on uncertainty. The areas labeled uncertainty are the specific values of uncertainty from each boxplot from Figure 5.8.

Influence of Slope Class on Uncertainty							
			Uncertainty (ft.)				
Parameter Class	Observations	Outliers	Min	1^{st} Quartile	Median	3^{rd} Quartile	Max
Low	3969	369	0.01	0.06	0.12	0.26	0.56
Medium	3347	219	0.01	0.10	0.31	0.68	1.55
High	799	77	0.01	0.67	1.08	2.02	4.01

Section 6
Geomorphic Change Detection with Repeat MBES

6.1 Traditional Bathymetric Differencing

In the simplest form of geomorphic change detection all that is needed is to subtract a DEM from a DEM created from a recent survey. The resulting positives are deposition and the negatives are erosion. However, this does not take into account the vertical uncertainties that exist within the surveying methods and are subsequently passed onto the DEM. To account for the vertical uncertainties of surveying methods it is common practice to establish a threshold or minimum level of detection. The threshold is set at the known vertical inaccuracy of the surveying equipment. In a study performed by the U.S. Geological Survey (USGS) using MBES on the Colorado River vertical inaccuracies of MBES were reported as 0.10 meters (Hazel et al., 2010). Using this number as a threshold any result in the differenced surface that is 20 cm or less (combining the uncertainty of both surveys) would not be included in the final analysis as this change could be due to surveying inaccuracies.

This technique, while conservative, is certainly valid. However, many researchers support the concept that uncertainty is spatially dependent and not random (Milan et al., 2011; Wheaton, 2008; Wheaton et al., 2010). Spatial attributes previously identified such as surface roughness, beam angle and slope contribute to how a survey technique will perform. To apply the same uncertainty term across the DEM does not incorporate this concept and thus falls short at quantifying uncertainty. This has potential to influence the final volumetric totals of erosion and deposition as there is potential to discard real change because it is below the minimum level of detection.

6.2 Emerging Concepts in Bathymetric Differencing

6.2.1 Moving from a Minimum Level of Detection to Probability Theory

There are a number of concepts that need to be adopted in order to move away from the minimum level of detection of geomorphic change. The first is the application of probabilistic statistical confidence to geomorphic change. Rather than discarding potential change entirely because it is below a minimum level of detection, a measure of statistical confidence is applied to geomorphic change. To accomplish this first a measurement of uncertainty, δz, must be calculated for each DEM involved in the calculation.

Many different methods have been proposed for estimating the vertical uncertainty, δz, of an elevation estimation. The simplest method is applying the factory reported vertical inaccuracy of a surveying method. Other methods applicable to MBES include repeat surveys of unchanging surfaces (fiduciary surfaces), complete uncertainty budgets, bootstrapping experiments and differencing points surveyed multiple times in the same survey as in Section 5.3 (Wheaton et al., 2010).

Once an uncertainty term has been computed for each DEM it be combined into a propagated uncertainty term to be applied to the DEM of difference (DoD) through the equation:

$$\delta \upsilon = \sqrt{(\delta z_{new})^2 + (\delta z_{old})^2} \tag{6.1}$$

where $\delta \upsilon_{DoD}$ is the propagated uncertainty in the DEM of difference (DoD), δz_{new} is the individual uncertainty term for the more recent DEM, and δz_{old} is the uncertainty term for the older DEM (Brasington et al., 2003). The next step is to use the output from this equation to calculate a t-score.

This is accomplished on a cell by cell basis for the change observed in the DoD with the equation:

$$t = \frac{| Z_{DEM_{new}} - Z_{DEM_{old}} |}{\delta \upsilon_{DoD}} \tag{6.2}$$

where $Z_{DEM_{new}}$ and $Z_{DEM_{old}}$ represent the Z values from each respective DEM at a particular location and $\delta \upsilon_{DoD}$, is the propagated uncertainty in the DoD. Finally this can be updated to a probabilistic threshold through the equation:

$$U_{critical} = t \times \sqrt{(\delta z_{new})^2 + (\delta z_{old})^2} \tag{6.3}$$

Using standard statistic tables the $U_{critical}$ can then be converted to a probability of real geomorphic change. To apply this statistical inference it is necessary to assume that uncertainty in each raster cell is random and independent (Wheaton et al., 2010). For more information about this assumption and the model of the distribution of error created from these equations refer to Appendix C.

This method now produces a DoD that does not discard changes below a minimum level of detection but rather views them as statistically improbable. Although subtle, this shift allows for the application of a fuzzy inference system and Bayesian probability that have mechanism to better quantify the spatially variable nature of elevation uncertainty.

6.2.2 Incorporating a Fuzzy Inference System

In a broad sense fuzzy logic is a system of concepts, principles and methods for dealing with modes of reasoning that are approximate rather than exact (Demicco and Klir, 2004). Fuzzy inference is suitable for dealing with uncertainty because of its ability to deal with ambiguity in values, its ability to quantify linguistic variables, and its representation of values as degrees of truth rather than denial or affirmation.

The concepts discussed in Section 5 have identified landforms and areas of the swath that will either decrease or increase vertical uncertainty in the measurements. Although it can be said that surface roughness leads to high uncertainty, the term high uncertainty

does not have a quantitative value associated with it. A fuzzy inference system is able to quantify these ambiguous terms into actual values.

In this study fuzzy logic will be used to convert the previously identified sources of survey uncertainty, surface roughness and slope, into a spatially variable vertical uncertainty estimation, δz. For vertical uncertainties, δz, to be spatially variable a system is needed that can combine attributes from multiple variables influencing δz, account for the variables' influence on one another and convert these into a quantitative value. For an overview of fuzzy inference systems refer to Appendix D. In Section 6.3.2 the development of a FIS specific to MBES is detailed.

6.2.3 The Spatial Contiguity Index & Incorporating Bayesian Probability

Bayesian probability is a school of statistics that allows for the incorporation of new information obtained a-priori to probability calculations. This new information is used to update the initially calculated probability to better reflect the phenomenon. In Section 6.2.1 a *DoD* was presented that represents the statistical likelihood that the geomorphic change observed is actual change, either erosion or deposition. Erosion and deposition are unique processes that follow general principles as to where they occur. By understanding and using these principles as guidelines the original probability of geomorphic change provided in the *DoD* can be updated with Bayesian probability when particular situations occur.

The use of a spatial contiguity index for erosion and deposition cells allows for Bayesian updating of probability in a geomorphic change study (Brasington et al., 2003; Wheaton, 2008; Wheaton et al., 2010). A spatial contiguity index is based on the concept that erosion and deposition tend to occur in groupings. Building from this concept a moving window operation counts the number of cells in the window that are erosion and/or deposition. The more cells in the moving window that are the same as the center cell the more likely that the center cell would be of that type. Through this process a cell that would have been given a low probability due to its low change and higher propagated uncertainty can be

given a higher probability of being actual geomorphic change.

The moving window can be defined as any size but the cell resolution of the *DoD* and the size of features that are attempting to be represented should both be considered when determining window size. For example if the cell resolution is 2 ft. by 2 ft. and sandbars in a typical reach are 10 ft. wide then a 5 x 5 cell window would be appropriate.

In some river systems deposition is more of a widespread phenomenon with the total volume of deposition dispersed over a larger area than erosion. This would result in many cells of small positive values in the *DoD* that would be likely to be given low probability of being real geomorphic change. This causes deposition to be more sensitive to minimum levels of detection and as minimum levels of detection are increased more deposition would be discarded than erosion (Brasington et al., 2003; Fuller et al., 2003). The spatial contiguity index window aims to solve this issue and increase the probability of small value deposition cells when they are in a neighborhood with a large number of deposition cells.

The spatial contiguity index also helps to alleviate a 'checkerboard' or 'island' patterns that can occur in a *DoD*. When an area has many alternating erosion and deposition cells, a checkerboard pattern, then the window can decrease the original probability of the cells in the window because of their lack of similar neighbors. In the same way if one deposition cell lies in a window of all erosion cells then its original probability would be reduced.

By combining knowledge of a river system through a spatial contiguity index, Bayesian probability is used to return potentially meaningful change back into the final analysis. In the same way erroneous geomorphic change can be discarded from the final analysis because of its unlikely location in relation to the values of its neighboring cells.

6.3 Case Study Application - Aligning Rasters and Developing a FIS

6.3.1 Orthogonality and Concurrency

It is crucial to adhere to the concepts of orthogonality and concurrency when differencing (or performing any calculations between) two rasters. Orthogonality is the idea that rasters have the same resolution and are aligned in both easting and northing which ensures they have the exact same grid centers. Concurrency means that rasters have the same extent. If these two principles are not followed then the results of the differencing is meaningless and different locations are being differenced.

To accomplish this raster extents should be in whole numbers and the width and height both evenly divisible by the cell resolution. This can be accomplished by inputting any raster into the raster calculator of GIS software and manipulating the environment settings on the raster calculator to meet the above specified criteria. There is no noticeable difference in the output of the rasters from this calculation; however, applying the same concurrent and orthogonal settings to the extents of both rasters ensures that calculations between the two will apply to the same cells in each.

6.3.2 Developing a Fuzzy Inference System

The Fuzzy Logic Toolkit from Matlab was used to formally create a two variable FIS to be used in this study. However, the real work of creating a FIS lies in the knowledge of the variables influencing uncertainty in the survey technique combined with statistical exploration of the relationships that exist between uncertainty and these variables. The parameter groups and their specific effect on uncertainty presented in Section 5.3 were used as guidelines for developing the FIS. Specifically knowing the distribution of the surface roughness and slope and how the values influence measurement uncertainty. Basic data exploration and spatial distribution of surface roughness and slope are presented in Figures 6.1, 6.2, 6.3 and 6.4.

Figures 6.2 and 6.4 reveal that in general this reach is characterized by relatively low surface roughness and slope but it contains isolated regions of high topographic complexity.

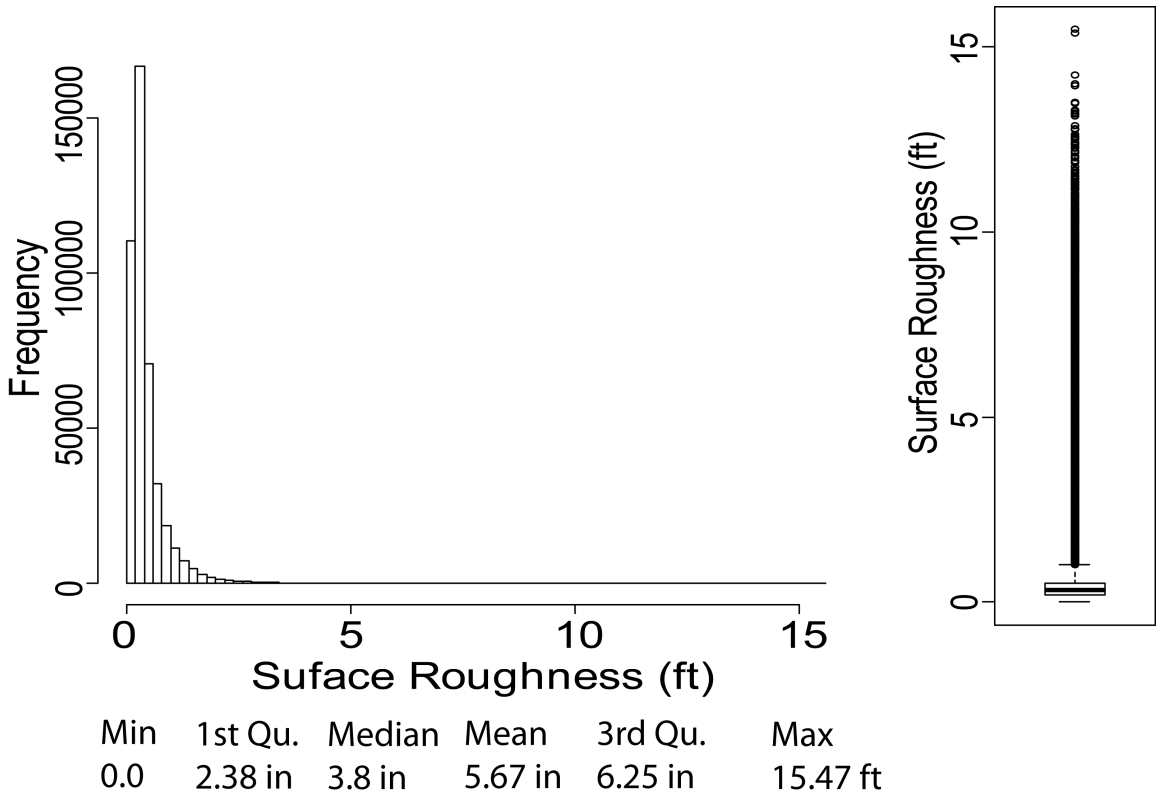

Figure 6.1. Exploration of the statistical distribution of surface roughness in Wild Sheep Reach.

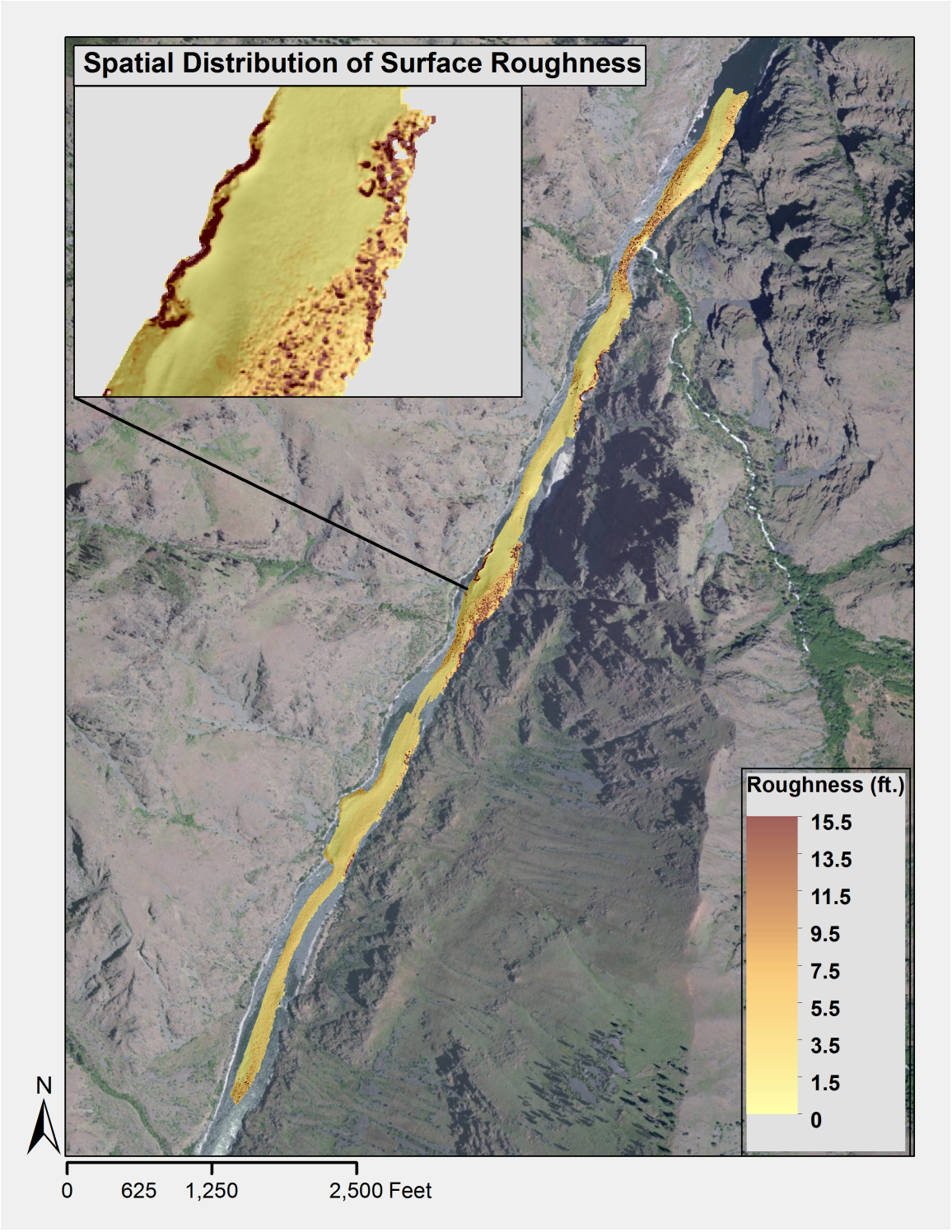

Figure 6.2. Spatial distribution of surface roughness in Wild Sheep Reach. Low surface roughness tends to be isolated in the center of the channel while values are at their highest along the banks.

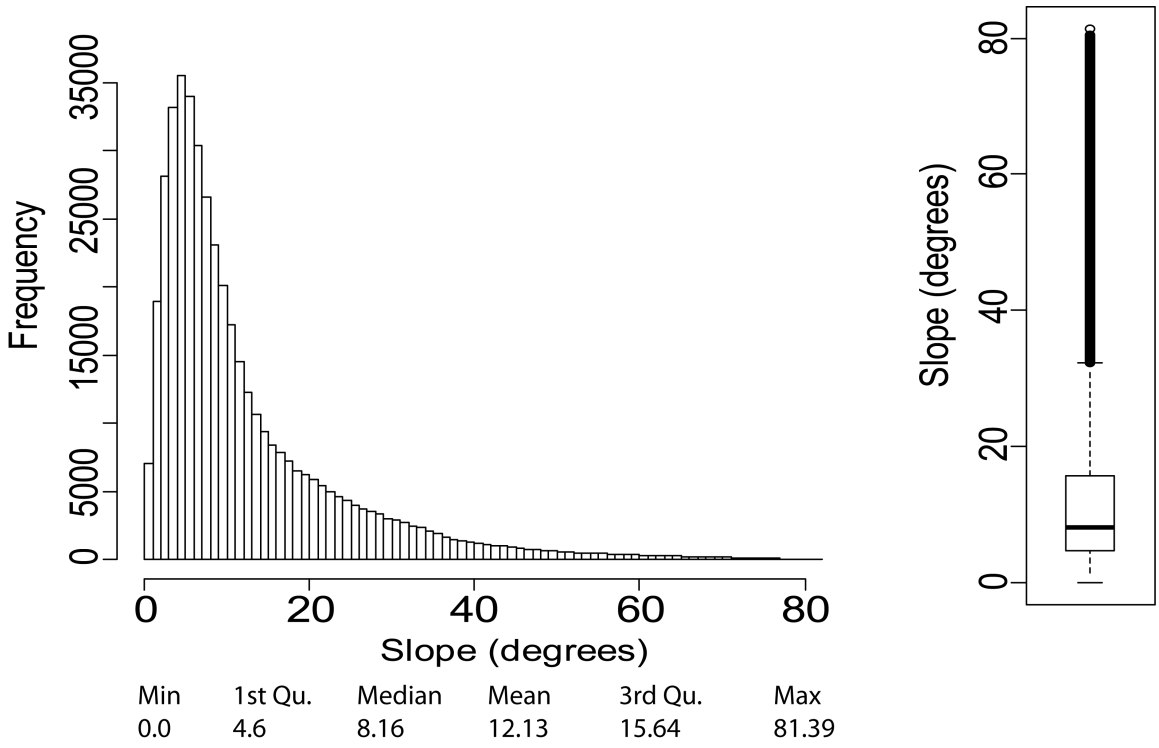

Figure 6.3. Exploration of the statistical distribution of slope in Wild Sheep Reach.

Additionally Figures 6.1 and 6.3 show that neither parameter could be considered normally distributed in a statistical sense. For this reason, as was presented in Section 5.3, a non-parametric metric for dividing the data, a boxplot, was used to distinguishe classes. However, the classes created in Section 5.3 are 'crisp' groups and have strict boundaries. To make the groups fit into a FIS the boundaries need to be loosened and overlap created between each group. Rather than arbitrarily creating overlap between the groups a method again was employed that utilizes viewing the quartiles of data but in this case each quartile of the overall dataset was broken further broken down into quartiles of its own. Due to the non-parametric nature of quartiles, which involve ranking the values from smallest to largest in order, predictable percentages of the data can be extracted from each group. Specifically a quartile of the entire population represents 25% of the data, when a quartile is divided into quartiles each 'sub-quartile' represents 6.25% of the entire population. These sub-quartiles were utilized to create the overlap between each group because of the ability to predict how much of the data would be included in the overlaps (with the exception of

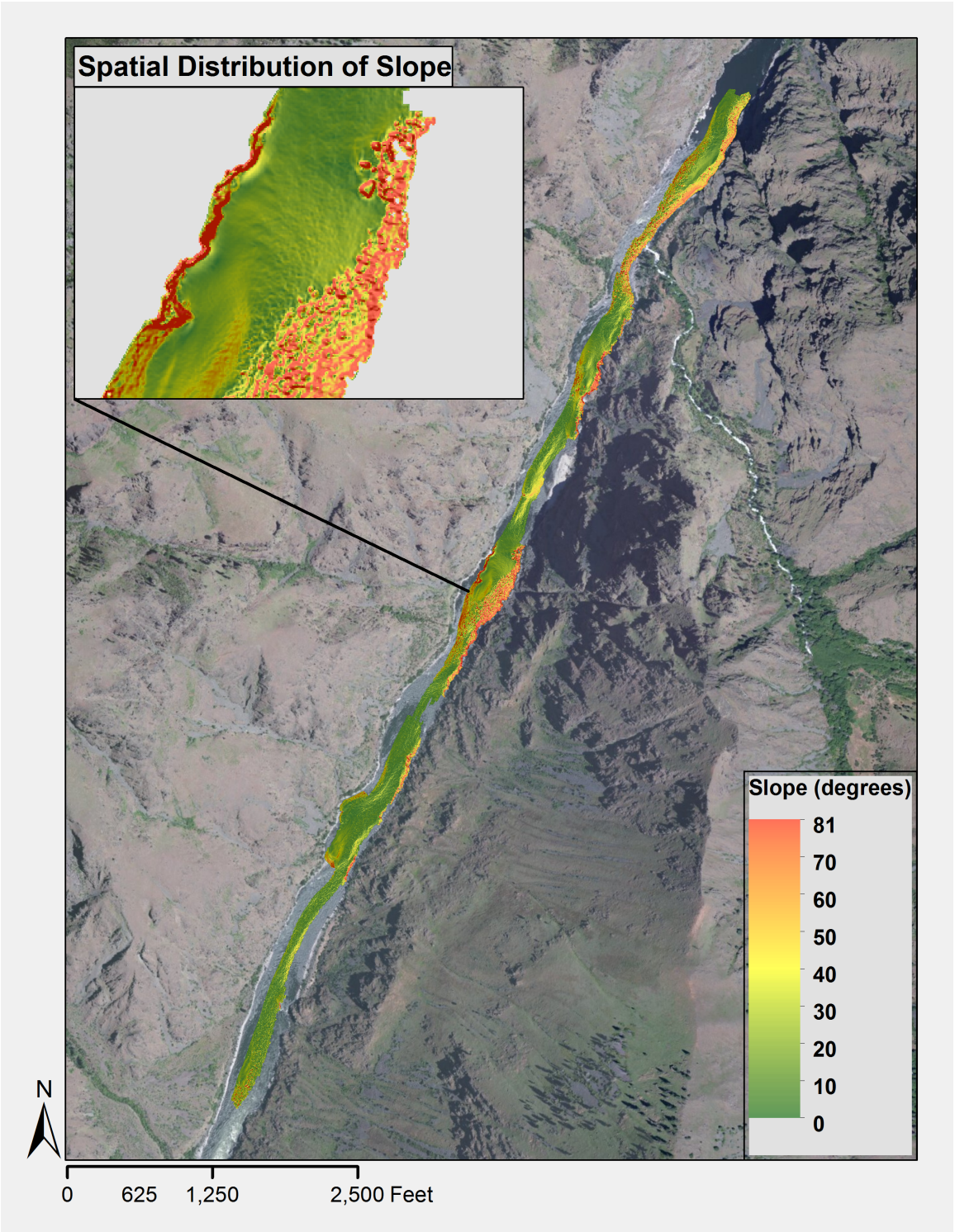

Figure 6.4. Spatial distribution of slope in Wild Sheep Reach. Slope values are generally less than 15° and are maximum along the banks of the river.

the overlap with the high classes) and additionally provide an iterative way of calculating FIS groups and their overlap.

Three input membership functions were created for surface roughness and slope of low, medium and high. As was shown in Section 5.3, the low group represented everything below the population median, or 50% of the data, in both surface roughness and slope, and to create overlap it then overlapped to the lower hinge of the sub-quartile of the third quartile of the population. While the medium category had all values greater than the median and less than the upper whisker of the 4th quartile to create overlap into the high group it then extended to the lower hinge of the sub-quartile of the population outliers. To create overlap with the lower group the medium group extended to the upper hinge of the sub-quartile from the 2nd quartile of the population. While the high group was comprised of values greater than the upper whisker to create its overlap with the medium group it spread to encompass to the upper hinge of the sub-quartile of the 4th quartile of the population. Although this description has a defined way in which each group overlaps, this is more for purposes of repeatability and in reality knowledge of the variables in a FIS can provide guidance to create the overlap as well. The final output of a FIS has been shown to be relatively insensitive to the amount of overlap that exists between groups.

With input membership functions in place the next necessary step to develop a FIS is to create output membership functions. Output membership functions relate each possible combination of input membership to one another and translate that into an actual value of uncertainty. To aid in the development of output membership functions roughness and slope values were extracted at locations where an estimation of uncertainty existed, classified as to which crisp group each point belonged to for both roughness and slope, further classified by all possible combinations of input membership functions, and their resulting influence on uncertainty was explored. A plot of this information is presented in Figure 6.5 and a summary of the specific values in Table 6.1. In this plot each dot represents a combination

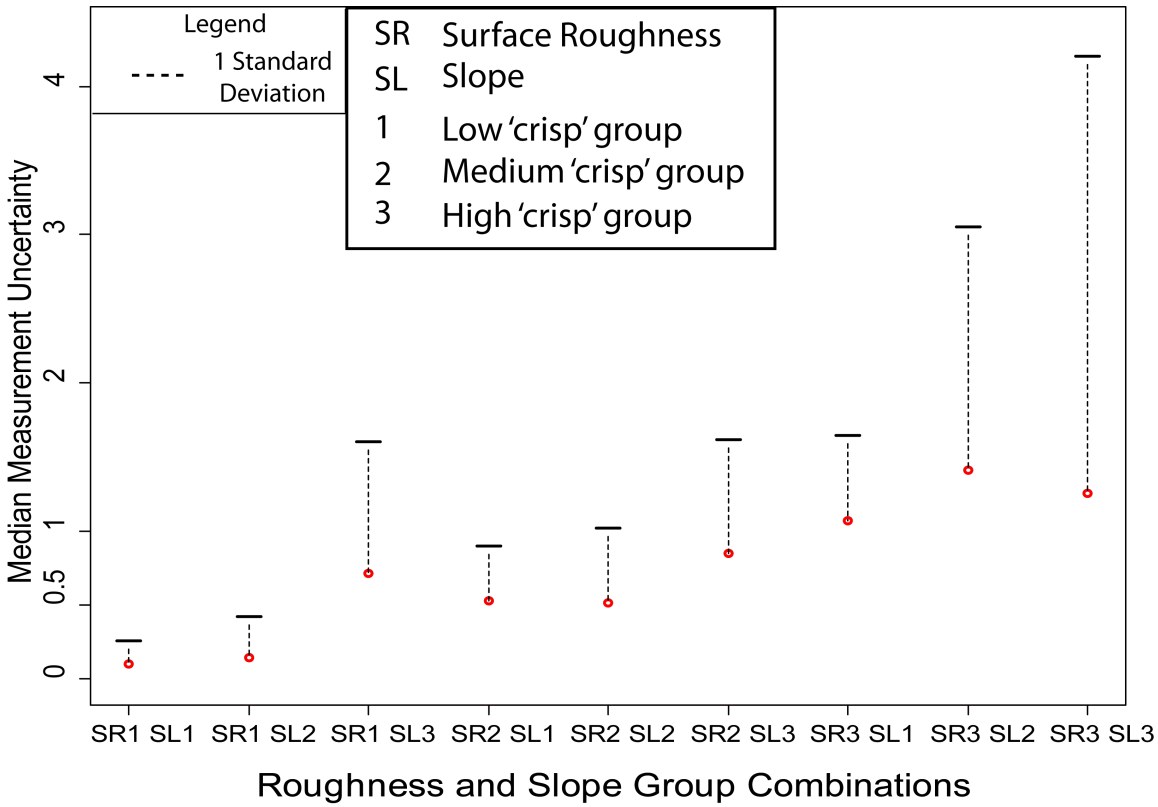

Figure 6.5. Plot of all possible combinations (rules) of the crisp groups of the input parameters to the FIS. The red dots represent the median value of uncertainty and the dotted lines are one standard deviation. This plot was used to identify combinations with similar effects on uncertainty in order to create the output membership functions.

of input groups. For example SR1 and SL1 is the summary of the observed uncertainty at all points where roughness was below the median roughness of the reach and slope was below the median slope of the reach. In terms of classification these equate to low roughness and low slope. By analyzing Figure 6.5 and Table 6.1, clear distinctions exist between different combinations of parameters and these differences were used to create the output membership functions.

Based on the values from Table 6.1, four separate groups of low, medium, high, and extreme uncertainty were created as there are distinctions as well as similarities between median values of the different parameter combinations and their effect on uncertainty. To ultimately create the specific values of each group and their overlap with other groups a

Table 6.1. Summary of the results presented in Figure 6.5. The different output membership functions are distinguished by color. The low uncertainty class is green, medium is yellow, high is orange, and red is extreme uncertainty.

Fuzzy Inference System Output Membership and Rules Development Guide							
		Uncertainty (ft.)					
Group Combinations	Rule	Median	Mean	StDev	Min	Max	Observations
SR1SL1	1	0.10	0.15	0.16	0.01	1.76	3390
SR1SL2	2	0.14	0.23	0.28	0.01	2.50	1492
SR1SL3	3	0.71	0.85	0.89	0.02	3.51	21
SR2SL1	4	0.53	0.59	0.37	0.01	2.76	568
SR2SL2	5	0.51	0.61	0.51	0.01	4.13	1611
SR2SL3	6	0.85	0.97	0.77	0.01	4.86	212
SR3SL1	7	1.07	1.08	0.58	0.14	2.27	11
SR3SL2	8	1.41	1.80	1.64	0.01	12.12	244
SR3SL3	9	1.25	2.26	2.95	0.01	23.29	566

degree of judgment is necessary. For the purpose of this study the standard deviation of each group was considered within relation to the standard deviations of groups that it would have overlap with. For example the low uncertainty group, represented by green in Table 6.1, has a general median value of 0.14 ft. with a standard deviation of anywhere from 0.16 to 0.28 ft. While the medium uncertainty group has a median uncertainty of 0.53 ft. and a standard deviation ranging from 0.31 to 0.51 ft. the overlap should lie somewhere in between the overlap that is provided by these standard deviation in relation to their median values. This process is somewhat subjective and expert judgment is necessary to create the final groups.

The final rules that result from this analysis are shown in Table 6.2. Due to the ability for a particular value to belong to multiple input membership functions any one cell in a FIS analysis can relate to multiple rules from this rules table. When this occurs in order to derive a final uncertainty value aggregation and defuzzification are necessary. To better understand how a fuzzy inference system derives a concrete uncertainty value from the input fuzzy memberships and their associated uncertainty class it is helpful to detail an example

Table 6.2. Fuzzy rule set.

Rule	**Roughness**	**Slope**	**Uncertainty Class**
1	Low	Low	Low
2	Low	Medium	Low
3	Low	High	High
4	Medium	Low	Medium
5	Medium	Medium	Medium
6	Medium	High	High
7	High	Low	High
8	High	Medium	Extreme
9	High	High	Extreme

of defuzzification. An example of this is presented in Appendix D.

With input membership functions, output membership functions, and a rules table to relate the two in place, the FIS can be applied on a cell by cell basis to compute an uncertainty value for each raster cell in an analysis. The result and process of computing the propagated uncertainty from a FIS is shown in Figures 6.6 and 6.7. This is a spatially distributed propagated uncertainty that is computed by overlaying the two inputs and applying the rules set. The values from this raster are then used in the equation from Section 6.2.1 along with the values from the two DEM to compute a probabilistic threshold. Applying a FIS spatially on a cell by cell basis is conceptually shown in Figure 6.6.

The interpolation error raster developed in Section 5.2 can be combined with the FIS to further quantify surface uncertainty in a DEM. However the interpolation error raster represents an exact measurement of uncertainty and is difficult to incorporate into a FIS that deals in vague values. To combine the FIS propagated uncertainty and the interpolation error rasters into a final propagated uncertainty surface first the two are added to another and then combined with similar equivalent rasters from another year through Equation 6.1 from Section 6.2.1. As was shown in Section 4.2.3 the mean interpolation error is low for nearly 95% of all cells and because of this the result of adding an interpolation error term is an increased propagated uncertainty value at areas of extreme topography as demonstrated

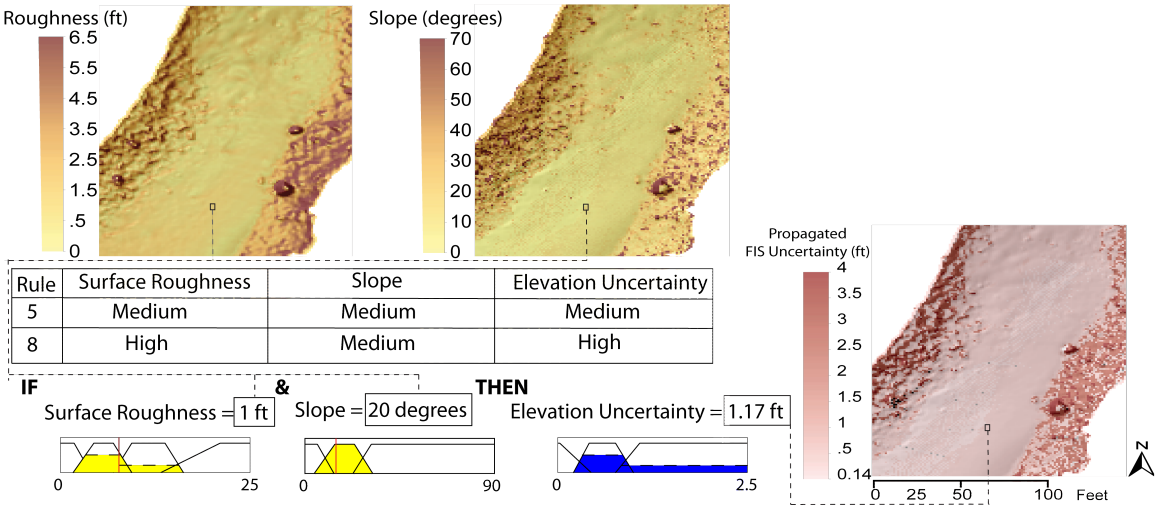

Figure 6.6. A fuzzy inference system (FIS) is used to calculate uncertainty on a cell by cell basis. In the figure a cell having the same geographic location is highlighted in each raster. The values of those cells are applied in the context of the FIS rules structure to compute a final uncertainty value.

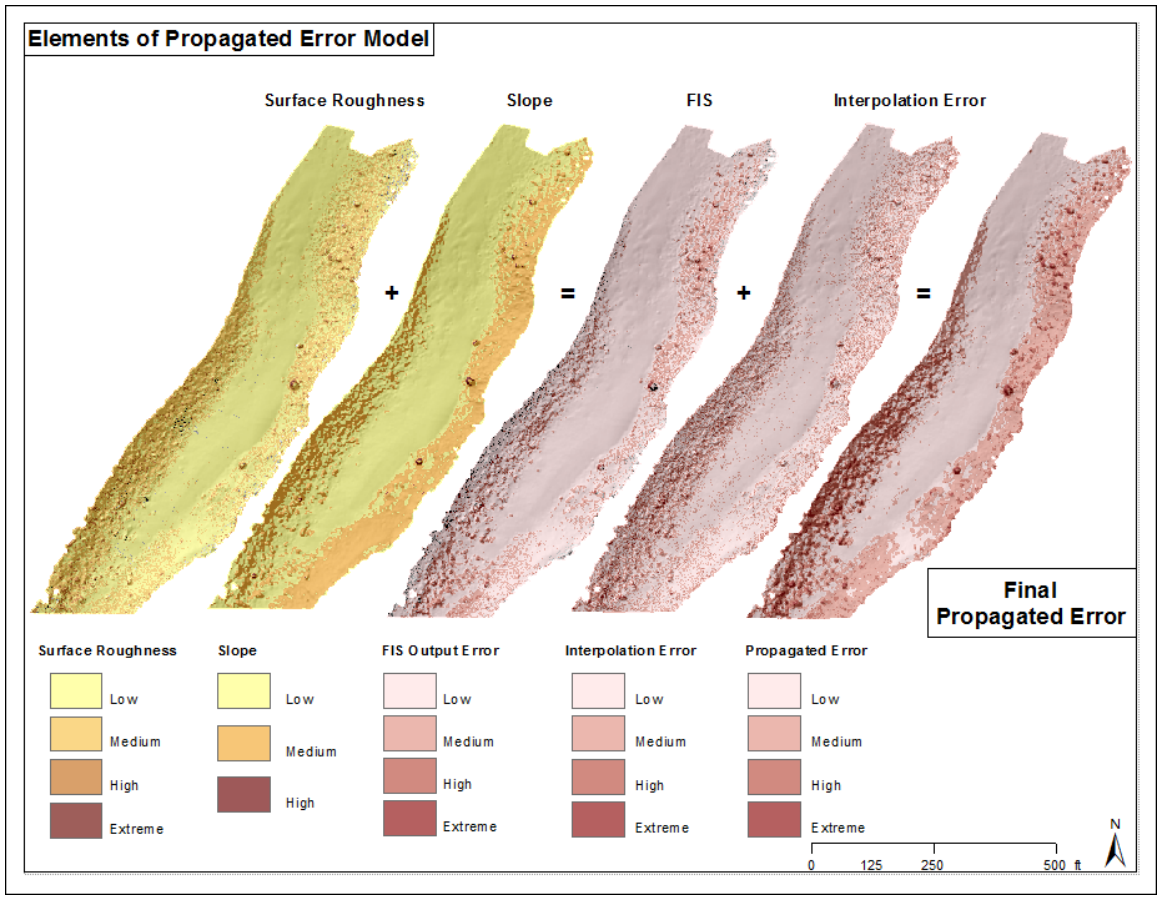

Figure 6.7. Propagated uncertainty raster for 2008 of a sub-reach.

in Section 4.2.3.

6.3.3 Checking Validity of FIS

To check if the FIS is properly representing the measurement uncertainty the propagated uncertainty at sample points can be extracted and plotted against the slope and surface roughness at these points. The same statistical analysis that was performed in Section 5.3 was performed with the attention placed not upon the statistical significance, as this inherently will exist, but rather if the plots can capture the same patterns as those created by plotting measurement uncertainty versus the same variables. This is presented in Figure 6.8. It is difficult to compare the modeled uncertainty from the FIS to the error observed in Section 5.3 as the maximum value of modeled uncertainty is 2.5 ft. while the maximum observed was 30 ft. However when related to surface roughness the modeled uncertainty only increases with increased surface roughness and their variability of uncertainty is not present that can be seen in Figure 5.6 when surface roughness was plotted against observed uncertainty. Modeled uncertainty when related to slope better reflects the increase in variability of uncertainty with increasing slope originally seen in Figure 5.7. This is mainly due to the fact that surface roughness, by design, is the dominating factor of the FIS and has more influence than slope does on the modeled uncertainty.

Although an increase in surface roughness or slope increases the potential for high uncertainty it does not guarantee it as there are still causes where the uncertainty remains low under these circumstances. This is a difficult pattern to quantify in a FIS or any mathematical model. The current FIS falls short of modeling this pattern however it does offer a method for addressing the spatially varying nature of uncertainty and represents an improvement on using a minimum level of detection.

The values of modeled uncertainty at the same points of observed uncertainty used in Section 5.3 were differenced to gauge if the FIS was comparable at these locations. Nearly 75% of the compared points were within 4 inches of the observed uncertainty. The percent

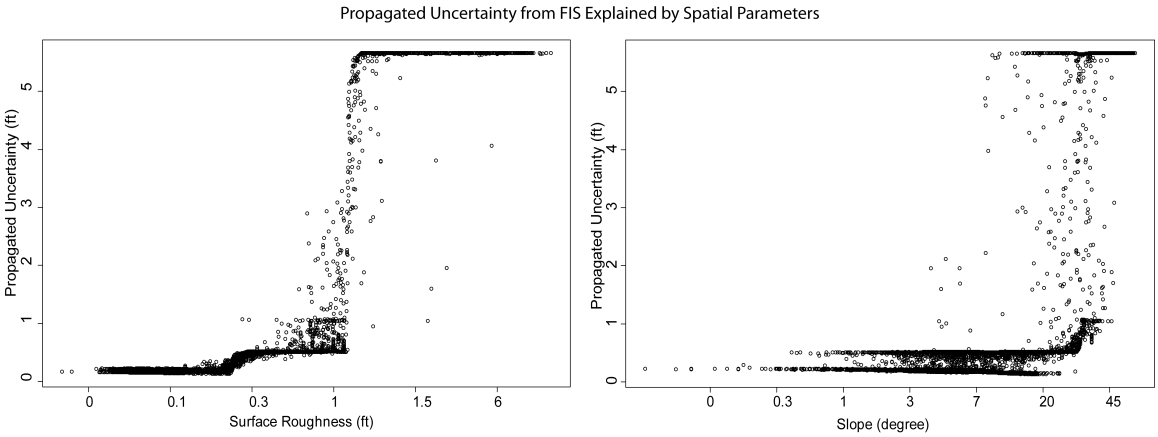

Figure 6.8. FIS modeled propagated uncertainty plotted against the logarithm of surface roughness and slope (axis labels have been converted back from logarithm to reflect more easily understood values).

of modeled uncertainty values within a range of values of observed uncertainty is presented in Figure 6.9.

The mean difference in points was an underestimation of uncertainty by the FIS of 1.2 inches while the median was an overestimation of slightly more than half of an inch. The difference in mean and median is due to the influence of the large values of observed uncertainty of upwards 30 ft. that the FIS was not able to model. The distribution of the difference between observed uncertainty and FIS modeled uncertainty is presented in Figure 6.10.

A nearly one to one relationship between modeled and observed uncertainty can be seen in the quartile-quartile plot in Figure 6.11. However, this 1 to 1 relationship exists only until the uncertainty values of 1.25 ft. The reason for this tail off can be explained by understanding the relationships shown in Figures 5.6 and 5.7, where an increase in either roughness or slope increases the likelihood that uncertainty will be a larger value; it does not guarantee an increase. The FIS is unable to model this increase in variance of uncertainty seen in the observed uncertainty values as slope and/or roughness increase. This graphic clearly shows the FIS inability to model extreme uncertainty seen in the observed values. However, the values that tail off only represent a small subset, n = 36 of significant

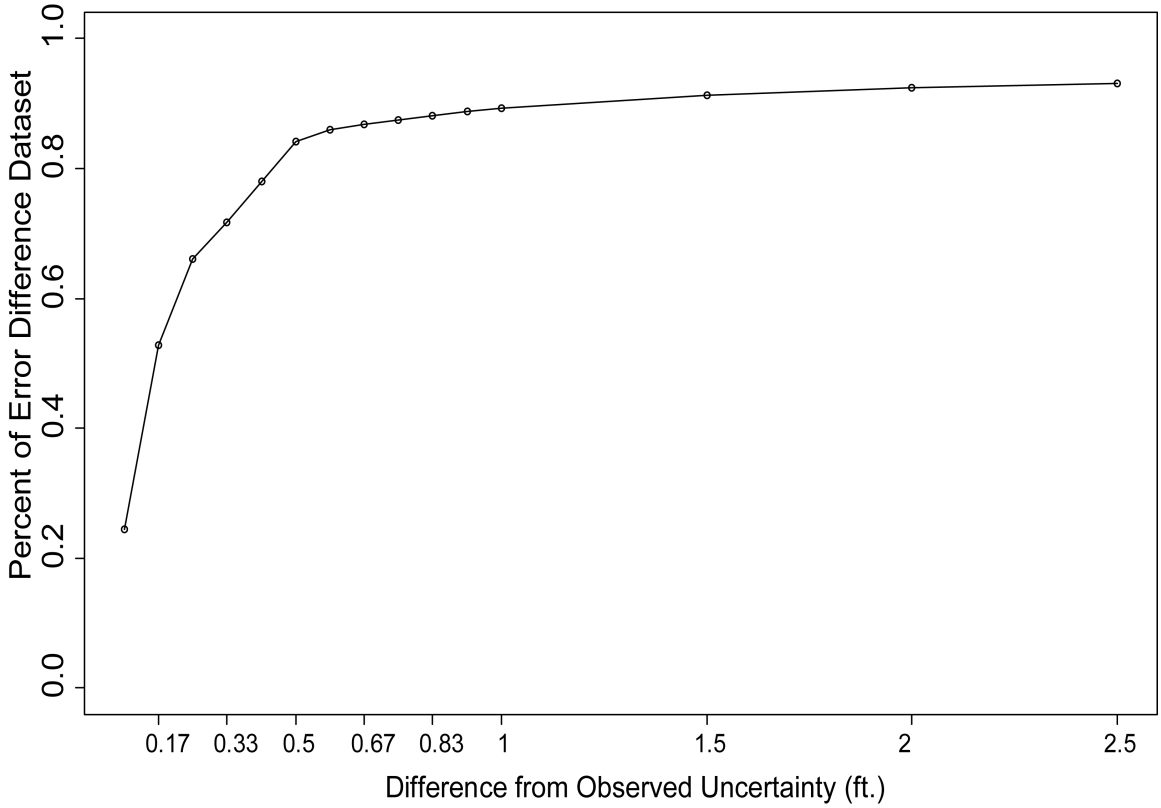

Figure 6.9. Percent of FIS data within different values of the observed uncertainty.

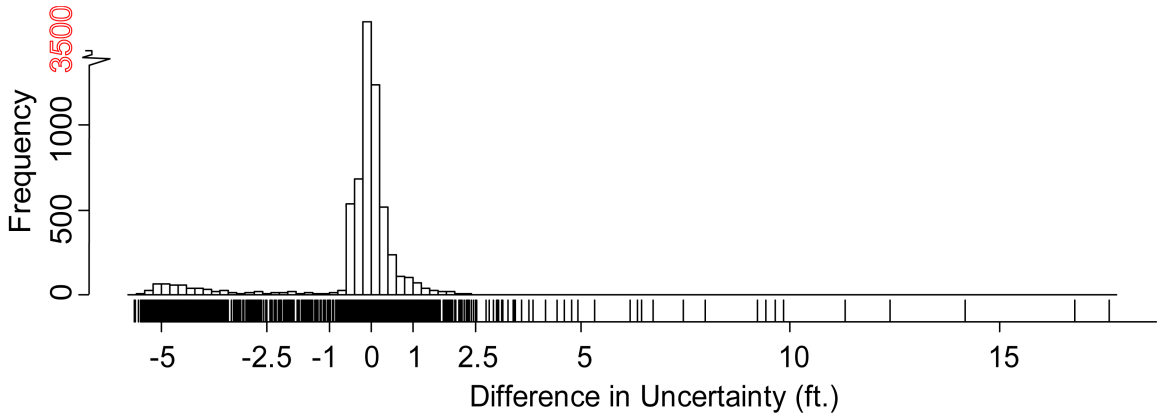

Figure 6.10. Histogram of the difference between observed uncertainty and fuzzy inference system modeled uncertainty. Each black tick mark above the x-axis labels represents one occurrence of that value.

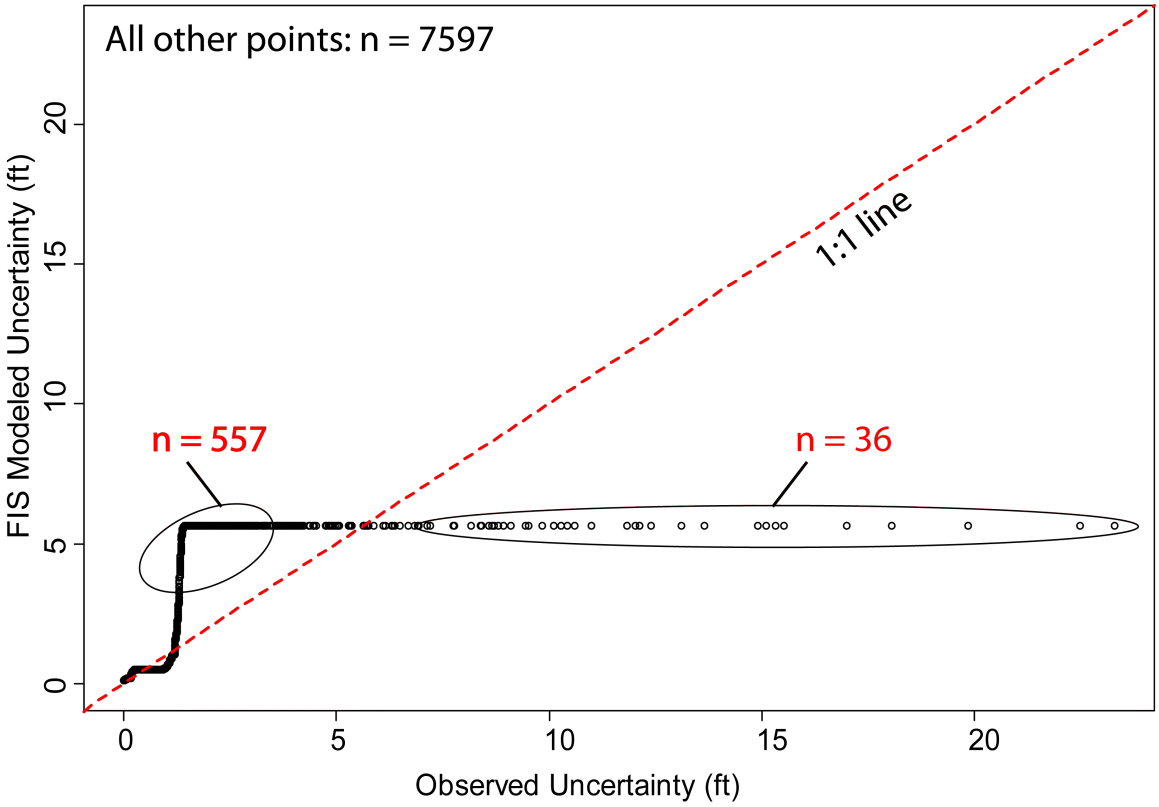

Figure 6.11. Quantile-quantile plot of observed uncertainty to fuzzy inference system (FIS) modeled uncertainty. The dashed red line is a 1:1 line that represents a perfect fit.

underestimation and n = 557 of significant overestimation (significant being described as greater than 2 ft.) of the data set used to assess the FIS. These 593 points are locations of extreme topographic complexity with a mean surface roughness of 4.4 ft. and mean slope of 46°, which is in contrast to a surface roughness mean of 0.36 ft. and 11° slope for the rest of the dataset (n = 7597). A plot with the subset of n = 593 points removed is presented in Figure 6.12.

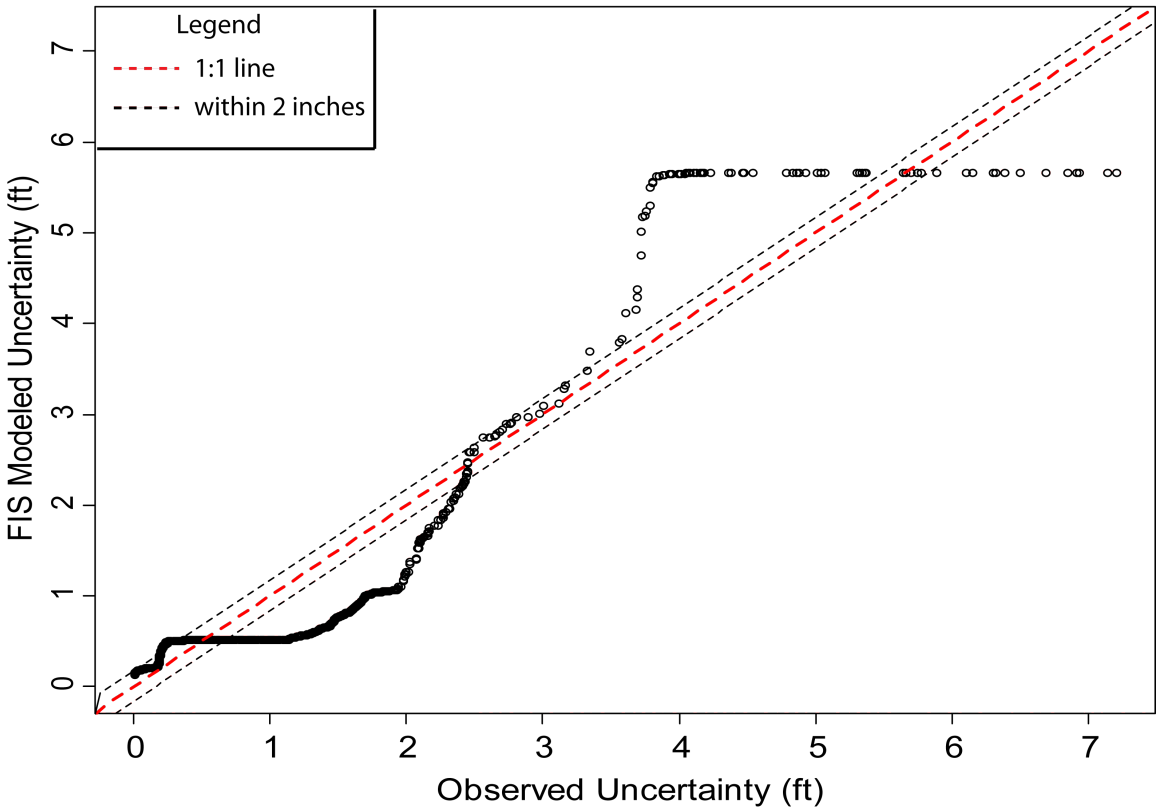

Figure 6.12. Quartile-quartile plot of observed uncertainty and fuzzy inference system (FIS) modeled uncertainty. The dashed red line is a 1:1 line while the dashed black lines set a boundary of values within plus or minus two inches.

Section 7

Interpretation of Change Detection Results

7.1 Assessing the Effects of Emerging Methods on Change Detection Results

Placing geomorphic change into the realm of statistics, implementing a FIS to quantify uncertainty, and using a spatial coherence index in conjuncture with Bayesian probability produces more robust results than simply removing potential geomorphic change that is below a minimum level of detection. The effects that these techniques have on a geomorphic change detection study are compared to a study without any uncertainty model in this section. To better display and discuss the differences between models a smaller section of Wild Sheep Reach is presented, specifically the same reach as was used in Section 4.2.3 and summarized in Table E.1 in Appendix E. First basic change detection with no uncertainty term is applied for comparison purposes, followed by propagating uncertainty in a fuzzy inference system, then a spatial coherence index, and finally the interpolation error term is added. The DoDs are compared in Figure 7.1 and volumetric totals are compared in the histograms of Figure 7.2. The calculations used in this analysis can be carried out in the raster calculator of popular GIS; however, the Geomorphic Change Detection software developed by Joe Wheaton packages all of the necessary operations into an easily manageable plug-in for ArcGIS (available for free download at `http://gcd.joewheaton.org/`). This software was used in the analysis of this section and is highly recommended.

In the top left of the comparison pane of Figure 7.1 the results of basic change detection calculations can be observed. In this graphic all change is considered to be real geomorphic change. There are clearly large regions of both deposition and erosion that appear to be distinguished patterns of sand bars and scour areas. However, in addition to these landforms there is also a large amount of unrealistic 'checkering' patterns on the banks of the river. This is perhaps unrealistic as many of these areas have been identified in surface roughness

rasters as being areas of large boulders that would not change through time. The histogram of this graphic is in the top left of Figure 7.2. All change is considered real change and this is clearly presented in the histogram. The result is a system that is displaying overall erosion.

The top right of the comparison panel of Figure 7.1 is geomorphic change with the two input FIS discussed in Section 6.3.2 applied to a 95% probabilistic threshold confidence interval. A large portion of the perceived change from the basic change detection has not passed statistical significance and is not displayed. The result is isolating the clear patterns discussed in the previous paragraph but the exclusion of much of the noise and checkering patterns. This result is similarly apparent in the histogram where virtually all of the change below 6 inches has not passed statistical significance. This histogram depicts a system that is displaying overall erosion. It should be noted that 95% probabilistic thresholding was selected to stay consistent with statistical confidence levels historically used in statistical inference; however, other thresholding levels may be chosen. For a brief explanation of the sensitivity of the critical threshold error to thresholding at different confidence intervals refer to Appendix C.

In the bottom left of the comparison panel of Figure 7.1 the spatial coherence index is applied in conjuncture with the two input FIS to 95% significance. Here some small magnitude erosion on the southeast bank that previously did not pass significance with just the two input FIS has been returned to the analysis. Similarly the patterns of deposition and erosion in the northwest of the graphic have increased in size as now more cells pass significance. Additionally the large bar feature in the southeast has increased in size. The result, which can be seen in the associated histogram, is the inclusion of geomorphic change below 1 ft. and even below 6 inches. This is the work of Bayesian probability updating as the probability of this small change being real was increased because of the large number of its neighbors being of the same flux class. The limit to update the probability was set at over 90% of cells neighborhood in a 5 x 5 window had to be of the same class to improve

the probability while less than 50% in the same window would decrease a cell's probability of being real change.

The final analysis in the bottom right of the comparison pane of Figure 7.1 is the two input FIS to 95% probabilistic threshold confidence with the spatial coherence index and the application of an interpolation error term. The effects of the interpolation term are more subtle but accomplish a number of important details. The first is that the deposition patterns on the east bank (very edge of surveyed area) of the image have been slightly decreased in size. These decreases or holes in the deposition patterns are large boulders such as the one represented in the point cloud of Figures 4.4 and 4.5 where an interpolator and thus the DEM was not able to properly model regions of abrupt elevation change. These were the areas established as high interpolation errors in Section 4.2.3. The second noticeable effect of the interpolation term is nearly all of the small specks of changes seen throughout the other graphics of Figure 7.1 no longer pass statistical significance. The result is a more fluid geomorphic change depiction that isolates regions of large change that fit the known patterns of erosion and deposition.

It is worth noting that although each of these techniques had an effect on the number of cells that were included in the final reporting of sediment flux, none of the techniques changed whether the system was displaying net erosion or deposition. Across all techniques this reach displayed overall erosion; the differences between methods was only the net volume of erosion. All methods using an uncertainty model ranged a maximum of 3,253 ft^3 in their net volume estimations of sediment flux. While this may seem like a considerable volume, it is quite small when considering there is a total volume of sediment transport of 137,223 ft^3 in this sub-reach.

7.2 Exclusion v. Subtraction

Once a probabilistic threshold confidence limit has been established there are two main

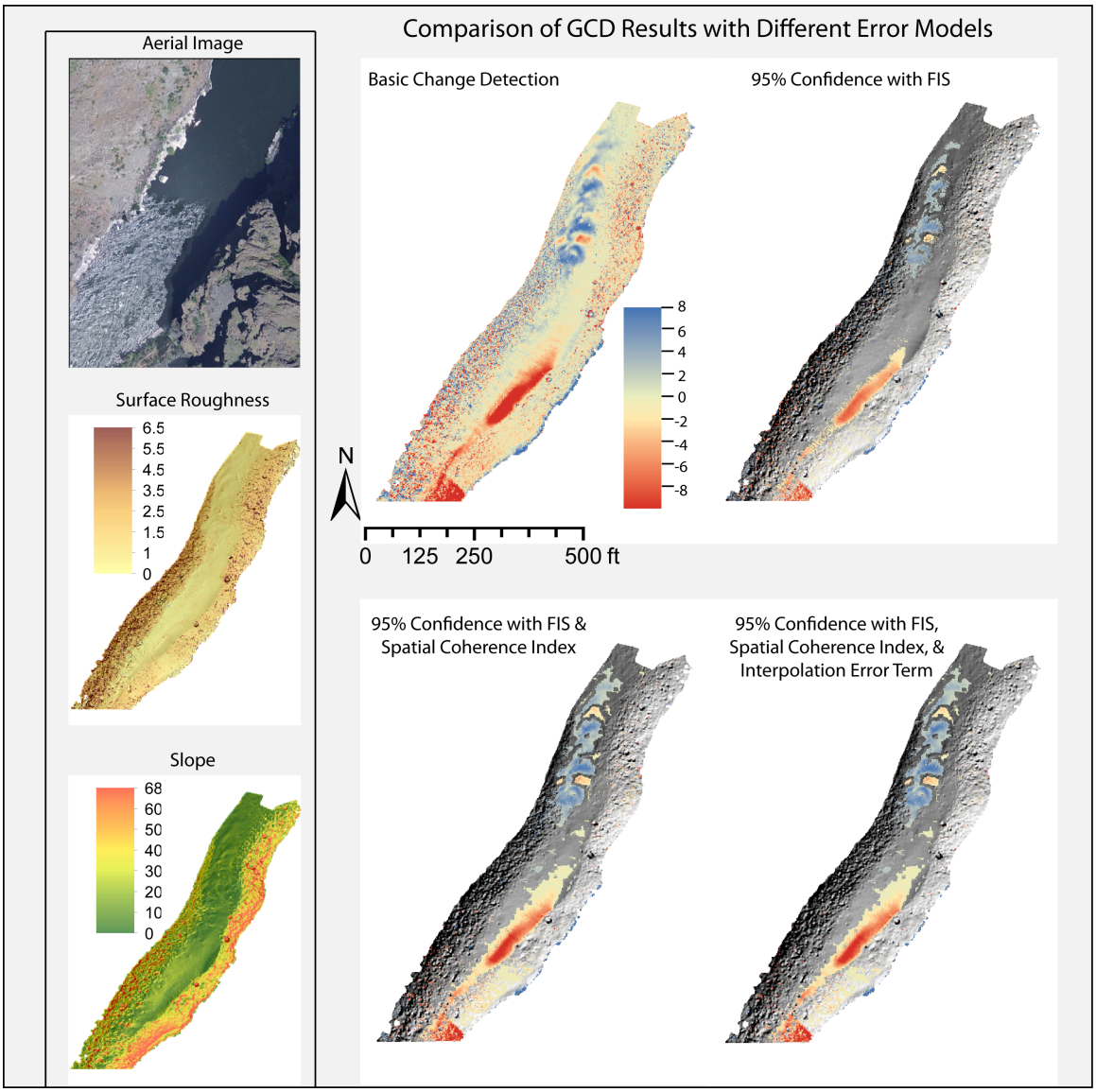

Figure 7.1. Geomorphic change detection results of sub-reach of Wild Sheep Reach. In the main panel the top left is a basic geomorphic change detection, top right is a two input FIS to 95% probabilistic threshold confidence, bottom left is a two input FIS to 95% probabilistic threshold confidence with a spatial coherence index, and bottom right is a two input FIS with interpolation error term to 95% probabilistic threshold confidence with a spatial coherence index. The gray area is a hillshade and represents areas that have been removed from the final DEM of difference by the different error models.

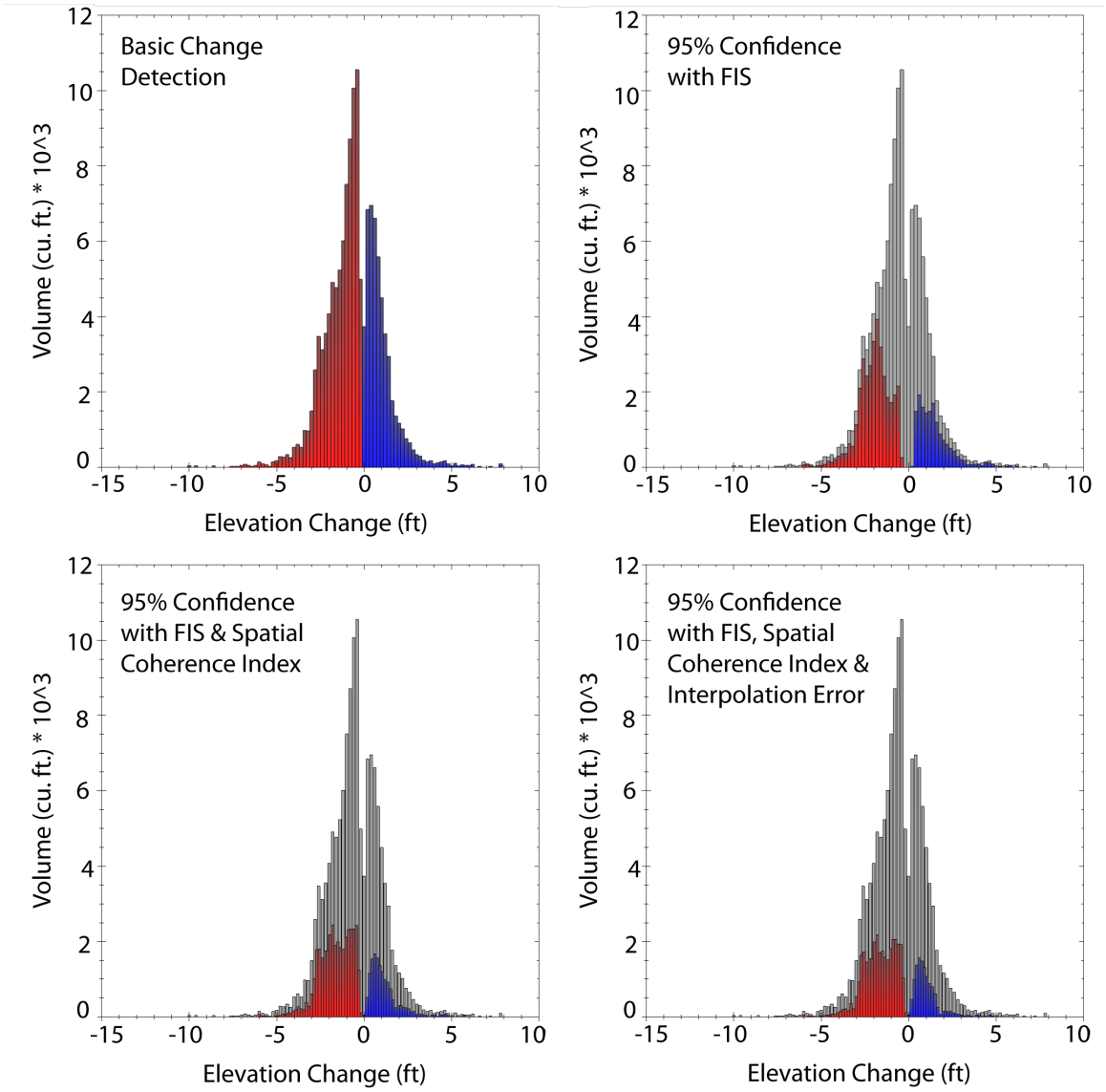

Figure 7.2. Histograms of geomorphic change detection results of sub reach. In the main panel the top left is a basic geomorphic change detection, top right is a two input FIS to 95% probabilistic threshold confidence, bottom left is a two input FIS to 95% probabilistic threshold confidence with a spatial coherence index, and bottom right is a two input FIS with interpolation error term to 95% probabilistic threshold confidence with a spatial coherence index.

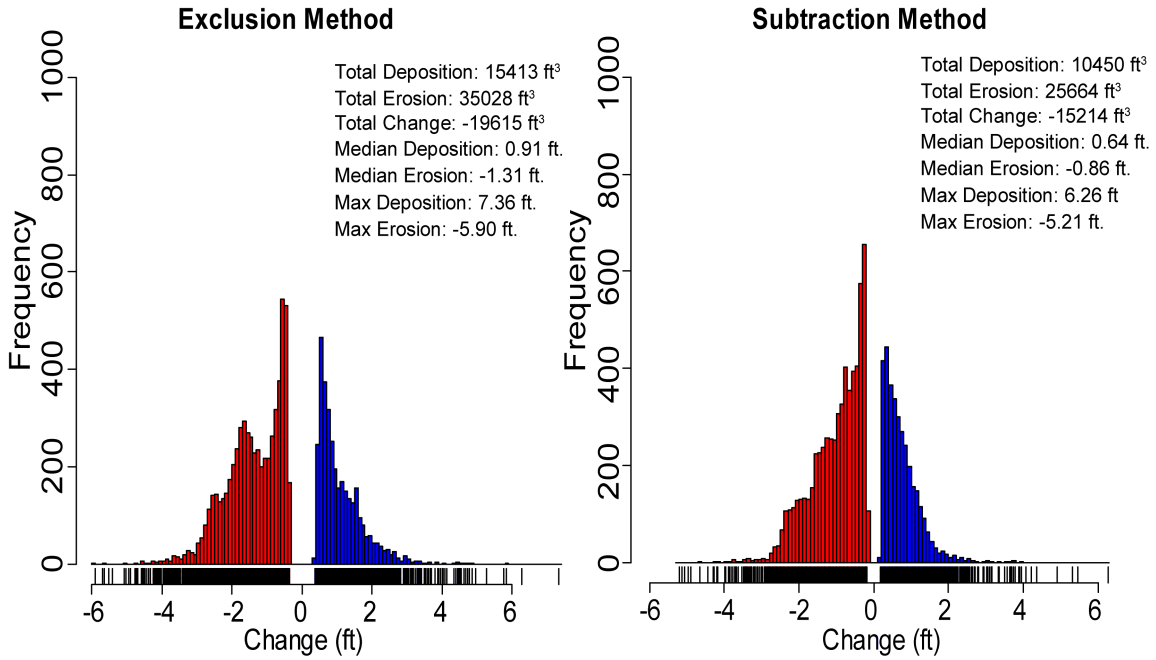

Figure 7.3. Histogram comparison of the change reported for the first sub-reach of Wild Sheep Reach. The more conservative subtraction method considerably reduces the amount of geomorphic change reported for each group when compared to the exclusion method. However, it results in a larger overall volume of change.

methods for determining the actual level of geomorphic change: exclusion or subtraction. The difference between the two methods is how they utilize the propagated uncertainty rasters. The subtraction method is a more conservative approach which subtracts the propagated uncertainty from deposition cells and adds uncertainty to erosion cells that probabilistic thresholding has established as real change. This removes the uncertainty completely from the estimate of geomorphic change (Milan et al., 2011). The exclusion method, which was the approach used in Section 7.1, is a more liberal approach that only uses the propagated uncertainty raster for calculating the statistical likelihood and significance of change in Equations 6.2 and 6.3. Once a change has passed the significance test then the amount calculated is considered to be real change (Wheaton et al 2010). The effect these methods have on the volume of change from the sub-reach used in Section 7.1 is presented in Figure 7.3.

The more liberal exclusion method results in 50,441 ft^3 some sort of change (+ or -) in this sub reach in comparison to the conservative subtraction method which results in 36,144 ft^3 some sort of change, a difference of 14,327 ft^3. The 14,327 ft^3 is the amount of uncertainty present in the cells that have been established at 95% probabilistic threshold confidence. For example if a cell calculated with the exclusion method was reported to be 1.46 ft. of change with 0.413 ft. of uncertainty, which is derived from the propagated uncertainty raster, then this cell actually represents a range of 1.46 $\pm$ 0.413 to 95% probabilistic threshold confidence. The 95% probabilistic threshold confidence is established because when adding the uncertainty term to the cell value it will not change from erosion to deposition or vice versa. The same cell in the subtraction method subtracts the 0.413 ft. of uncertainty from 1.46 ft. This results in reporting 1.05 ft. of change, the low end of change in the same cell when using the exclusion method. If a cell value is negative change when using the subtraction method the uncertainty term is added to the value. The above example of the range of values for a cell in the exclusion method is presented in Figure 7.4. In this figure the left bar is the amount of change reported that would be reported for the cell when using the subtraction method.

This concept can be viewed in Figure 7.5 when looking at the large groupings of erosion and deposition in area of interest inset map. The lighter shades of red and blue in the subtraction method indicate a decrease in reported change in comparison to the exclusion method. This is also quite apparent in the histograms of Figure 7.3; here the 14,327 ft^3 difference in reported net volumetric change can be seen when comparing the taller height of the larger values of both erosion and deposition in the exclusion method histogram to the subtraction method histogram.

7.3 Interpreting Output from a Geomorphic Change Detection Study

The change reported from a geomorphic change detection study can be broken down into areal, change as reported in ft^2, or in volumetric, change reported in ft^3, totals. Areal

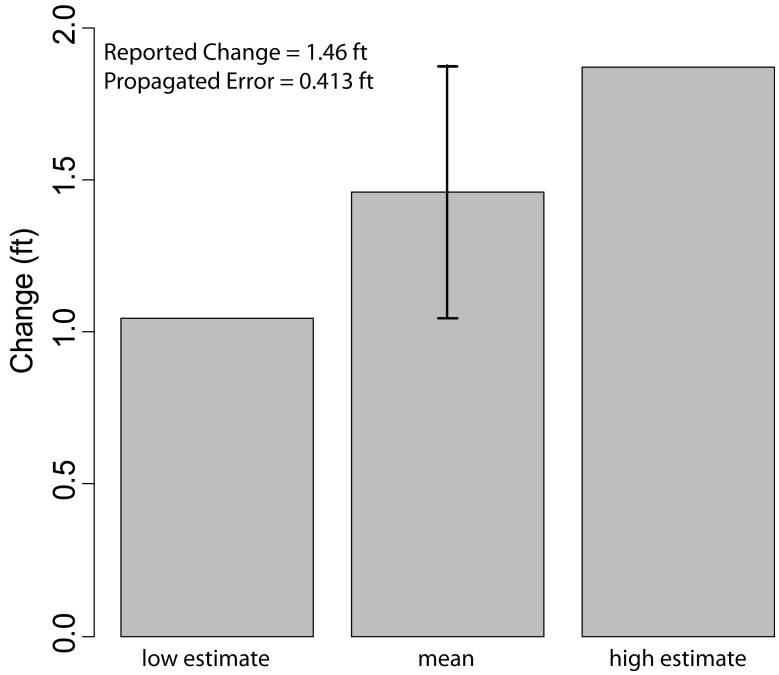

Figure 7.4. Example of propagated error in the exclusion method for one cell in a digital elevation model (DEM).

totals are the area of channel floor exhibiting change, number of cells multiplied by cell resolution, and volumetric totals are the areal total multiplied by the amount of change (z value) associated with each cell. To better characterize the phenomenon of sediment flux, areal and volumetric totals can be partitioned into groups of erosion or deposition totals. Additionally, as each cell has an amount of uncertainty associated with it, it is also helpful to report the amount of error in terms of volume. The Geomorphic Change Detection Software used to perform the analysis of Section 7.1 provides a table that is helpful in presenting this information. An example of this table is presented in Table 7.1. Table 7.1 is associated with the results of change detection to the 95% probabilistic threshold confidence using a FIS, Bayesian probability and the interpolation error term from Section which coincides with the bottom right of the comparison panes of Figures 7.1 and 7.2.

In the first row of Table 7.1 there are two 2 columns: Raw and Thresholded DoD. The Raw column reports the amount of change present in the system without removing any of

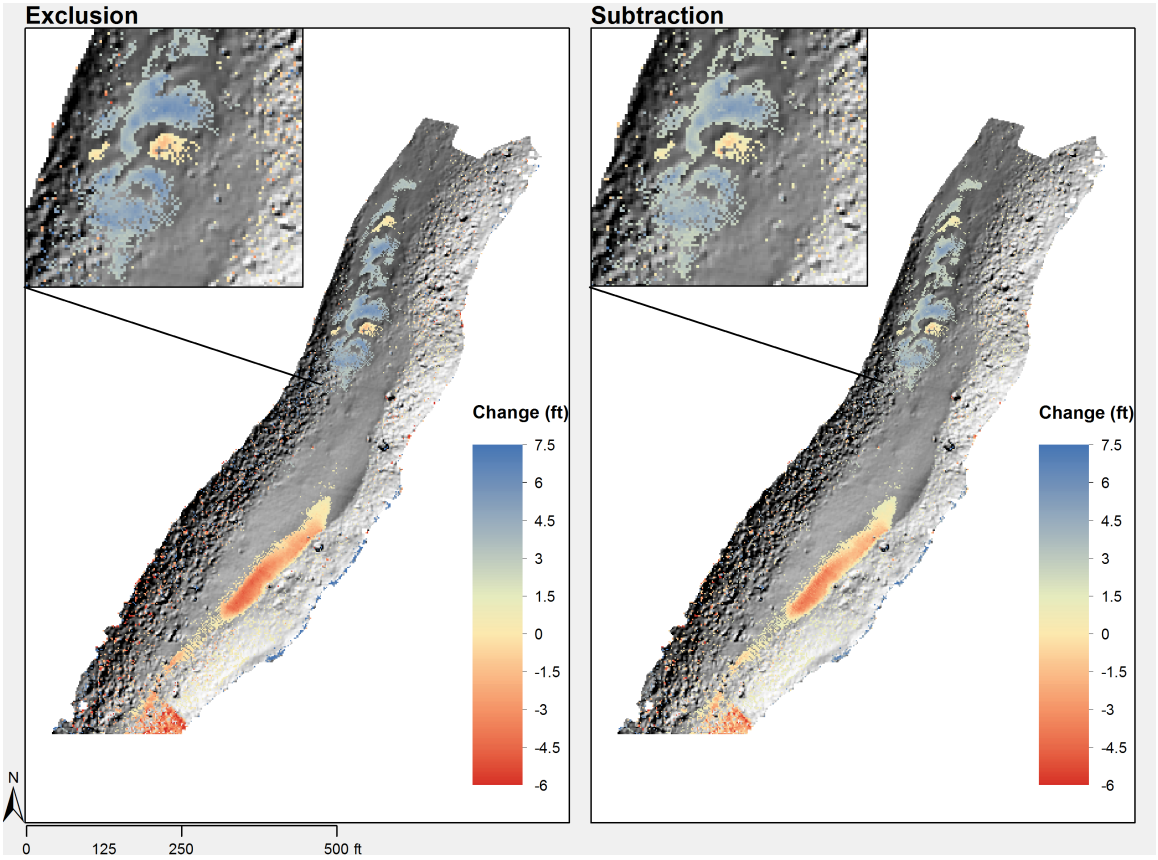

Figure 7.5. Spatial comparison of exclusion to subtraction methods of dealing with propagated error. Although subtle in this map the subtraction method reports much lower values of change when compared to the exclusion method as demonstrated by the lighter shades in the figure.

Table 7.1. Geomorphic change reporting table for the bottom right pane of Figures 7.1 and 7.2.

Attribute	**Raw**	**Thresholded DoD Estimate**		
AREAL				
Total Area of Erosion (ft^2)	150,816	66,192		
Total Area of Deposition (ft^2)	108,408	26,924		
VOLUMETRIC			± Error Volume	%Error
Total Volume of Erosion (ft^3)	77,788	43,272	± 73,817	171%
Total Volume of Deposition (ft^3)	59,126	24,525	± 12,330	50%
Total Volume of Difference (ft^3)	136,914	67,797	± 86,148	127%
Total Net Volume of Erosion (ft^3)	-18,663	**-18,747**	± **74,840**	-399%
PERCENTAGES (BY VOLUME)				
Percent Erosion	57%	64%		
Percent Deposition	43%	36%		
Percent Imbalance (departure from equilibrium)	-7%	-14%		

the noise associated with uncertainty of measurement values. Referring to this column is a good way to see quantitatively how much change has been removed from the DoD through probabilistic thresholding. The Thresholded column presents for erosion, deposition and net totals the amount of change reported after the survey noise due to uncertainty has been removed, the volume of uncertainty and the ratio between these two. Analysis of Table 7.1 reveals 43,272 ft^3 of erosion with 73,817 ft^3 uncertainty and 24,525 ft^3 of deposition with 12,330 ft^3 of uncertainty for a net volume of erosion of 18,747 ft^3 with 74,840 ft^3 of uncertainty. The uncertainty numbers are the sum of all uncertainty of the cells passing significance and partitioned by group. Having passed the probabilistic threshold generally the total volumes of erosion and deposition should be greater than the uncertainty volume. However, when a spatial coherence index is used, as is the case for the DoD presented in Table 7.1, it is possible to have higher uncertainty volumes than volume of erosion or deposition because the spatial coherence index returns cells to the final reporting that would not have passed the probabilistic threshold based on their values alone. Referring to Figure 7.4 it was shown that through the exclusion method each cell represents a range of potential values but the mean is reported; for example the cell from Figure 7.4 has a reported change

of 1.46 ft. with 0.413 ft. of uncertainty. The reported uncertainty volumes from Table 7.1 represent the potential shift if every cell in the analysis was reported as its minimum value or its maximum value. Although a larger net uncertainty volume than net difference volume means that the sediment budget for a reach is indeterminate due to survey noise, it does not mean that there is not meaningful statistically significant change occurring in the reach. It is understandable as to why change at a reach scale would be indeterminate as the majority of meaningful change involves smaller scale features. Many of the smaller scale features of sandbars and scour pools will still be statistically meaningful change.

To isolate these smaller scale changes and provide a closer look at the type of change occurring within a reach it is possible to segregate a sediment budget based on polygons of specified features, landforms, flow regimes, or any other attribute of interest. While an overall sediment budget may be indeterminate segregating the budget in this way can reveal a more robust and insightful view of geomorphic change within a reach.

In addition to reporting volumetric totals Table 7.1 also reports the percent of the total geomorphic change budget that erosion and deposition make up. Before probabilistic thresholding it can be seen that the system was exhibiting slightly more erosion (57%) than deposition (43%), while probabilistic thresholding led to an increase in the reported erosion to 64% and decreased deposition to 36%. However, when a budget has been shown to be indeterminate, as in this reach, these numbers are much less meaningful and more emphasis should be placed on the change occurring in small scale features.

Section 8

Workflow Recommendations

By working through a geomorphic change detection study a basic workflow has been established that is comprised of six basic steps:

1. Determine sampling resolution
2. Determine grid resolution
3. Create an interpolation error grid
4. Create survey uncertainty grids
5. Create a FIS
6. Difference DEMs to 95% confidence using probabilistic thresholding and a FIS, Bayesian updating and an interpolation error term.

The determination of sampling resolution helps the user determine what level of detail that can be captured by the survey and the amount of support that the survey provides at different cell resolutions. Determining a cell resolution of analysis based on sampling resolution and preforming an information sensitivity loss analysis ensures that a desired amount of information obtained in the survey is retained in future raster calculations. This is a compromise of computational capacity and desired information retention. The creation of an interpolation grid quantifies the inability of interpolation techniques to correctly model abrupt changes in the landscape. The creation of survey uncertainty grids seeks to quantify the spatially varying effect that landscape attributes, like surface roughness and slope, have on the ability of multi-beam SONAR to capture accurate measurements. The implementation of a FIS to a 95% probabilistic threshold confidence level provides structure to combine the interpolation error and survey uncertainty grids into a coherent rule-driven system of propagated uncertainty. The addition of Bayesian probability allows for the integration of

observed spatial patterns that exist in erosion and deposition.

These steps were developed with the idea of limiting and quantifying uncertainty by including emerging concepts from geomorphic change detection literature and best practice methodology. The result is a DoD with a quantified uncertainty term and a method of expressing the statistical likelihood that change in a river system is real or indeterminate due to survey noise.

Section 9

Discussion

The methods discussed in this paper, particularly the implementation of probabilistic thresholding, use of a FIS to quantify and propagate uncertainty, and updating of probability based on Bayesian probability, provide some of the most advanced methods of realistically analyzing and presenting geomorphic change detection study results. However, there are a number of shortcomings of these methods that should be addressed.

These methods currently only focus on vertical inaccuracies while horizontal inaccuracies are generally thought to be negligible. This concept may be true in more traditional survey techniques; however, horizontal inaccuracies are an issue with MBES. Horizontal inaccuracies have the potential to influence the results of a change detection study as much as vertical inaccuracies. An example of this can be seen in row 2 of Figure 4.5 where a large boulder and break in slope has large vertical differences (>10 ft.) over less than 1 horizontal ft. Depending on the magnitude of a horizontal inaccuracy in this situation, a surveyed point could contain more than 10 ft. of uncertainty due to the large relief over such short horizontal distances. To fully deal with the uncertainty in an MBES horizontal uncertainty must be addressed.

In general, the discussed methods in this paper only discard small geomorphic change but there is no method to discard large geomorphic change. While the interpolation error term somewhat addresses this, there are still blatantly large values ($\pm$10 ft.) of change present in the final result. This is mainly due to the way that the t-score is calculated in Equation 6.2 from Section 6.2.1. In this equation if change is significantly large and the FIS modeled uncertainty is not significantly large (which is difficult to design a FIS to represent adequately high uncertainty values for rare occasions as was shown in Section 6.3.3 than due to this it will be considered to be statistically significant change. A method to question

unusually large geomorphic change would improve the methods. Ideally this could be dealt with in the initial equations of probabilistic thresholding or using Bayesian probability updating.

The concept discussed in Section 6.2.3, that deposition tends to occur in large groups of lower level amounts than erosion which tends to be more spatially unique, may not hold true for large river environments such as Hells Canyon. More research needs to be done observing this phenomenon in multiple types of river environments to confidently apply it to all river systems. Additionally, in previous literature explaining the concepts behind the spatial coherence index (Brasington et al., 2003; Wheaton et al., 2010) erosion and deposition are described as separate phenomenon but are treated in the same manner by a spatial coherence index. Developing distinct algorithms for each may improve the application of the spatial coherence index.

In Section 5.1 and Figure 5.2 the influence of beam angle on accuracy of survey measurements is discussed, but a method to quantify its effect on uncertainty is never presented. This information is crucial to quantifying uncertainty in a multi-beam survey and is blatantly lacking. This specific information or a proxy for it needs to be included in a FIS or form similar to the interpolation error surface to correctly account for uncertainty specific to MBES.

The strategy to overlap several passes used in the data collection of this experiment can have an adverse effect on the end product in GIS. Although this surveying strategy is a method of providing better coverage of the river bed, the beam footprint collection style of MBES and overlap in beam footprints due to overlap in survey may result in a smoothing of the actual surface. This phenomenon will be more pronounced at greater depths and could have little effect at shallow depths where beam footprints are quite small (<1 ft^2).

Section 10

Conclusion

This paper has detailed a coherent context for estimating sample resolution, determining cell resolution of analysis, identifying proper interpolation techniques, quantifying interpolation and survey uncertainty, integrating a fuzzy inference system, and Bayesian probability updating specifically geared towards a geomorphic change detection study derived from a multi-beam SONAR survey. The result is a workflow aimed at limiting and quantifying survey, surface, and processing uncertainty.

The presented workflow moves geomorphic change detection by repeat MBES survey away from simple minimum levels of detection and towards a spatially variable uncertainty model. The discussion and statistical analysis of data collection methods and spatial attributes specifically influencing MBES measurement uncertainty highlights spatially quantifiable relationships between uncertainty and these variables. Uncovering these relationships provides the building blocks for a FIS to construct a spatially variable uncertainty model.

The application of probabilistic thresholding by propagating uncertainty through a FIS provides more robust results reporting than basic change detection studies. The results better quantify the spatial variability of uncertainty and provide a context for communication of geomorphic change based on probability that is more intuitive to a layman than the concept of survey noise and indeterminate geomorphic change.

Appendices

Appendix A
Overview of SONAR Basics

A.1 Data Collection with SONAR

MBES was developed with the main purpose of producing accurate depth measurements of underwater environments. To accomplish this it must produce depth measurements which are consistent with locations on the water-body floor and produce these measurements in a sensible amount of time (L-3-Communications-SeaBeam-Instruments, 2000). The basics of how this is accomplished are detailed in this section. For a more technical and complete explanation of this refer to the users manual of specific MBES systems or refer to L-3 Communications SeaBeam Instruments (2000), Beaudoin (2010), and Diaz (2000).

The process of measuring depths using SONAR technology can be divided into four stages: ping generation, propagation, echoing and reception. Ping generation is the process of creating a sound wave, known as a ping, through a projector. A projector is a device that creates a sound wave in water and in SONAR systems allows the user to precisely control the characteristics of the sound wave.

The next stage is the propagation of the sound wave through the water. Sound travels as a compression wave through water at the local speed of sound. In a typical ocean environment the local speed of sound is 1500 m/s with variations depending upon temperature, salinity and pressure. This variation in the speed of sound in water requires the use of a sound speed profiler to adjust the measuring equations of the multi-beam system.

The local speed of sound can be determined by the equation:

$$Speed of Sound = \nu \times \lambda \tag{A.1}$$

where ν is frequency, described as the number of peaks that pass a specific point in a unit of time and λ is wavelength, which is the distance between peaks or pressure fronts in a propagating sound wave. When a change in temperature, salinity or pressure occurs the wavelength is changed but the frequency remains the same, because of this frequency is used to describe sound waves. As a sound wave propagates through water it losses some of its energy, this is known as attenuation. The amount of attenuation is dependent upon the frequency; low frequencies attenuate very little while high frequencies attenuate quite rapidly. This attenuation affects how far the sound wave can travel and thus how deep of a floor it can detect. The shorter travel distances required of sound waves in shallow water allow for higher frequencies to be used.

The next stage in SONAR is echoing. When the propagation of the sound wave is impeded by another object, ideally the water-body floor but potentially a fish or other object, the portion of the sound wave not absorbed by the object, known as an echo, is scattered in all directions. Of this, an important portion is directed back towards the source of the sound wave in what is known as the angle of incidence. The energy returned in the form of an echo maintains the frequency of the source sound wave. The echo returning via the angle of incidence is then used to determine the distance of the obstructing object to the boat. Echoing is visually depicted in Figure A.1. An amount of energy is absorbed by the object struck by the echo which is described by a property known as impedance. Different surfaces and materials have unique impedance factors, as will be discussed in Appendix A.2, and this has implications for the acoustic backscatter.

The final stage of the SONAR process is known as reception. To measure the depth at a particular location, also known as the range to the bottom, a device known as a hydrophone is used. A hydrophone converts the oscillations of the received echo into an electrical signal. Through this conversion the hydrophone measures the time between ping generation and the return of its echo via the angle of incidence to determine the range to the bottom. This

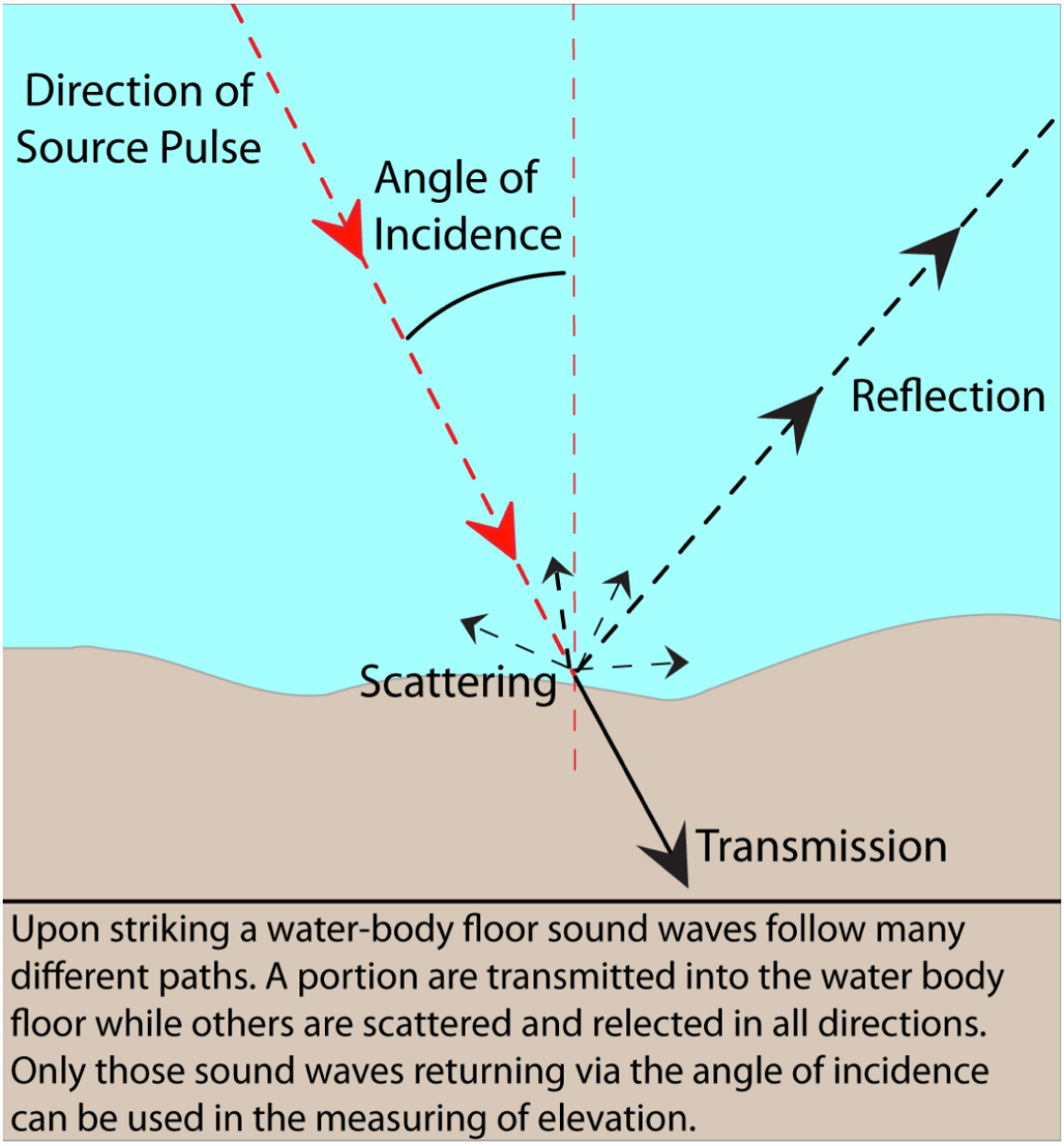

Figure A.1. Depiction of the behavior of a sound wave after it has struck the water-body floor. (Adapted from L-3 Communications SeaBeam Instruments, 2000).

can be expressed by the equation:

$$Range = 0.5 \times v \times echo\ time \tag{A.2}$$

where 0.5 is used to account for the sound wave traveling to and from the boat, v is velocity and is the local speed of sound, and echo time is the total amount of time it takes the sound wave to travel from the boat and back. When a depth measurement is achieved for an area of the water body floor that portion of the floor is said to have been ensonified.

A.2 Acoustic Backscatter

As was briefly mentioned in Section A.1 when a ping hits an object an amount of energy is absorbed by the object. The amount of energy that is absorbed by an object is unique to the type of material or surface and has an effect on how the energy is scattered as well as the amount of energy that is ultimately returned to the hydrophone in the form of an echo. Known as acoustic backscatter, the unique signature that a particular object imparts upon the echo due to absorption of energy into the object and scattering patterns creates measurable differences in the backscattered energy. These noticeable differences can be used to classify the substrate into different materials. This concept is similar to using aerial or satellite remote sensing signatures to classify vegetation or rock type. Classifications of water bottom material as sand, mud, clay, cobble, etc. are possible from acoustic backscatter measurements.

The amount of energy reverberated back into the echo is generally referred to as the backscatter coefficient. The physical properties of the water body floor, grain size, density and seafloor roughness are the main factors in determining the coefficient with the velocity of the ping also having an influence. This coefficient is used to describe the amount of scatter that occurs when a ping is echoed off of an object. For example a flat surface will

tend to cause less scattering than a rough surface.

Although it is a relatively new method of using MBES, the use of acoustic backscattering to classify water body floors is a powerful tool in bathymetric mapping. Bottom material has a direct influence on MBES and its ability to provide accurate vertical measurements. Beyond improving the visualization of an underwater surface, classified acoustic backscatter has the potential to be used as surface roughness models because of the different reflective characteristics of substrate. Surface roughness plays a crucial role in estimating vertical measurement uncertainty in an MBES and advanced methods of obtaining metrics of it are valuable for bathymetric mapping and scientific applications.

Appendix B

Overview of Interpolation

B.1 Interpolation Techniques

Interpolation techniques fall into two main categories: deterministic and geostatistical. Deterministic methods rely on mathematics and operate in a set algorithm for every input dataset regardless of its unique characteristics. Geostatistical methods use statistics to integrate spatial relationships and characteristics within the input dataset to create a final interpolated surface. The application of geostatistical techniques is a more data-driven method of interpolation. Important to geostatistical techniques is the concept of spatial autocorrelation, the tendency of nearby objects to vary in concert (Bolstad, 2008; Johnston et al., 2001). To better distinguish between the two methods and analyze the validity of specific interpolators a brief review of interpolation techniques commonly used in geomorphology and DEM creation is presented.

The interpolation methods included in this review are inverse distance weighting (IDW), multiquadratic radial basis function (MRBF), regularized spline with tension (RST), ordinary kriging (OK) and universal kriging (UK). All of these techniques are exact interpolation techniques, they honor the actual survey point values, which is one of the main reasons they are recognized as acceptable interpolation techniques for creating DEM.

Inverse distance weighting is one of the simplest deterministic interpolation methods. It assigns values to unmeasured locations by averaging a user defined number of locations and places the highest weight on values closest to the unmeasured location. The equation is defined as:

$$Z_j = \frac{\sum_i \frac{Z_i}{d_{ij}^n}}{\sum_i \frac{1}{d_{ij}^n}} \tag{B.1}$$

where Z_j is the value at the unmeasured location j, d_{ij} is the distance from known point i to unknown point j, Z_i is the value for the known point i, and n is a user defined exponent used to increase or decrease the influence of distant points. Increasing n reduces the influence of distant points. It is generally accepted practice to use values of 1 to 3 for n (Aguilar et al., 2005). In GIS software this equation is usually performed on a search window of 3 x 3 map unit but in practice could be run on any user defined neighborhood or set of points. IDW is an exact interpolator as equation B.1 reduces to Z_i at a measured location (Bolstad, 2008).

IDW is a widely used interpolation method because of the few user defined model parameters and as in all deterministic techniques no assumptions are required of the data. Using IDWs equation B.1 limits the minimum and maximum values to surveyed points only. Values decrease or increase with distance away from the maximum or minimum respectively. When using IDW it is important to recognize that it is sensitive to outliers because it must honor the surveyed values and it has the potential to produce bulls eye relics in the interpolated surface.

Multiquadratic radial basis function and regularized spline with tension are both part of a group of deterministic interpolation techniques known as radial basis functions. These functions have been compared to the fitting of a rubber membrane to the measured values, meaning that they must pass through all surveyed points but have a great deal of freedom as to how they bend to create the surface at unmeasured points (Johnston et al., 2001). In contrast to IDW radial basis functions can predict maximum and minimum at unmeasured values; this is shown in Figure B.1. Radial basis functions are reliable interpolators when interpolating elevations that have gradual changes. However, they do not perform well when large variations occur over short distances. The key parameter to radial basis functions is the kernel parameter which controls how smooth the interpolated surface will be, the higher

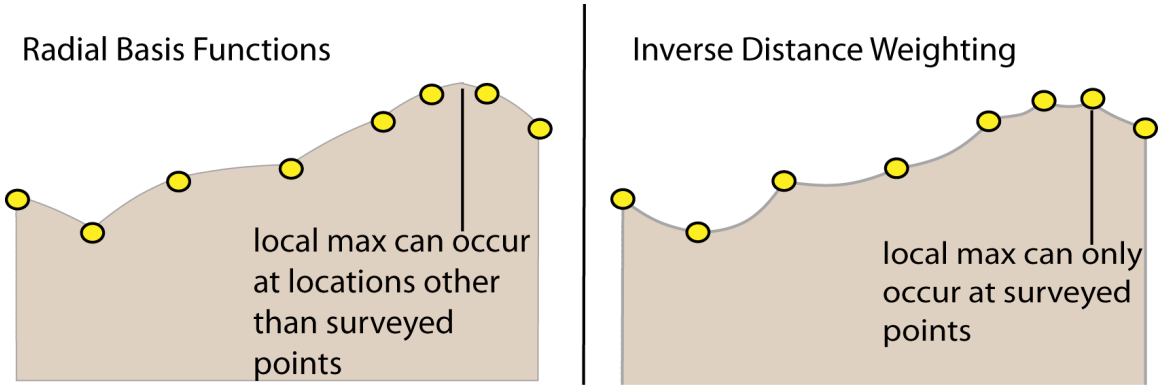

Figure B.1. Comparison of interpolation with radial basis functions (RBF) and inverse distance weighting (IDW). Local maximum can occur at unsurveyed locations in RBF but can only occur at surveyed points in IDW (figure adapted from (Johnston et al., 2001)).

the kernel parameter the smoother the output surface will be. Generally there is little difference between output surfaces of the different radial basis functions (Johnston et al., 2001).

Ordinary kriging and universal kriging are both geostatistical methods and differ only in the assumptions they place on the data before applying geostatistical techniques. To better understand these kriging methods it is helpful to outline concepts of geostatistical methods before detailing each kriging technique specifically. As previously stated, geostatistical methods make statistical inferences about the input data in order to interpolate it uniquely. These methods make predictions for random processes that have spatial autocorrelation or what can be thought of as rules of dependence. For DEM these rules of dependence are in essence the geomorphic principles locally simplified into mathematical relationships. In a basic sense the task of geostatistics is to uncover the spatial autocorrelation (rules of dependence) and to make predictions based on them. To do this there are a number of tools that exist within geostatistics, specifically semivariogram and covariance functions as well as generalized linear regression. Semivariogram and covariance functions are used to determine the spatial autocorrelation (in a process known as variography) while generalized linear regression is used to predict unknown values.

Important to variography is the concept of stationarity which is the idea that predictions can be derived and uncertainty estimates for the predictions can be understood by repeated observations (i.e. there are patterns that exist within the data that are uncovered through continued observation). Stationarity forms the basis for three important ideas in geostatistics: mean stationarity, second order stationarity, and intrinsic stationarity. Mean stationarity is the idea that through these repeated observations the mean is constant between samples and is independent from location. Second Order stationarity and intrinsic stationarity assume that covariance and variance, respectively, are the same between any two points that are the same distance and direction apart regardless of direction. These assumptions are what allow geostatistical techniques to uncover the spatial autocorrelation, if any, contained in the data.

Ordinary kriging and universal kriging are quite similar, the main difference being that ordinary kriging assumes an unknown constant mean while universal kriging assumes a known mean and uses a 2nd order deterministic function to estimate the mean. One of the main advantages of kriging methods over deterministic methods is it provides an estimation of error for interpolated point. Additionally if measurements in the dataset occur at the same location kriging is able to give an estimate of measurement error for the data.

B.2 Triangulated Irregular Networks (TINs)

One of the most commonly used methods of interpolation when creating a DEM is the triangular irregular network (TIN). This method uses three vertices of x,y,z sets to create a surface based on triangles. The sampling points are linked to their neighbors by straight lines to create triangles that do not contain any of the vertices. TINs are an exact interpolator and when an extent is adequately surveyed can be considered a local interpolator. However, when an insufficient number of surveyed points are available a TIN will interpolate over large distances. This generally occurs in TINs along the edges. A strong disadvantage to TINs is the inability to perform common calculations on them that

are easily performed on rasters. For this reasons a TIN often serves as an intermediate piece of data to be used to edit the surface by removing erroneous points and creating a realistic extent of the channel. Due to the high point density of MBES data, which results in little difference between interpolation techniques, and the inability to perform calculations on TINs they will not be used in this study.

Appendix C

Overview of Probabilistic Thresholding

Due to the lack of direct verification of elevation measurements resulting from surveying sub-aqueous surfaces, statistical estimation of uncertainty is required. This statistical estimation is governed by the laws of probability and is represented by Equations 6.1, 6.2, and 6.3. The combination of these equations is used to model the distribution of uncertainty for each cell within a geomorphic change detection study. The propagated uncertainty calculated in Equation 6.1 is an estimation of the standard deviation of the distribution of uncertainty for each cell. By assuming the uncertainty in each raster cell is random and independent, the standard deviation can be used to create a normal distribution centered on zero. An example of using these equations to compute the standard deviation to model a normal distribution for uncertainty is shown in Figure C.1.

In this study computing the 95% probabilistic threshold level is equivalent to computing the threshold value to which 95% of the uncertainty values would be contained. To compute a 95% probabilistic threshold (Equation 6.3) the standard deviation of uncertainty (result from Equation 6.1) is multiplied by 1.96, the standard value for computing the threshold for which 95% of values would lie within the mean. This distribution and 95% threshold is shown in Figure C.2. To compute a different probabilistic threshold the Standard T-Distribution Critical Values Table is referred to. The comparison of different critical t-scores and their effect on the critical threshold error are shown in Figure C.2. By viewing these values it can be understood that lowering the probabilistic threshold level is synonymous with lowering the critical threshold error. By viewing the differing critical t-values it can be understood that the sensitivity of changing the probabilistic threshold level is a simple linear relationship that increases linearly with increasing propagated uncertainty. For example the difference between the critical threshold error for a propagated uncertainty of 0.2496 ft. at 95% and 80% threshold levels is 0.07875 ft. While when a higher propagated

uncertainty of 2.5 ft. is used the difference between 95% and 80% threshold level is 0.7875 ft.

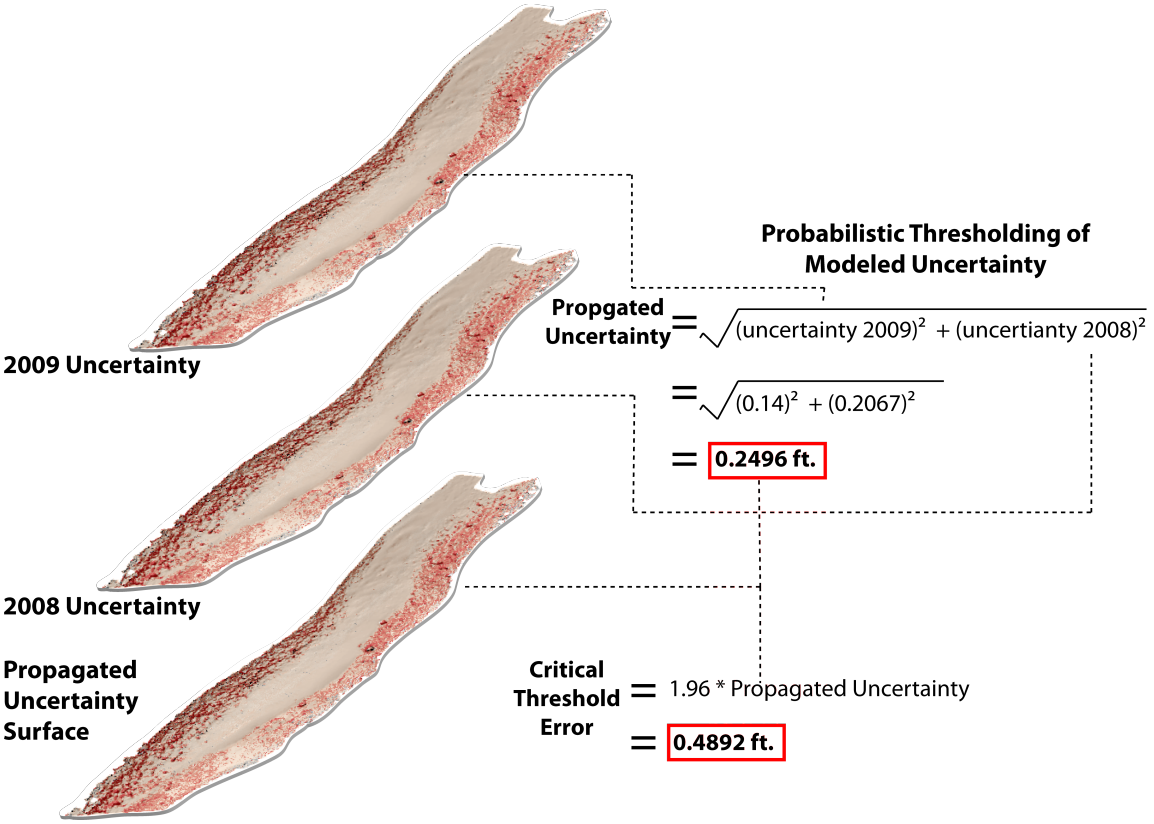

Figure C.1. An example of computing the probabilistic threshold at 95% for a single cell.

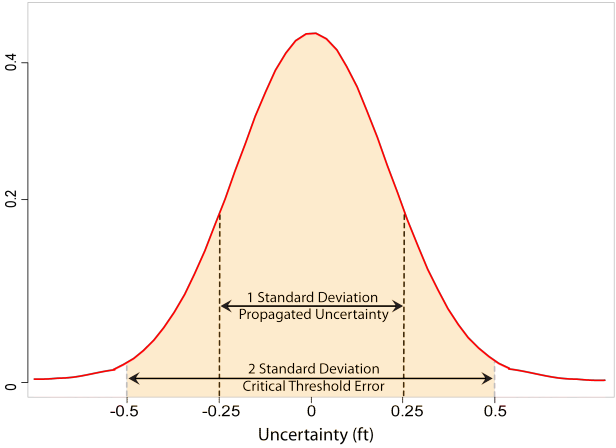

Comparing Probabilistic Thresholding Values for 0.2496 ft.		
Threshold Level	Critical Threshold Error (ft)	Critical T-Value
99%	0.640	2.576
95%	0.489	1.960
90%	0.411	1.645
80%	0.319	1.282
70%	0.259	1.036
60%	0.210	0.842
50%	0.168	0.674

Figure C.2. Example of the normal distribution computed at a 95% probabilistic threshold for a propagated uncertainty value of 0.2496 ft. The table within this displays the different critical t-values, which are independent of propagated uncertainty, and their effect on the critical threshold error.

Appendix D

Overview of Fuzzy Inference Systems

Fuzzy inference systems are a method to deal with ambiguity in parameters seen in many real world problems. They are applied in a wide variety of fields with documented applications in environmental impact assessments, geology, engineering and many others (Ross et al., 2002; Shepard, 2005). The main building blocks of a FIS are fuzzy sets, fuzzy membership functions, fuzzy operation methods, rule implication methods, aggregation methods and defuzzification methods. This section will explore these concepts in more depth.

The basic unit to a FIS is the fuzzy set. Examples of fuzzy sets are shown in Figure D.1. The domain or universe of discourse, which is represented by the x-axis, defines all possible values for a variable. The support set, also on the x-axis, is all possible values that can have a degree of membership to the fuzzy set. The y-axis in Figure D.1 is the degree of membership to the fuzzy set. A values position in relation to the shape of the fuzzy set determines its degree of membership to that fuzzy set, similar to a function in classical mathematics.

There are four main shapes that fuzzy sets take on: triangular, trapezoidal, Gaussian bell-shaped and singleton. The slope of the lines that make up the sides of the fuzzy set are the fuzzy membership function and provide a means to determine the degree of membership a value has in that set. Specifically steep slope would represent an exclusive fuzzy set with few values having high membership while a gradual slope is more inclusive and may have many values that have high degrees of membership. For example a triangular shape represents a phenomenon that has one ideal value and depending on the degree of slope of its sides will decrease in degree of membership rapidly with steep slopes or more gradually with more gradual sloping sides. While the presence of a horizontal line at the top of a trapezoid means this membership function has a larger range of values that can have full

membership when compared to a triangular membership function. The Gaussian bell-shape is similar to the trapezoidal membership function but has a sharper decline from the high grade membership values. A singleton is a special membership function represented by a vertical line; it has one value that defines its support set and is said to function as a crisp value within a fuzzy logic system (MathWorks, 2013; Shepard, 2005). These concepts are visually explored in Figure D.1.

The examples in Figure D.1 represent one fuzzy set. However, as in this study, a parameter is generally made up of many groups of fuzzy sets, each with their own support sets, which define the complete domain for the parameter. This concept is shown in Figure D.2. This figure also explores the idea that fuzzy sets allow for partial degrees of membership to different fuzzy sets when overlap occurs with another fuzzy set within the same domain. Partial membership is a key feature of fuzzy logic and naturally combines with concepts of ambiguity in parameters.

A basic FIS can function to help define a single parameter in more ambiguous terms that can often be more intuitive when classifying complex parameters as is demonstrated in Figure D.2. But more frequently a FIS is used to relate multiple parameters that have been classified into fuzzy sets and combine the relationships between these fuzzy sets into final output fuzzy sets. To accomplish this fuzzy operators, implication methods, and aggregation methods are used. Fuzzy operators relate the parameters to one another. The most frequently used fuzzy operators are the Boolean logic operators AND and OR. Fuzzy operators form the first clause in FIS rules statements, known as the antecedent, that establish relationships for how parameters are related. An example antecedent is if surface roughness is medium and slope is low. Implication methods form what is known as the consequent of a FIS rule and close out the antecedent by using basic mathematical functions to create new fuzzy sets for each applicable rule created. There are four main implication methods to apply rules: minimum, product, maximum, and probabilistic. Minimum and

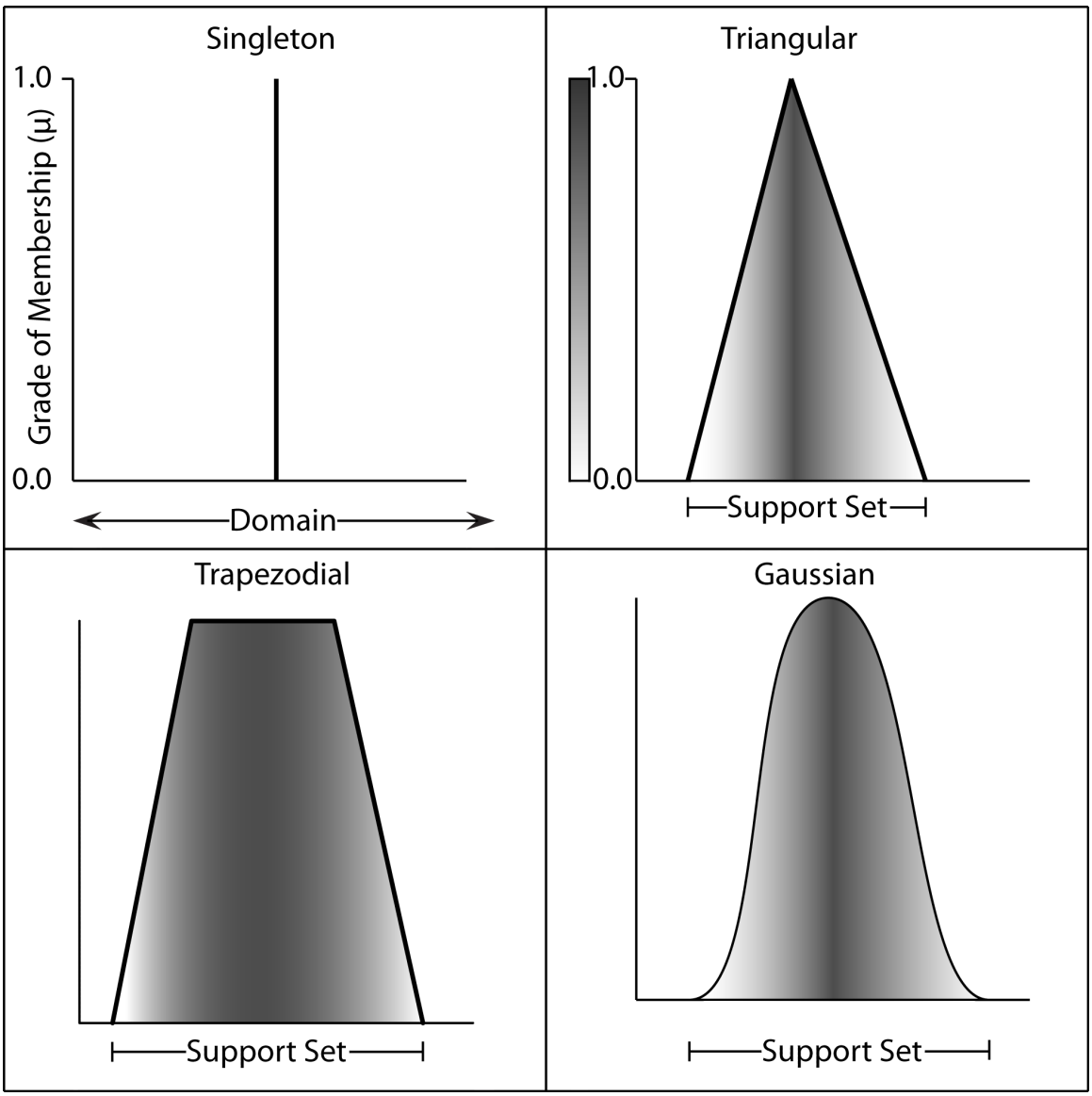

Figure D.1. Basic fuzzy sets & membership functions: Singleton, Triangular, Trapezoidal, and Gaussian. The ranging shades of gray represent different degrees of membership to the fuzzy set. The slopes of lines of each shape are the membership functions for each set. Comparing the triangular to trapezodial it the angular nature of the triangle makes it a more exclusive membership function.

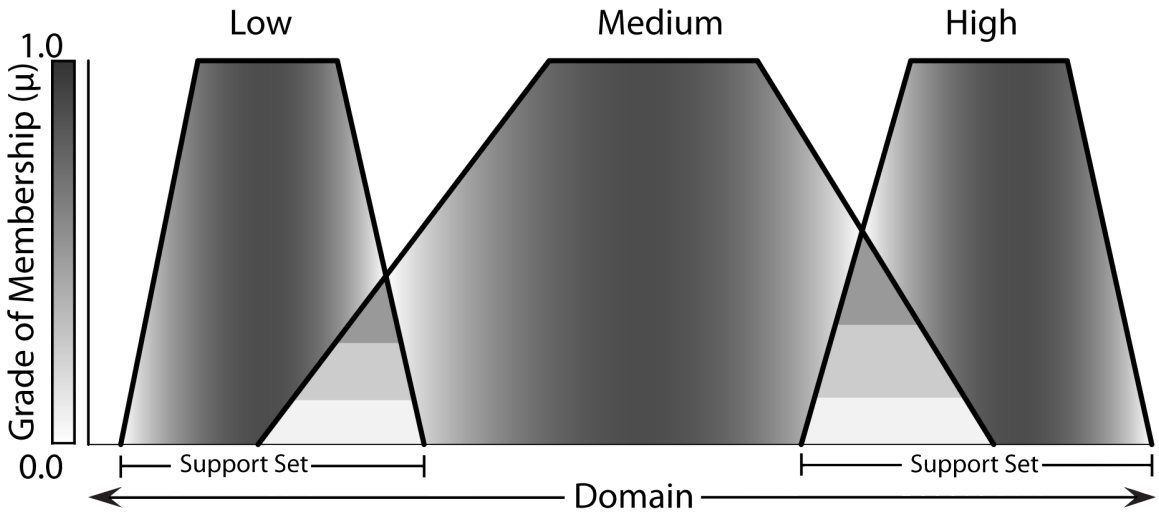

Figure D.2. The entire domain of a parameter is classified by three fuzzy sets in this figure. Varying shades of gray represent degrees of membership to a particular fuzzy set while the vertically striped regions are areas where overlap in fuzzy sets exists, meaning values occurring in this region have degrees of membership with two fuzzy sets.

product apply to the 'AND' operator while maximum and probabilistic apply to the 'OR' operator. Minimum simply takes the minimum of the input membership values while the product multiplies the membership values to compute its output. The maximum operator takes the maximum value of the input membership values. The probabilistic method adds the input membership values and from this subtracts the product of the input membership values. Application of the fuzzy operators in combination with rules implication places the parameters into new degrees of memberships to the output fuzzy sets. An example of this is visually explored in Figure D.3.

Due to the concept that a particular value can have degrees of membership in multiple fuzzy sets, many FIS rules can apply to the given inputs. To handle this, a FIS uses aggregation methods to combine all fuzzy sets created from the implication methods to create a final consequent fuzzy set. There are three main types: maximum, probabilistic and sum. The maximum method takes the maximum of each degree of membership and combines them. The probabilistic method acts as it did when used as an implication method, it adds all degrees of membership and from this subtracts their product. The sum adds all degrees

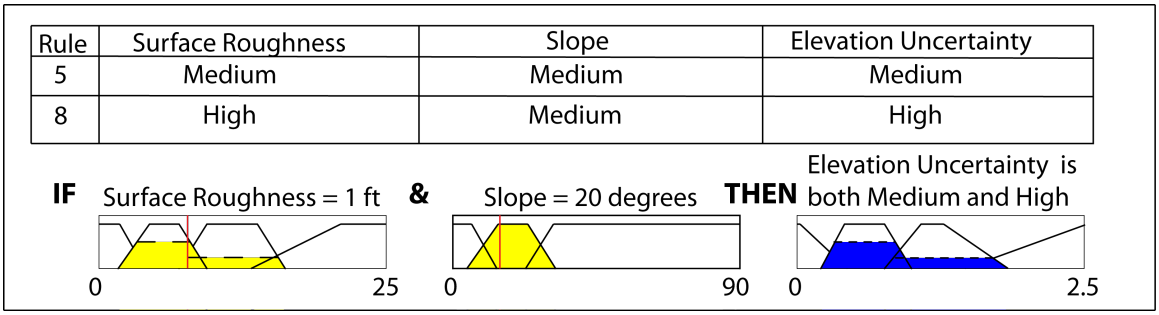

Figure D.3. In this figure the & fuzzy operator is combined with the minimum implication method to derive a membership to the output uncertainty fuzzy sets. The surface roughness value of 1 ft. has membership in two groups, medium and high which results in the application of two rules, rules 5 and 8, from the FIS.

of membership to create the final output fuzzy set. This concept is explored in Figure D.4. All of these aggregation methods create a range of values that need to be converted into a final single value, this is accomplished through defuzzification.

The final step is the conversion of the aggregated fuzzy set into a single value known as defuzzification. There are five main options for defuzzification: centroid, bisector, middle of maximum, largest of maximum, and smallest of maximum. Middle of maximum, largest of maximum and smallest of maximum are all quite similar; they identify the maximum or highest degree of membership in the output fuzzy set and define the final value as the vertical middle value, largest value and smallest value respectively. If there is only maximum within the final output fuzzy set then the middle of maximum, largest of maximum, and smallest of maximum will all defuzzify to the same value. The bisector method outputs the value that if a vertical line were drawn from it would divide the region into two equal area sub-regions. The centroid method is the most widely used defuzzification method. It takes the aggregated fuzzy set and finds a center of mass to calculate the final single value (MathWorks, 2013; Shepard, 2005). The bisector and centroid methods are quite similar and generally their output is quite similar and can often be the same value. These defuzzification methods and a comparison of their final output are presented in Figure D.5.

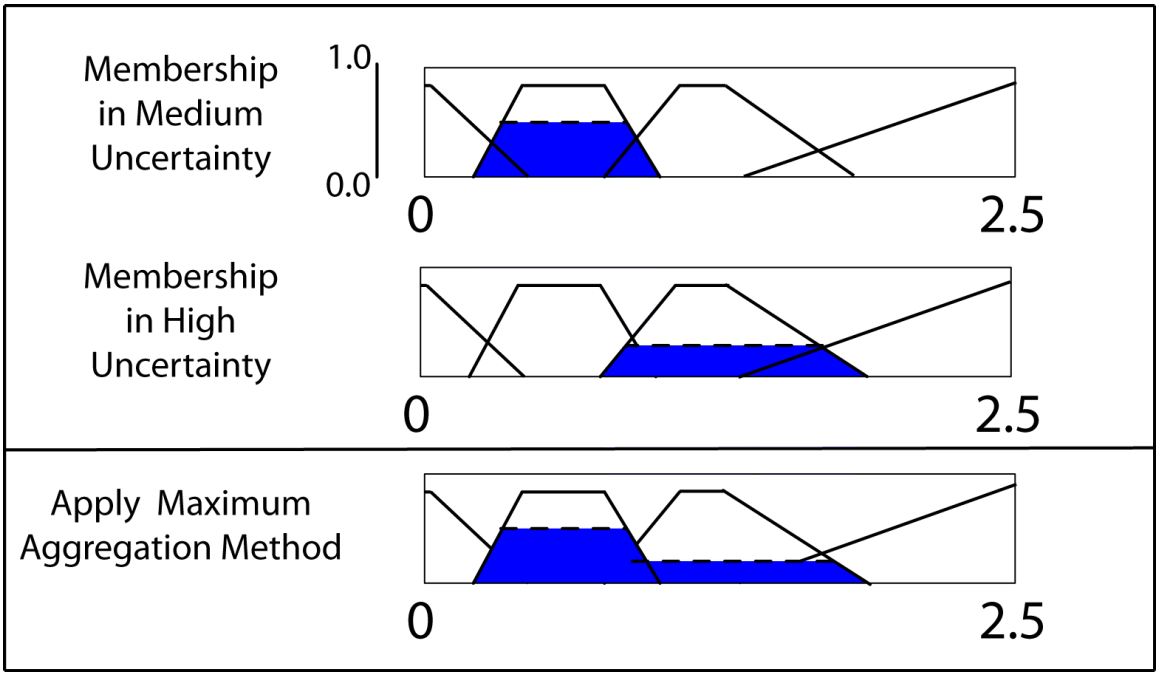

Figure D.4. The maximum aggregation method is used to combine a membership in two output fuzzy sets. The result is a final value that spans the range of both the medium and high groups. A defuzzification method is used to convert from these ranges of values to a single output value.

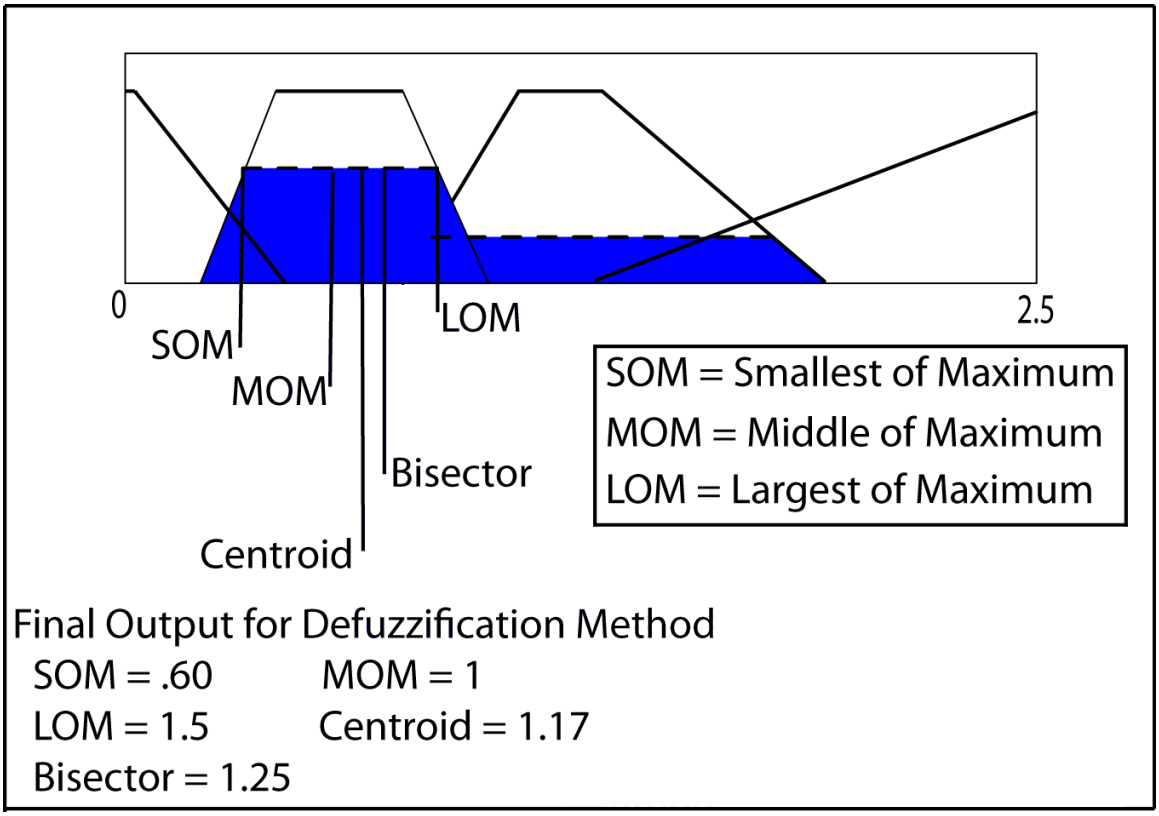

Figure D.5. This figure presents the five defuzzification methods: smallest of maximum, middle of maximum, largest of maximum, centroid, and bisector. The output value of each method coincides with where the vertical lines intersect the x-axis. Quite a bit of variation is seen between the different methods; however, the two most commonly used methods, centroid and bisector, are fairly close in their final output (figure adapted from Matlab Fuzzy Logic Toolkit online documentation).

Defuzzification is the final step of using a FIS as the final value is in a single value that can be more easily used rather than a range of values or an ambiguous understanding of a value. The main pieces of a FIS; a fuzzy set, membership functions, fuzzy operators, implication methods, aggregation methods, and defuzzification methods have been presented in this section. To connect all of these concepts in a fluid example all of these pieces are presented in the context of a functioning FIS used in a geomorphic change detection study in Figure D.6. The purpose of this FIS is the same as in this paper: to provide a structure to quantify the spatial parameters of slope and surface roughness and their influence on the final uncertainty of a surface produced from surveying under these conditions.

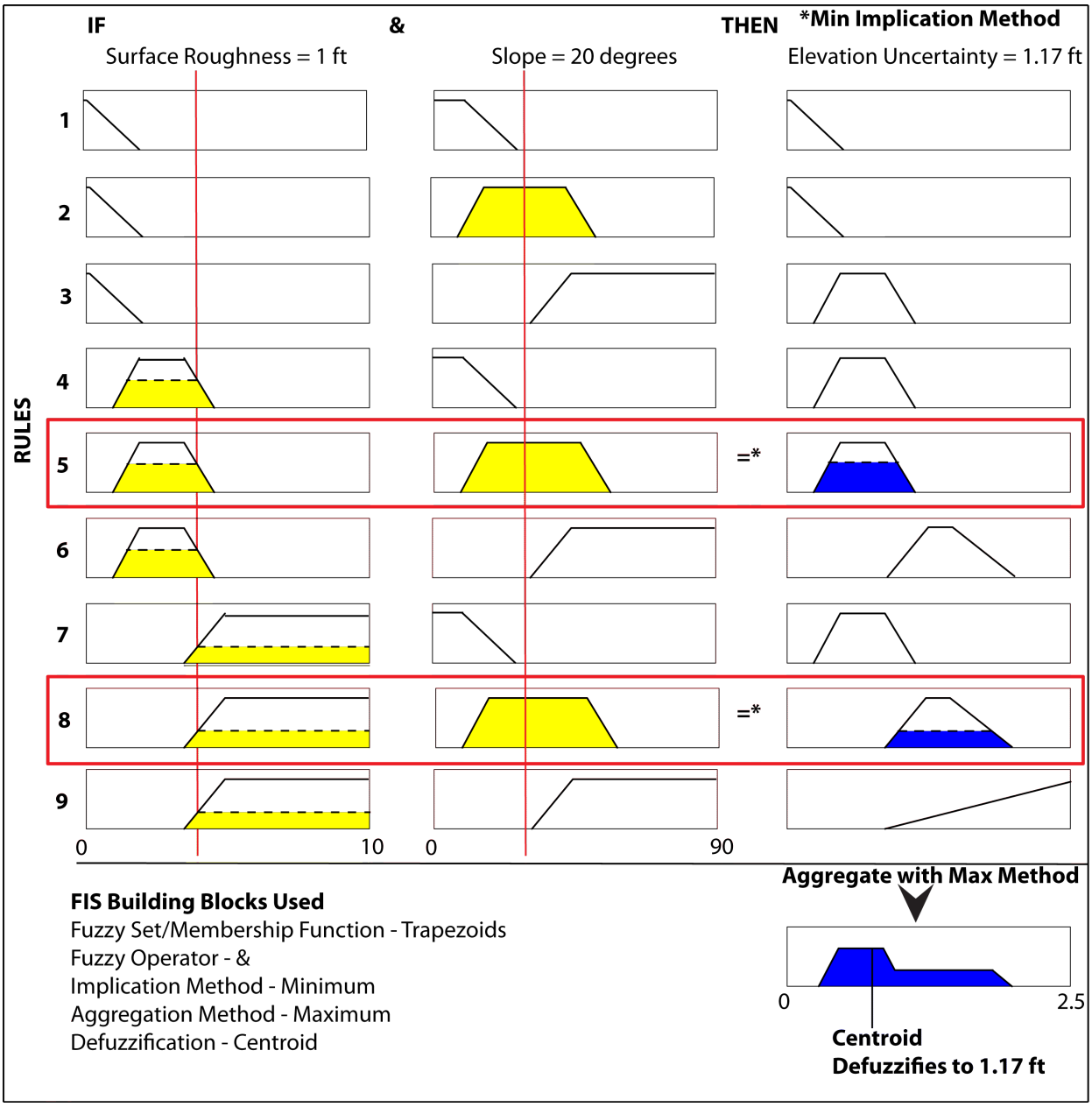

Figure D.6. A fully functioning fuzzy inference system (FIS) to relate surface roughness and slope and how they influence surface uncertainty in digital elevation models (DEMs) from a surveyed surface are presented in this figure. Three fuzzy sets each makeup the surface roughness and slope groups while the elevation uncertainty is represented by four fuzzy sets. All rules are shown; however, only rules 5 and 8 are rules that deal with values that encompass the provided values for both parameters.

Appendix E

Supplementary Tables

Table E.1. Basic summary statistics of population of roughness and slope by sub-reach.

	Surface Roughness (ft.)				**Slope (°)**				
Site	Median	Mean	Max	StDev	Median	Mean	Max	StDev	Observations
All Sites	0.32	0.47	21.34	0.63	8.16	12.13	81.39	11.41	
s1	0.13	0.26	7.09	0.36	10.51	14.06	71.12	10.50	62802
s2	0.32	0.50	6.38	0.57	14.57	17.69	67.90	12.73	34866
s3	0.14	0.29	18.07	0.91	7.91	11.97	81.82	12.82	50847
s4	0.16	0.19	9.31	0.26	7.00	8.945	75.46	7.00	41087
s5	0.18	0.48	21.34	1.04	15.72	20.66	82.33	15.52	63886
s6	0.18	0.22	6.44	0.29	5.09	7.488	73.91	8.07	48867
s7	0.20	0.24	10.78	0.34	6.33	8.214	77.07	7.31	62891
s8	0.27	0.29	3.37	0.22	6.28	7.385	60.53	4.96	30122
s9	0.21	0.27	3.42	0.27	7.08	8.818	67.05	7.00	29664

Table E.2. Results of statistical significance tests of influence of roughness and slope on uncertainty for each sub-reach.

	Surface Roughness (ft.)		**Slope (°)**		**Degrees of Freedom**	
Site	**F-Statistic**	**Probability**	**F-Statistic**	**Probability**	**Numerator**	**Denominator**
s1	691.6	<0.0001	211.7	<0.0001	1	645
s2	908.4	<0.0001	168.3	<0.0001	1	1291
s3	1232.3	<0.0001	639.6	<0.0001	1	1318
s4	1150.0	<0.0001	569.9	<0.0001	1	699
s5	1720.6	<0.0001	702.2	<0.0001	1	1379
s6	412.3	<0.0001	125.3	<0.0001	1	1027
s7	1077.9	<0.0001	456.6	<0.0001	1	2065
s8	143.2	<0.0001	61.8	<0.0001	1	353
s9	532.6	<0.0001	115.2	<0.0001	1	1966

REFERENCES

Aguilar, F., Aguera, F., Aguilar, M., Carvajal, F., 2005. Effects of terrain morphology, sampling density, and interpolation methods on grid DEM accuracy. Photogrammetric Engineering & Remote Sensing 71-7, 805–816.

Anderson, K., Morehead, M., Wilson, T., Butler, M., Conner, J., Hocker, B., 2011. Multi-beam bathymetry to measure volumetric change and particle size distributions in the Snake River through Hells Canyon. American Geophysical Union Fall Meeting.

Beaudoin, J., 2010. Real-time monitoring of uncertainty due to refraction in multibeam echo sounding. The Hydrographic Journal 134, 3–13.

Bolstad, P., 2008. GIS Fundamentals A First Text on Geographic Information Systems. Eider Press.

Brasington, J., Langham, J., Rumsby, B., 2003. Methodological sensitivity of morphometric estimates of coarse fluival sediment transport. Geomorphology 53, 299–316.

Brasington, J., Richards, K., 1998. Interactions between model predictions, parameters and DTM sacles for TOPMODEL. Computers & Geosciences 24-4, 299–314.

Brasington, J., Rumsby, B., McVey, R., 2000. Monitoring and modeling morphological change in a braided gravel-bed using high resolution GPS-based survey. Earth Surface Processes & Landforms 25, 973–990.

Butler, M., 2002. Topographic integration for Hells Canyon studies. Tech. rep., Idaho Power Company.

Chaplot, V., Darboux, F., Bourennane, H., Leguedois, S., Silvera, N., Phachomphon, K., 2006. Accuracy of interpolation techniques for derivation of digital elevation models in relation to landform types and data density. Geomorphology 77, 126–141.

de Jong, C., Lachapelle, G., Skone, S., Elema, I., 2002. Hydrography: Navtech Part #1150. DUP Blue Print, Delf University Press.

Demicco, R., Klir, G., 2004. Fuzzy Logic in Geology. El Sevier Academic Press.

Diaz, J., 2000. Analysis of mulitbeam sonar data for the characterization of seafloor habitats. Master's thesis, University of New Brunswick.

Dix, M., Abd-Elrahman, A., Dewitt, B., Nash, L., 2012. Accuracy of terrestrial LIDAR and multibeam sonar systems mounted on a survey vessel. Journal of Surveying Engineering 138, 203–213.

Ernstsen, V., Noormets, R., Hebbeln, D., Bartholoma, A., Flemming, B., 2006. Precision of high-resolution multibeam echo sounding coupled with high-accuracy positioning in shallow water coastal enivronment. Geo-Marine Letters 26-3, 141–149.

Fuller, I., Large, A., Charlton, M., Heritage, G., Milan, D., 2003. Reach-scale sediment transfers: An Evaluation of two morphological budgetin approaches. Earth Surface Processes and Landforms 28, 889–903.

Hare, R., Eakins, B., Amante, C., Taylor, L., 2011. Modeling bathymetric uncertainty. US Hydro April.

Hare, R., Godin, A., Mayer, L., 1995. Accuracy estimation of Canadian swath (multibeam) and sweep (multi-transducer) sounding systems. Tech. rep., University of New Brunswick, Ocean Mapping Group.

Hazel, J., Grams, P., Schmidt, J., Kaplinski, M., 2010. Sandbar Response in Marble and Grand Canyons, Arizona, Following the 2008 High Flow Experiment on the Colorado River. Tech. rep., USGS.

Heritage, G., Milan, D., 2009a. Influence of survey strategy and interpolation model on DEM quality. Geomorphology 112, 334–344.

Heritage, G., Milan, D., 2009b. Terrestrial Laser Scanning of grain roughness in a gravel-bed river. Geomorphology 113, 4–11.

Hocker, B., 2012. Total propagated uncertainty computations for change detection. Tech. rep., David Evans & Associates.

Huevelink, G., 1998. Error Propagation in Environmental Modeling. Taylor & Francis Inc.

International-Hydrographic-Bureau, 2005. Manual on Hydrography: Publication M-13. International Hydrographic Bureau, 1st Edition.

Johnston, K., Ver Hoef, J., Krivoruchkov, K., Lucas, N., 2001. Using ArcGIS Geostatistical Analyst. ESRI.

Kaplinski, M., Hazel, J., Parnell, H., Breedlove, M., Kohl, K., Gonzales, M., 2009. Monitoring fine-sediment volume in the Colorado River ecosystem: bathymetric survey techniques. Tech. rep., USGS.

Kearns, T., Breman, J., 2010. Bathymetry - the art and science of seafloor modeling for modern applications. GEOconnexion International Magazine July/August, 1–37.

L-3-Communications-SeaBeam-Instruments, 2000. Multibeam Sonar Theory of Operation. L-3 Communications SeaBeam Instruments, East Walpole, MA.

Laan, M., Hsu, J., Rose, S., 2010. Statistics Ready for a Revolution. Amstat News, American Statistical Association September.

Lane, S., James, T., Crowell, M., 2000. Application of digital photogrammetry to complex topography for geomorphological research. Photogrammetric Record 16(95), 793 – 821.

Lane, S., Westaway, R., Murray Hicks, D., 2003. Estimation of erosion and deposition volumes in a large, gravel-bed, braided river using synoptic remote sensing. Earth Surface Processes and Landforms 28, 249–271.

MathWorks, 2013. Fuzzy Logic Toolbox User's Guide. MathWorks.

McKean, J., Isaak, D., Wright, W., 2008. Chapter 2 Stream and Riparian Habitat Analysis and Monitoring with a High-Resolution Terrestrial-Aquatic LiDAR. PNAMP Special Publications: Remote Sensing Applications for Aquatic Resource Monitoring, 7–15.

Mechelke, K., Kersten, T., Lindstaedt, M., 2007. Comparitive investigation into the accuracy behaviour of the new generation of terrestrial laser scanning systems. Optical 3-D Measurement Techniques VIII Vol I, 319–327.

Milan, D., Heritage, G., Large, A., Fuller, I., 2011. Filtering spatial error from DEMs: Implications for morphological change estimation. Geomorphology 125, 160–171.

Ross, R., Booker, J., Parkinson, W., 2002. Fuzzy Logic and Probability Applications: Bridging the Gap. Series on Statistics & Applied Probability 11. ASA-SIAM.

Rumsby, B., Brasington, J., Langham, J., McLelland, S., Middleton, R., Rollinson, G., 2008. Monitoring and modelling particle and reach-scale morphological change in gravel-bed rivers: Applications and challenges. Geomorphology 93, 40–54.

Rychkov, I., Brasington, J., Vericat, D., 2012. Computational and methodological aspects of terrestrial surface analysis based on point clouds. Computers & Geosciences 42, 64–70.

Shepard, R., 2005. Quantifying Environmental Impact Assessments Using Fuzzy Logic. Springer Science bib+ Business Media.

Wheaton, J., 2008. Uncertainty in Morphological Sediment Budgeting of Rivers. Ph.D. thesis, University of Southampton.

Wheaton, J., Brasington, J., Darby, S., Sear, D., 2010. Accounting for uncertainty in DEMs from repeat topographic surveys: improved sediment budgets. Earth Surface Processes and Landforms 35, 136–156.